Universidade de Aveiro
Ano 2022

Guilherme Matos Lopes

Desenvolvimento de sensores óticos de pH para aplicação em aquacultura e integração em plataforma híbrida multi-parâmetro

Development of optical pH sensors for application in aquaculture and integration in a hybrid multiparameter platform

Universidade de Aveiro
Ano 2022

Guilherme Matos Lopes

Desenvolvimento de sensores óticos de pH para aplicação em aquacultura e integração em plataforma híbrida multi-parâmetro

Development of optical pH sensors for application in aquaculture and integration in a hybrid multiparameter platform

Dissertação apresentada à Universidade de Aveiro para cumprimento dos requisitos necessários à obtenção do grau de Mestre em Engenharia Física, realizada sob a orientação científica do Doutor Carlos Alberto Ferreira Marques, Investigador Principal do Departamento de Física da Universidade de Aveiro e da Doutora Sónia Oliveira Pereira, Investigadora Pós-Doutoramento do Departamento de Física da Universidade de Aveiro

Este trabalho foi desenvolvido no âmbito do projeto i3N, UIDB/50025/2020 & UIDP/50025/2020 & LA/P/0037/2020, e do projeto DigiAqua PTDC/EEI-EEE/0415/2021 financiados por fundos do FEDER através do programa COMPETE 2020 e da FCT – Fundação portuguesa para a Ciência e Tecnologia.

Dedico este trabalho à Isa e à minha família.

o júri / the jury

presidente / president

Professor Doutor Luís Miguel Rino Cerveira da Silva
Professor Auxiliar da Universidade de Aveiro

vogais / examiners commitee

Professor Doutor José Luís Campos de Oliveira Santos
Professor Catedrático da Faculdade de Ciências da Universidade do Porto

Doutora Sónia Oliveira Pereira
Bolseira de Investigação de Pós-Doutoramento da Universidade de Aveiro

agradecimentos

O trabalho desenvolvido nesta dissertação resulta da colaboração e ajuda de várias pessoas e entidades, sem quais a realização do trabalho não teria sido possível, e por essa razão, pretendo mostrar a minha gratidão.

Em primeiro lugar, gostaria de agradecer aos meus orientadores, Doutor Carlos Marques e Doutora Sónia Pereira, não só por toda a orientação, conhecimento e ajuda que me prestaram ao longo de todo o trabalho, mas sobretudo por serem exemplos de profissionalismo e dedicação que levarei para a vida.

Ao Departamento de Física da Universidade de Aveiro e ao laboratório do grupo de Nanofotónica e Optoeletrónica do i3N-Aveiro pela disponibilização do espaço, instalações, materiais e equipamentos necessários, em especial, aos membros que frequentam o laboratório, pela sua presença e disponibilidade para ajudar sempre que preciso.

Um agradecimento muito especial ao Professor Doutor Santosh Kumar e ao seu grupo da Universidade de Liaocheng, China, pelo fornecimento dos tapers que foram uma parte central do trabalho.

Ao Professor Doutor Nunzio Cennamo da Universidade de Nápoles pelo fornecimento das fibras óticas de plástico D-shapes revestidas em ouro, que me permitiram posteriormente reutilizá-las.

Ao técnico António José Fernandes pela aquisição das imagens por SEM.

À Doutora Ana Catarina Moreirinha pela aquisição dos espetros de FTIR.

A todo o pessoal da oficina que fizeram várias versões dos recipientes necessários à realização das caraterizações dos sensores, em especial aos técnicos Miguel e ao Jorge.

Um agradecimento também ao Rafael e ao Doutor Nuno pela ajuda e discussões que tivemos para implementar os sensores que ambos produzimos na plataforma híbrida.

Igualmente um grande agradecimento aos meus amigos e colegas que conheci durante este percurso, pois de uma forma ou de outra tornaram esta caminhada ainda mais especial.

Agradecer também à minha família, sobretudo ao meu pai, mãe e irmã, pois sem a confiança e apoio que me dão todos os dias a conclusão desta etapa não era possível.

Por último, e mais importante, agradecer à Isa. É imensurável a quantidade de coisas que fazes por mim, mas sobretudo obrigado por estares sempre presente e me deixares feliz.

Muito obrigado a todos!

palavras-chave

aquacultura, pH, sensor, *taper*, *D-shape*, polianilina.

resumo

Os sensores em fibra ótica têm-se mostrado muito promissores para a aplicação em ambientes marinhos na monitorização de vários parâmetros cruciais ao bom crescimento e reprodução dos peixes, dos quais o pH é dos mais importantes no setor da aquacultura. No caso deste trabalho, dois tipos de sensores em fibra ótica foram produzidos: *tapers* feitos a partir de uma fibra de sílica monomodo com uma rede de *Bragg* e fibras óticas de plástico com uma D-*shape*. Em relação às fibras óticas de plástico D-*shape*, foram usados dois tipo diferentes: umas produzidas no laboratório, usando uma máquina de polir, e outras foram reutilizadas a partir de sensores antigos de cortisol.

A polianilina (PANI) foi sintetizada por polimerização oxidativa da anilina na presença das fibras e o tempo de síntese escolhido, para o qual se obteve melhores resultados, foi 20 minutos. A sensibilidade e comportamento do sensor são determinados pelas modificações de geometria aplicadas nas fibras que permitem que a onda evanescente tenha acesso ao meio circundante e, em combinação com a polianilina, isto resulta numa diminuição da transmissão dos espetros à medida que o pH aumenta.

Os sensores apresentam um certo grau de reprodutibilidade e repetibilidade, com os *tapers*, as fibras D-*shape* produzidas no laboratório e as reutilizadas com sensibilidade de –0.25 dB/pH, –500 contagens/pH e –2500 contagens/pH, respetivamente. Contudo, isto apenas é válido no sentido ascendente de pH.

Relativamente ao tempo de estabilização, para os extremos das regiões de pH, quer seja muito ácido, totalmente protonado, ou muito básico, totalmente desprotonado, o tempo de estabilização é mais curto. Já para os valores de transição de pH este tempo é mais elevado, pois a PANI também está numa fase de transição. Foram ainda efetuados testes de sensibilidade cruzada no que diz respeito à força iónica e à temperatura, sendo que os sensores não mostraram uma alteração espetral na zona de interesse. Adicionalmente, integrou-se o sensor de pH numa plataforma híbrida com um sensor de nitritos e observou-se a resposta ótica ao adicionar nitritos a uma solução de PBS, o que resultou em variações pouco significativas.

As fibras *tapers* são bastante úteis devido às suas capacidades de monitorização remota e multiplexagem, daí terem sido fundidos com um sensor de nitritos. No entanto, estes carecem de robustez mecânica e facilidade de fabrico. Por outro lado, nas fibras D-*shape* o oposto é observado. Estas são mais robustas mecanicamente e fáceis de fabricar, mas a possibilidade de multiplexar ou monitorizar remotamente é desconhecida ou mais complicada.

Como trabalho futuro pretende-se que os sensores de pH produzidos sejam aplicados diretamente nos tanques de aquacultura a fim de identificar possíveis interferentes da água nas medidas e de realizar testes para otimizar a estrutura híbrida.

keywords

aquaculture, pH, sensor, taper, D-shape, polyaniline.

abstract

Optical fiber sensors have shown a lot of potential for application in marine environments e regarding monitoring multiple parameters crucial to the growth and well-being of fish, of which pH is one of the most important. Regarding this work, two types of optical fiber sensors were produced: tapers made from a silica single mode fiber with a fiber Bragg grating, and D-shape plastic optical fibers. There were used two different types of D-shape plastic optical fibers: home-made, using a polishing machine, and reused, from old cortisol sensors.

Polyaniline (PANI) was synthesized by oxidative polymerization of aniline that was carried out onto the fibers and the selected synthesis time, for which better results were obtained, was 20 minutes. The sensitivity and the sensors' behavior are determined by the geometry modifications applied onto the fibers, which allow the access of the evanescent wave to the surrounding medium which, in combination with polyaniline, results in a transmission decrease of the spectra as pH increases.

The sensors present a certain degree of reproducibility and repeatability with the tapers, the D-shapes home-made and reused having a sensitivity of –0.25 dB/pH, –500 counts/pH and –2500 counts/pH, respectively. However, this is only valid for the increasing order.

Regarding the stabilization time, for extreme pH values, whether very acidic, totally protonated, or very basic, totally unprotonated, the stabilization time is shorter. On the other hand, for the transition values of pH, this time is longer, since the PANI is in a transition phase. There were also made cross-sensitivity tests related to ionic strength and temperature, where the sensors did not show a spectra variation in the range of interest. Additionally, the pH sensor was integrated in a hybrid platform with a sensor of nitrites and the optical response to the increment of nitrites in a PBS solution was observed, having only slight variations.

The tapers are very useful due to their remote sensing and multiplexing, which is the reason they were spliced with a sensor of nitrites. However, these lack mechanical robustness and ease of fabrication. On the other hand, the opposite happens in the D-shapes. These are more robust and easier to manufacture, but the possibility of multiplexing or remote sensing is challenging or unknown.

As a future work, it is intended that the pH sensors produced are applied directly on the aquaculture tanks in order to identify possible water interferences in the measurements and perform tests to optimize the hybrid structure.

Index

List of Symbols

α	Acceptance angle
ε	Strain
Λ	Periodicity of the Bragg grating
λ^{m}_{LPG}	Wavelength corresponding to the coupling of a cladding of a long period grating
λ^{m}_{TFBG}	Wavelength corresponding to the coupling of a cladding of a tilted fiber Bragg grating
λ_0	Wavelength of a light source
λ_{Bragg}	Bragg wavelength
$\lambda_{cut\text{-}off}$	Wavelength cut-off
θ_c	Critical angle
θ_i	Angle of incidence
a	Radius of the fiber core
A^-	Conjugate base
a_H	Activity of Hydrogen
B	Base
d_p	Penetration Depth
E	Cell Potential
E^0	Standard Cell Potential
F	Faraday constant
HA	Acid
HB^+	Conjugate acid
In	Indicator
In^-	Conjugate base of an indicator
K_a	Acid dissociation constant
n_0	Refractive Index of the external medium
NA	Numerical Aperture
n_{clad}	Refractive index of the cladding
n_{core}	Refractive index of the core
Nd:YAG	Neodymium-doped yttrium aluminum garnet
n_{eff}	Effective refractive index
$n_{eff}^{clad(m)}$	Effective refractive index of a cladding mode
n_{eff}^{core}	Effective refractive index of the core
R	Gas Constant
T	Temperature

List of Acronyms

CE	Counter Electrode
CMS	Combiner Manufacturing System
DC	Direct Current
DPV	Differential
EW	Evanescent Wave
FAO	Food and Agriculture Organization
FBG	Fiber Bragg Grating
HE	Hybrid Modes
ISFET	Ion Selective Field Effect Transistor
LIG	Laser induced graphene
LPG	Long-Period Grating
MOSFET	Metal-Oxide Semiconductor Field Effect Transistor
NP	Nano Particles
PANI	Polyaniline
PANI-PVA	Polyaniline-Polyvinyl Alcohol
PBS	Phosphate Buffered Saline
PEGDA	Poly(ehylene glycol) Diacylate
PMMA	Poly(methylmethacrylate)
POF	Plastic Optical Fibers
PPY	Polypyrrole
PTH	Polythiophene
RAS	Recirculating Aquaculture Systems
RE	Reference Electrode
RI	Refractive Index
SEM	Scanning Electrom Microscopy
SMF	Single Mode Fibers
TE	Transverse Electric
TFBG	Tilted Fiber Bragg grating
TIR	Total Internal Reflection
TM	Transverse Magnetic
UV	Ultraviolet
WE	Working Electrode

List of Figures

1. Introduction

Projections indicate that the world population will grow from the current 7.7 billion to 9.7 billion people by 2050, and this growth needs to be accompanied by a fast and continuous development of the food industry, to meet the nutritional demands of the population [1]. Thus, there is a need to obtain protein and alternatives to wild fisheries. Aquaculture is an industry that can fill in this necessity for high-quality protein, and this is supported by the Food and Agriculture Organization (FAO), as well as framed within the 2030 Goals set by the United Nations. Thus, this growth needs to be accompanied by a development of technology to monitor important water parameters that can define the fish well-being. Optical fiber sensors due to their advantages are a technology that can be easily deployed on aquaculture tanks.

1.1. Motivation

Fish is an important part of human food, not only to achieve the desirable animal protein, without over relying on the livestock industry, but also due to its high nutritional profile. However, following the population growth reports, fish consumption will grow past the production capacity of the oceans and seas. Thus, the growth and development of the aquaculture industry, which is defined as the farming of aquatic organisms including fish, mollusks, crustaceans, and aquatic plants in selected or controlled environments, could respond and act as a solution to this increase in the demand of fish and decrease the pressure on the oceans and traditional fishery [2,3].

This interest in expanding the aquaculture industry is backed by the FAO, which has set a goal that, by 2030, 60% of the consumed fish will be provided by aquaculture. For aquaculture to keep growing in an ethical and sustainable manner, improved methods and technology to monitor fish health and the management of the tanks are a necessity [2].

All of the reasons mentioned above make the advancements and improvements on the aquaculture industry framed within three of the goals set out by the United Nations to accomplish by 2030: End hunger, achieve food security and improved nutrition and promote sustainable agriculture (Goal 2); Build resilient infrastructure, promote inclusive and sustainable industrialization and foster innovation (Goal 9); Conserve and sustainably use the oceans, seas and marine resources for sustainable development (Goal 14) [4].

In 2018, from the 179 million tons of fish caught, 82 million tons came from aquaculture, where China was the country at the forefront, contributing to a total of 70% of this value, and it has already replaced the traditional capture as the main source of fishing. Portugal produced 82 thousand tons, which represents a growth of 11.5% when comparing it to 2017, although aquaculture is still not growing as fast as desired. One way the farms and marine organisms can be cultivated is in seawater, either in sheltered coasts or offshore waters. Thus, it would be expected a decent growth and investment since Portugal has a vast coastal zone. However, the profitability has not been as high as expected, due to the adverse conditions of the coast and the high technological cost associated with aquaculture systems [5,6].

The most common aquaculture production system are ponds, and despite being the most traditional method, its biggest disadvantage is that it relies heavily on natural processes to remove waste and provide oxygen. Other systems include utilizing cages on existing bodies of fresh or salt water to grow fish in large quantities, where fish are confined and grown in large numbers, and, once again, the water movement and circulation is critical, since tight confinement with high densities of fish increase the risk of disease. Another system are raceways, which are usually located downstream of a river or stream, since they require a large and continuous water flow into

the system, and the number of fish that can be grown is directly correlated to the quantity and the quality of the water flow and supply. Thus, it is difficult to find places that fit these types of conditions, reducing the amount of locations where this system can be deployed [3]. On top of the limitations of these methods, it is also important to note their possible environmental impact from water pollution and transmission of parasites, but also territory occupation and invasion of species, which will affect local biodiversity.

Recirculating Aquaculture Systems (RAS) attempt to tackle these issues, by allowing the development of fish on land in a controlled environment, with lower environmental impact, lower territorial area, independence from weather and reusing water. As a result of the continuous filtering and addition of oxygen that these systems provide, it is necessary to have a continuous source of external power and mechanical process to maintain the water quality. RAS, as schematized in Figure 1.1, is the most intensive form of aquaculture, and its complex systems regarding fish biomass and water quality are challenging to manage and monitor. This is relevant, because small variations of these parameters can cause stress on the fish and affect their feed intake, which in turn can lead to lower growth and eventual death. Thus, these systems offer the highest potential reward, but also the greatest risk of failure [7].

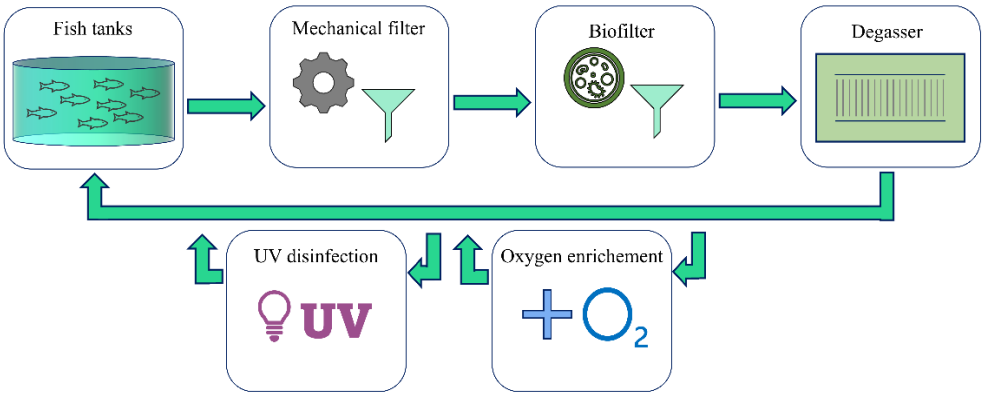

Figure 1.1 –Schematic representation of RAS functioning.

Therefore, to combat these issues, and since aquaculture is one of the fastest growing protein production markets right now, it needs to be accompanied by a high-tech progress as well, to monitor and control harmful substances in the water, so detrimental events in the quality of life of the fish are avoided, and, consequently, quality of food for human consumption is ensured [6].

Fish do all their basic activities, such as breathing, feeding, growing, excreting wastes, maintaining a salt balance, and reproducing, all under water, thus understanding the physical and chemical properties of water is essential to effective aquaculture. Some of the key water parameters that define fish health in aquaculture tanks are temperature, light, salinity, water flow, feeding rate, oxygen, carbon dioxide and pH. But also, newer parameters being studied right now, which may have a strong influence on growth and feeding conversion ratio, but have no commercial solutions available, such as stress, and micro and nano plastics.

One critical parameter of the above mentioned is pH, and its importance lies beyond if the water is either acid or basic, since the pH value can have an influence on the overall chemical behaviour of substances, either on its nutritional availability, biological function, or microbial activity [8–10]. Thus, it is a central parameter in various industries that have a great impact on our health, such as agriculture, aquatic ecosystems, water treatment, medicine and food [11], and also aquaculture.

The optimal pH required for fish development is between 6.5 and 9, and at slightly lower and higher pH values, up until 4 and 11, respectively, poor growth and reproduction will start to

be observed. Regarding pH values below 4 and above 11, fish cannot endure them for an extended time, eventually leading to their mortality [12].

Additionally, by eating feed and consuming oxygen, the fish will excrete waste products, such as feces, carbon dioxide, and ammonia. Ammonia is present in two forms, the ionized form (NH_4^+), which is not toxic, and the unionized form (NH_3), which is toxic and harmful for the fish. Toxic ammonia can be converted by biological mechanisms into non-toxic nitrates, however, due to the high stocking density of fish in aquaculture tanks, the amount of toxic ammonia rises. Additionally, the amount of toxic ammonia is dependent on temperature and also on pH, increasing as both of them increase [12].

For all these reasons, advanced monitoring methods are required to obtain the information that determines water quality. Numerous analytical techniques, such as mass spectrometry and spectrophotometry have been used to determine parameters that determine water quality. Although these techniques have high accuracy, sensitivity and repeatability, they are usually expensive and time consuming and require sophisticated instrumentation, as well as difficulty in performing real-time and *in situ* measurements [13]. Hence, there is a lack of probes or online technologies to measure and identify these parameters that determine water quality.

In the case of pH, the most common commercial pH sensor is the glass electrode, and although it produces reliable results, it has its limitations regarding continuous measurements in real time, fragility, and difficult miniaturization and integration in multiparameter platforms.

Therefore, fiber optic sensors are a viable alternative to combat this scarcity in the market, as they offer numerous advantages, such as immunity to electromagnetic interference, miniaturization, robustness and multiplexing and the possibility of real-time remote sensing and *in situ* measurements, and the prospect of applying this technology in aquaculture tanks is promising and a possible tremendous asset.

1.2. Objectives of the work

This work aims to develop and characterize different types of optical fiber sensors for pH detection and evaluate the possibility of deploying them in aquaculture tanks.

First, it was intended that these sensors were produced on two different types of geometrically modified optical fibers, allowing access of the evanescent wave to the surrounding medium and offering distinct advantages and disadvantages between them: a tapered single mode fiber and a D-shape in a plastic optical fiber. In the case of the tapered single mode fiber, a Bragg grating is subsequently inscribed in the tapered region. As for the D-shapes, two distinct sets of fibers will be used, one consists of a low-cost and home-made D-shape manufactured using a polishing machine, and the other one is made by reutilizing a D-shape previously used by other colleagues in the group, as a cortisol immunosensor. Afterwards, all three of these sensors were coated with polyaniline, a polymer sensitive to pH variations.

Subsequently, there was a need to determine the optimal synthesis time of the polyaniline coating, and fully characterize and evaluate the sensors performance regarding their sensitivity, possibility of reproducibility and repeatability of the results, stabilization time, and possible cross sensitivities, concerning temperature and ionic strength.

Lastly, after producing them, an optical pH sensor is integrated in a hybrid sensing platform with an electrochemical nitrite sensor, as this is also an important parameter in aquaculture. The incorporation of both these sensors in the same platform reinforces the importance of measuring pH, as this value is needed not only to determine water quality, but also to calibrate the nitrites sensor.

2. pH sensors: concepts and state of the art

In the following chapter, an introduction to the concepts of acids, bases and pH is provided, as well as why pH is an important parameter in a variety of different areas. Succeeding it, an exposure of the traditional ways used for measuring pH, such as colorimetric methods and glass electrodes is given, as well as novelty solutions using potentiometric and ion-selective field effect transistor techniques. Lastly, optical fibers are introduced, and how they can be exploited to be used as pH sensors. Briefly, different fiber sensing structures, whether it be geometry-modified or grating based, will be addressed, combined with different functional materials allowing to sense a variety of different parameters, namely the specific case of pH.

2.1. pH definition

The concepts of acidity and basicity were first introduced in the 19th century, in 1884, by Svante Arrhenius, with the ionic theory, which explains the relationship between hydrogen ions or protons, H^+, and hydroxyl ions, OH^-. Acids are defined as a substance that dissociates in water increasing the concentration of H^+, while analogously, a base is a substance which, by dissociation in the water, it increases OH^- concentration [14,15]. These concepts that Arrhenius introduced would be generalized in 1923 by Johannes Nicolaus Brønsted and Thomas Martin Lowry with how the acids and bases react with each other [15–17]. The Brønsted-Lowry acid is a proton donor, whereas the Brønsted-Lowry base is a proton acceptor, this definition can be expressed in terms of the following equation (1), for a given acid HA [15,17]:

$$HA + B \rightleftarrows A^- + HB^+ \tag{1}$$

On the left hand-side there is the acid, HA, and the base, B. As for the acid, it can donate its proton to B, and subsequently, they turn to its conjugate base, A^-, and its conjugate acid, HB^+, respectively.

However, even after the initial definitions provided by Arrhenius, the acidity or basicity of an aqueous solution was not exactly quantified up until 1909, when Søren Peder Lauritz Sørensen defined the concept of a pH scale to determine whether an aqueous solution is acid or basic [14,16,18–20]. Although there are some literature reports that discuss the original meaning behind the lower case "p" of pH, which can either mean "power of hydrogen" or "potential of hydrogen", chemist defined that the lower case "p" stands for "decimal logarithm of" and as for the following letter, capital "H" stands for hydrogen ion concentration [21]. This concept can be also applied for pOH, when related to hydroxide ions, or the acid dissociation constant, pK_a.

Although the most common form is as written in equation (2), a few years after Sørensen introduced a way to determine pH, the concept of hydrogen ion activity was introduced. Therefore, a more formal and generally accepted way to write the equation is as a function of the molality-based activity of hydrogen, a_H, as written in equation (3) [16,19,22]:

$$pH = -\log_{10}([H^+]) \tag{2}$$

$$pH = -\log_{10}(a_H) \tag{3}$$

Each acid has an acid dissociation constant, K_a, that quantifies the acid strength for a given solution, i.e., the ability to either accept or donate a proton, given by equation (4) [23]:

$$K_a = \frac{[A^-][H^+]}{[HA]} \tag{4}$$

Thus, the lower the pK_a, the stronger the acid and the greater its ability to donate protons. The relationship between pH and pK_a is given by the Henderson-Hasselbalch equation, using the equilibrium concentrations of the acid and base, as in equation (5) [23]:

$$pH = pK_a + \log_{10}\frac{[A^-]}{[HA]} \tag{5}$$

This equation provides an easy way to calculate the pH of buffer solutions (aqueous solution containing a weak acid and the conjugate base, or vice-versa). Since in buffer solutions, for weak acids, the dissociation is small enough to consider that the concentrations suffer very small variations when comparing to the initial concentration value, for both acid and base, just as long as $[H^+]$ is less than 5% of both $[A^-]_{initial}$ and $[HA]_{initial}$. Although, this approximation can fail for extremely low pH acids or high pH bases [22].

The pH scale is measured between 0 and 14, with the neutral value usually associated to 7, below this value the solution is acid, and above it is basic. However, this statement is only valid if the temperature is 25 ºC. By increasing the temperature, the neutral value decreases, and vice-versa, by decreasing the temperature the neutral value increases. Despite in any aqueous solution the concentration of hydrogen ions multiplied by the concentration of hydroxide ions being kept constant, this value changes depending on the temperature ($K_W = [H^+][OH^-] = 1 \times 10^{-14}$ for 25 ºC). This is due to the equilibrium constants being a function of temperature and being related to Gibbs free energy, according to the equation (6) [22,24]:

$$E = E^0 + \frac{RT}{F}\ln(a_H) = E^0 - \frac{2.303RT}{F}pH \tag{6}$$

where E is the cell potential, E^0 is the standard cell potential, R the gas constant, T the temperature and F the Faraday constant.

Although most pH measurements will fall between 0 and 14, it is possible to find pH values outside of this range. This is observed in both commercially available solutions and in nature. Saturated NaOH solutions have a pH of 15, or for negative pH, observed in hot springs or water from mines, ranging from −1 to −3 [25].

2.2. pH measurement

2.2.1. Traditional methods

The most traditional and commercially methods available are colorimetric and glass electrode.

Starting with the colorimetric methods, they are simple and rapid techniques that use the color of acid-base indicators to determine the pH and, if under optimum conditions, accurate values of pH values can be obtained. Indicators are natural or synthetic dyes that are weak acids or bases and have different colors depending on if they are in their acidic or basic states. For a given indicator, HIn, that dissociates, the ratio of $[In^-]/[HIn]$ is what determines the color of the indicator in the solution, and consequently, directly correlates the color to the pH of the solution. Following equation (5), if the ratio $[In^-]/[HIn]$ is less than 1/10, the solution will have the color corresponding to an acid, and if it is higher than 10, it will be basic [22].

Regarding the colorimetric measurement, it can be done in two ways, using indicator papers or by adding the indicator to the test solution. As for the papers, the dyes are strongly bound to the paper, for the dye to not bleed into the test solution. The paper is then immersed in the test solution, and the color it acquires is compared to a standard color chart to determine the pH, as Figure 2.1 shows. On the other hand, a measured amount of indicator is added for a certain quantity of the test solution, and the color that the solution acquires is compared to a reference

solution of a known pH. However, these colorimetric methods have a higher degree of inaccuracy, due to various possible errors, such as, by adding the indicator, since it is a weak acid, it could slightly change the pH of the solution. Additionally, the result analysis is subjective to the person doing it since it relies on comparing the color of the solution to the reference color and applying it to a narrow interval can be difficult, so lack of resolution is also a problem in this method. Also, due to high salt concentration, temperature or organic substances present in the test liquid may also change the pH.

Figure 2.1 – Example of a colorimetric method (Left) scale (Right) and indicator paper.

Thus, the most common way to measure the pH is through the glass electrode method, as schematically represented in Figure 2.2, which uses measuring and reference electrodes [16,24,26]. The tip of the measuring electrode consists of a thin glass bulb membrane, and upon contacting the test solution, a "gel layer" is developed in both outside and inside the glass membrane and it is in contact with a defined buffer solution, which is inside the electrode. This internal buffer has constant pH, and therefore its potential is constant. By contacting the test solution, H^+ ions diffuse either into or out of the "gel layer", depending on the pH value of the measured solution. If the test solution is basic, the H^+ ions will diffuse outwards, a negative charge will appear on the outside of the gel layer. However, if the test solution is acid, H^+ ions diffuse inwards, leaving a positive charge on the outside. Hence, the total electrode potential is a result of the difference between the inner and outer charge [22].

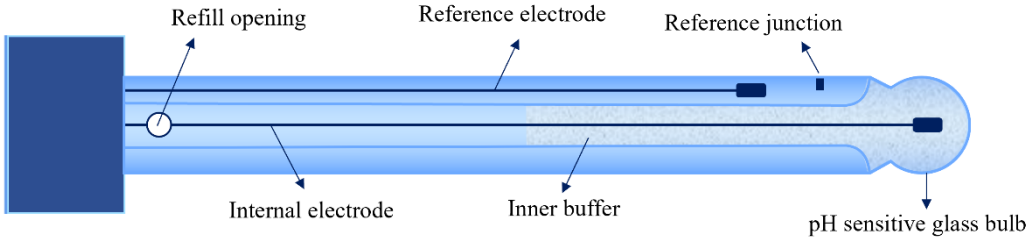

Figure 2.2 – Schematic representation of a glass electrode.

The reference electrode must have a well-defined stable potential, which is independent of the test solution, with the reference element, usually being silver or silver chloride, being immersed in an electrolyte, that needs to be in contact with the measured solution. This contact is usually made through a porous ceramic junction. The reference electrolyte has a high ion concentration leading to a low electrical resistance. Ideally, there should be no reaction between the reference electrolyte and the measured solution [22,24]. It is rare to find nowadays both these electrodes separated, as they are usually packed as combination electrodes, with both the measuring and the reference elements contained in the same electrode. The functioning method stays the same, but in this case, the combination electrode consisting of the glass electrode and the reference electrolyte are concentrically encircled [22,24].

The response of a pH electrode is defined by the equation (6), the Nernst equation, and as it is seen, the slope factor shows a dependence on the temperature. This is one of the reasons

the temperature highly influences the pH measurements, since the common value of the water dissociation constant, 10^{-14} mol dm^{-3}, is only valid at 25 ºC, which is the temperature at which electrodes are usually calibrated. Therefore, it is necessary some sort of temperature compensation, since a change of over 10 ºC in the temperature sample, will result in pH measuring errors of up to 0.2 pH units. Hence some modern electrodes have automatic compensation temperature techniques, which through a separate temperature sensor incorporated into the pH electrode, measures the temperature of the test solution, and automatically revaluates the pH value depending on the Nernst slope temperature factor [24].

The glass electrode is the standard for pH measurements, due to being the oldest and widest used approach for commercial pH meters. However, it poses a few disadvantages, such as slow response time, high temperature instability, high impedance, fragility, and difficult miniaturization. This is the reason that sensors based on two electrodes, where the sensing electrode is coated by a material that is sensitive to pH, to measure the potential across the cell, are still subject of development and research [9,27,28].

2.2.2. State of the art

To cite a few examples of recent potentiometric based sensors, in 2018, Khalil *et al.* [29] developed a pH sensor using iridium oxide nanoparticles (NPs) synthesized by the facile alkaline hydrolysis method, which were electrodeposited using cyclic voltammetry on a gold wire and presented a sensitivity of −73.7 mV/pH. Also in 2018, Mohammad-Rezaei *et al.* [30], reported a potentiometric pH sensor based on manganese oxide NPs electrodeposited on graphenized pencil lead electrode, with a sensitivity of -57.051 mV/pH. More recently in 2022, Singewald *et al.* [31] developed a low-cost potentiometric pH electrode based on niobium, using three different methods, thermal growth, and chemical and electrochemical deposition, with the electrochemical method producing the best results achieving higher reproducibility and higher sensitivity of −41 mV/pH, due to the higher porosity verified. In 2019, Park *et al.* [32] produced a two-electrode configuration with a polyaniline nanofiber array as the sensing electrode and Ag/AgCl as a reference electrode. The authors obtained sensitivities of 62.4 mV/pH. Due to their high flexibility, polyaniline can also be found as wearable pH sensors, such the one reported by Mazzara *et al.* in 2021 [33], a wearable polyaniline based for pH sweat monitoring with sensitivities of 62.3 mV/pH and pH ranges from 2 to 8.

The main problem associated with potentiometric methods lies in the main measurement mechanism, since by measuring the whole cell potential, it can be associated with poor selectivity [11,34].

An alternative to potentiometric sensors is using Ion Selective Field Effect Transistor (ISFET) sensors, with their advantages offering more robustness, lower impedance, and simple fabrication, due to their Complementary Metal-Oxide Semiconductor (CMOS) compatibility. An ISFET has a similar structure to a Metal-Oxide Semiconductor Field Effect Transistor (MOSFET), but instead of a top metal gate, it has a gold reference electrode in contact with the electrolyte solutions, which in turn is interacting with the gate oxide of the ISFET where the sensing film will be deposited. Most recent sensing films include Ta_2O_5, Al_2O_3, SnO_2 and AlN that are grown using different methods, such as electrochemical deposition, sputtering and sol-gel techniques [35,36]. For example, in 2019 Sinha *et al.* [36] reported an AlN gate ISFET based pH sensor, with the sensing film being deposited through pulsed DC magnetron assisted reactive sputtering technique with a sensitivity of 33 mV/pH [36]. The disadvantage of these sensors is their dependence on the ionic strength of the solution, signal, and behavior drift over time, and that the sensing film gets etched by being in constant contact with the electrolyte solutions.

The reasons mentioned above are why there is still a demand to find even more alternatives to the already existing pH sensors. Lastly, another option is optical sensors, with most

of them using an optical fiber coated with a pH sensitive film, with its main advantages being faster response times, resolution, miniaturization, and the multi-point and multiplexing ability of the fibers.

2.3. pH sensors using optical fiber

2.3.1. Optical fibers

An optical fiber is a structure that consists of a cladding concentrical with a core, which acts as means of transporting light through large distances with low losses. The way this light is transmitted is through the total internal reflection (TIR) phenomenon that happens due to the core (n_{core}) having a higher refractive index (RI) than the cladding (n_{clad}). If a light beam, travelling in a medium with a RI of n_{core}, reaches the interface of a medium with a RI of n_{clad}, in which $n_{core} > n_{clad}$, if the angle is inferior to the critical angle (θ_c, angle at which the angle of refraction is 90º) the light will be refracted. However, if the angle is superior to the θ_c the light beam is reflected and TIR happens. This is the principle at which light travels inside the fiber, being associated with the concept of numerical aperture ($NA = n_{ext} \sin \alpha = \sqrt{(n_{core}^2 - n_{clad}^2)}$, with n_{ext}, the refractive index of the external medium at which the fiber is placed, and α the acceptance angle). If any light beam at the external medium-core interface is entering with an angle below the acceptance angle, TIR will be achieved, if it is higher, the light refracts to the cladding [37,38].

When light is travelling inside an optical fiber, it propagates in different types of guided modes, and each of these guided modes, which carries a portion of the light from the input signal, consists of a variety of electromagnetic field configurations, transverse electric and magnetic (TE and TM, respectively), and hybrid modes, combinations of TE and TM modes, (HE). These modes are the number of possible allowed paths of light propagating inside of the fiber, with the modes that propagate at angles close to the θ_c being higher order modes, and angles higher than the θ_c being lower order modes [39].

The parameter that sets if there are single or multiple modes inside the fiber is V-parameter, $V = 2\pi\, a\, NA/\lambda$, with a representing the radius of the core and λ the wavelength of the light propagating inside the fiber. If $V < 2.405$ it is a single mode and only the zero-order mode propagates. In the opposite condition, the fiber is multimode and multiple modes propagate [40]. V can alternatively be written as a wavelength cut-off parameter ($\lambda_{cut\text{-}off}$), i.e., wavelength at which higher modes will start to propagate. The most standard commercially available fibers are silica single mode fibers (SMF) with a total diameter of 125 μm and a core diameter of 9 μm with a NA of 0.13, and plastic optical fibers (POF) that support multimode with a total diameter of 1000 μm and a core made of poly(methylmethacrylate) (PMMA) with a diameter of 980 μm and a fluorinated polymer cladding with a NA of 0.5 [39].

The optical fibers' characteristics well controlled in their fabrication step make them the desired transmission medium in long-distance telecommunication systems, since it can send large amount of data with low losses, especially SMF in the windows with low attenuation, the O-band and C-band, centered at around 1300 and 1550 nm, respectively [41]. These advances in telecommunications, as well as in optoelectronic devices, lead to more extensive production and research on optical fiber as sensors, with the first being reported in 1960 [42–44]. Fiber sensitivity to attenuation, depending on external disturbances, allows modulation of various light properties, for example, intensity, phase, polarization, or wavelength, and by monitoring one of these properties, an optical fiber sensor is obtained. Optical fiber sensors allow measuring parameters such as temperature, strain, RI and humidity, among others, and offer advantages in relation to traditional electronic sensors, namely immunity to interference from electromagnetic fields, high sensitivity, and possibility of multiplexing [43,44].

In the early 1980s, using ion or UV laser, it was possible to manufacture what would come to be a very popular type of optical fiber sensors, grating based sensors, of which the most common are fiber Bragg gratings (FBG). This technique consists on the inscription of microstructures longitudinally across the core of an optical fiber where periodic RI modulations take place. Due to the phase matching conditions associated with a sub-micron period, of all the reflected signals only in a very narrow spectral region will constructive interference happen. Acting as a wavelength selective reflection filter with a well-defined wavelength (Bragg wavelength, λ_{Bragg}), defined by equation (7), and the rest will be transmitted, as seen in Figure 2.3 [40,42,45–47].

$$\lambda_{FBG} = 2n_{eff}(\varepsilon, T)\Lambda(\varepsilon, T) \tag{7}$$

where n_{eff} is the effective RI, Λ the lattice parameter that defines the periodicity of the modulations of the RI and ε the strain.

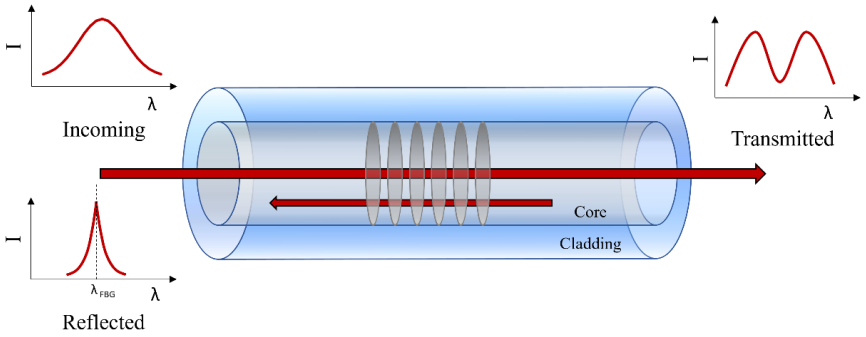

Figure 2.3 – Schematic of the light coupling occurring in a FBG and its respective spectra.

This technology allowed to produce satisfactory results regarding temperature and strain, as well as the measurement of both parameters simultaneously. However, it was found that there were limitations from the point of view of the maximum sensitivities reached and the variety of parameters possible to measure. Since, in a FBG, the light remains trapped in the core, thus it is not sensitive to RI or other parameters, besides temperature or strain, which are intrinsic to any FBG structure [47–49]. This is the reason why different gratings are still explored.

Another type of grating is long-period grating (LPG), which typically have sub-millimeter periods, and the higher spacing between the microstructures allows the coupling of the forward-going propagating core mode into forward-going cladding modes. The high attenuation of the cladding modes gives rise to several attenuation bands in the transmission spectrum, each with a discrete wavelength corresponding to the coupling of a cladding mode, accordingly to the following equation (8) [48,50,51], as seen in Figure 2.4:

$$\lambda_{LPG}^{m} = (n_{eff}^{core} - n_{eff}^{clad(m)})(\varepsilon, T, n_{ext})\Lambda(\varepsilon, T, n_{ext}) \tag{8}$$

In contrast to a traditional FBG, a LPG is not only sensitive to the usual gratings' parameters, temperature and strain, but also to the RI.

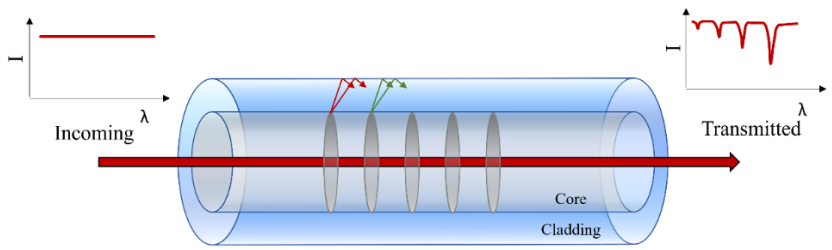

Figure 2.4 – Schematic of the light coupling occurring in a LPG and its respective spectra.

Lastly, for a tilted fiber Bragg grating (TFBG), the period of the grating resembles that of a FBG, however, in this case, the gratings are uniformly tilted by an angle, usually between 4º and 30º, between the grating plane and the transverse section of the fiber. Consequently, alongside the fundamental core mode, light is redirected to the cladding, which allows core and cladding mode coupling to occur, forming in the transmission spectra a comb of discrete resonance peaks, each at a specific wavelength, as seen in Figure 2.5, with the phase matching condition as represented in equation (9) [48,49,51–53]:

$$\lambda_{TFBG}^{m} = (n_{eff}^{core} + n_{eff}^{clad(m)})(\varepsilon, T, n_{ext})\Lambda(\varepsilon, T, n_{ext}) \tag{9}$$

It is important to note that despite the functioning mechanism between the LPGs and TFBGs both relying on the coupling of the cladding modes, the phase matching conditions represented in equations (7) and (9) are the key to the different results produced between them. Since in the LPG the phase matching condition depends on the difference between the core and cladding modes, because of the relative dispersion of the two modes, when applying LPGs as sensors, they can achieve high sensitivities. However, this can come as a disadvantage due to cross-sensitivities between the desired parameter and other effects, such as temperature and axial strain. Although TFBGs may not be as sensitive, the resonance peaks can be used as the sensing mechanism for the intended measurement, namely RI, and alongside it by monitoring the fundamental core mode that appears in the TFBG, since it follows the principles of a classic FBG only being sensitive to temperature and strain, cross-sensitivity is eliminated regarding those two parameters [52].

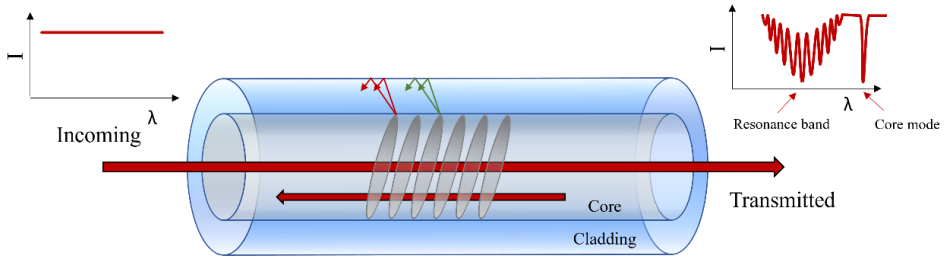

Figure 2.5 – Schematic of the light coupling occurring in a TFBG and its respective spectra.

An alternative to grating sensors is geometrically modified optical fibers sensors, in which the geometry of the fiber is changed to produce evanescent wave-based sensors. As the light travels throughout the core, a small part of the light penetrates the cladding. This light represents the evanescent wave (EW), and inside the cladding this evanescent field has a decay factor of 1/e. Due to the dimensions of the cladding in the non-tapered region, there is no evanescent wave that escapes to the surrounding medium. However, if the cladding were to either be removed, thinned, or reduced, the light propagating in the air-cladding interface would start to leak to the surrounding medium as an EW. The distance that the EW travels inside the cladding can be called penetration depth and can be determined by the following equation (10) [54–57]:

$$d_p = \frac{\lambda}{2\pi\sqrt{n_{core}^2 \sin^2\theta_i - n_{clad}^2}} \tag{10}$$

where λ is the wavelength of the light propagating in the fiber, and θ_i the angle of incidence at the core-cladding interface.

The main types of structured optical fiber sensors are uncladded, D-shaped, U-shaped and tapered, as seen Figure 2.6. The different geometries between them influences the way the EW leaks to the surrounding medium [48,49,58,59].

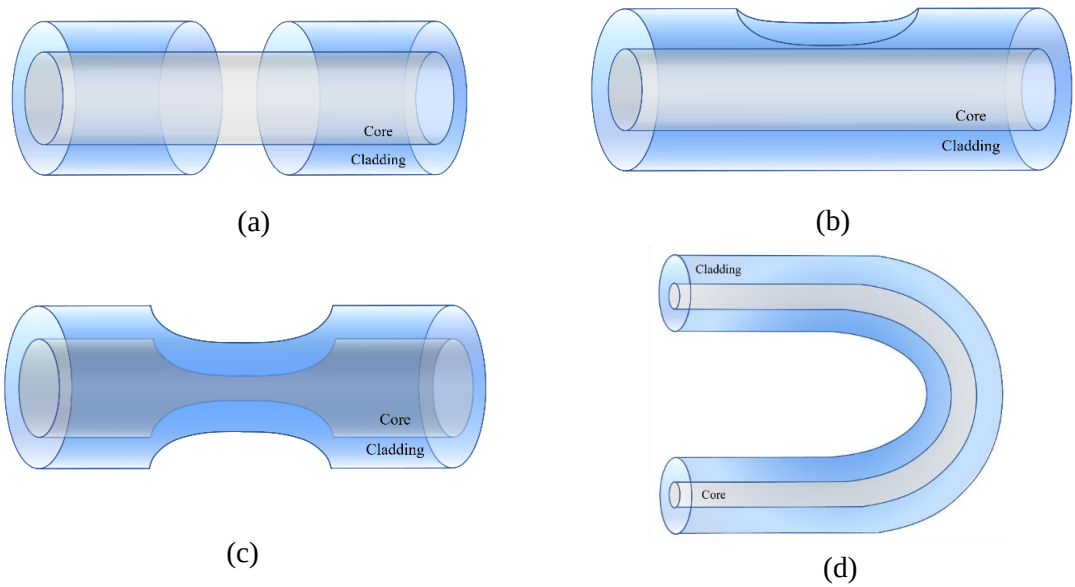

Figure 2.6 – Schematic of geometry-modified fibers: a) unclad; b) D-shape; c) Taper; d) U-shape.

The most straightforward geometry modified fiber sensor is the unclad configuration, in which a great part of the cladding, or the entirety of it, is removed, leaving the core naked and it is at this region that there is an EW output [60,61]. By leaving only the core completely exposed, the uncladded fiber becomes a more fragile and weaker mechanically structure, so an alternative to this is leaving the core exposed only in one side of the fiber, in what is called a D-shape. Therefore, by removing the cladding on just one side of the fiber, its structure is mechanically slightly stronger and more robust when comparing to the uncladded fibers, without compromising the sensitivity of the device, and thus, in literature, there are more examples reporting D-shaped than uncladded fibers [62,63]. Both structures can be employed on both SMF and POF, with the cladding removing mechanism varying depending on the fiber type. The POF methods are easier to manufacture since the fiber is not as fragile as a SMF. The cladding can be mechanically removed by a blade, although this is only viable in POF, as for the SMF either lasers or chemical etching can be used. Additionally, since for a D-shape only the side of the cladding in a fiber needs to be removed, the most common method for D-shaped fibers is through polishing techniques [64,65].

Another technique consists of bending the fiber to obtain an U-shape, and due to the bend, there is more light leaking in this sensing region, leading to an enhanced EW, and thus higher sensitivities are achieved [58,66,67]. It is reported that there is an optimum value for this bending radius, by passing it, more losses are induced in the fiber and sensitivity decreases [68]. This configuration is usually found frequently on SMF, and since bare bending will cause much stress on the fiber, a heat source is used to ease the bending process of the fiber. Although there is the potential to achieve high sensitivities using this structure, it is one of the most fragile.

Lastly, there are tapered fibers, in which the core and the cladding are reduced proportionally, leading to a structure that has a conical transition region connecting the rest of the main fiber to a uniform waist with reduced diameter. The reduction of the core and the cladding results in a decrease of the effective RI of the core mode, n_{eff}, and starts approaching the RI of the cladding. Consequently, when light enters the transition region, the incident angle gradually decreases and reaches the critical angle of total reflection, thus more light leaks into the cladding and core mode coupling to higher modes is supported, eventually leading to a higher EW output at the waist region [13,57,69]. To enhance the intensity and the penetration depth of the evanescent wave, it is reported that tapered fibers with smaller waist result in sensors with higher

sensitivities because, as the diameter of the core decreases, the fundamental mode becomes less confined in the core and couples with the higher order cladding modes. This reason makes tapered fibers the geometry-modified sensors where higher sensitivities can be obtained, when compared to other evanescent wave-based sensors where the core dimensions remain unchanged, such as thinned cladding fibers or any method that removes the cladding to expose the core to the surrounding medium [26,69,70]. However, the smaller the diameter of the waist, the frailer the structure becomes, thus there needs to be a compromise between the intended waist and robustness of the sensor.

2.3.2. State of the art

The coupling to the cladding modes or EW observed in grating based and geometry modified sensors, or even the combination of both, for example an unclad FBG [71], only allow by themselves the measurement of the refraction index. So, in order to apply these structures for the measurement of diverse parameters, such as pH, a functional material needs to be deposited on the surface of the fiber.

In 2021, Wen *et al.* [72] developed an etched LPG coated with a multilayer of Clitorea Ternatea and gold NPs as a pH sensor. The authors observed that the LPGs only with Clitorea Ternatea functional layer and no gold NPs, had a transmission loss sensitivity of 0.0635 dB/pH and a minimal wavelength sensitivity. By adding the gold NPs, the sensitivity was enhanced (0.173 nm/pH) due to the generation of localized surface plasmon resonance, which translates to an enhancement by a factor of 37.

In 2018, Cheng *et al* [62] produced a pH sensor using a FBG inscribed in a POF coated with a pH-sensitive hydrogel, poly(ethylene glycol) diacrylate (PEGDA), which when immersed in aqueous solutions of different pH values, produces different degrees of swelling and induces lateral stress in the fiber. This leads to a wavelength shift, with an associated sensitivity of −0.34 nm/pH, in the pH range from 2 to 6.5 with a response time of around 30 s [62].

In 2018, Aldaba *et al* [73] used a TFBG coated with polyaniline (PANI) through *in situ* chemical oxidative polymerization to develop a pH sensor. The authors determined the sensitivity by monitoring the wavelength shift of the resonant cladding modes in response to the pH changes. This demonstrates a compromise between the sensitivity and hysteresis related to the thickness of the polymer, showing a maximum sensitivity of 82 pm/pH with higher hysteresis, and a minimum of 30 pm/pH with lower hysteresis [73].

Another sensor that uses polyaniline as pH sensitive layer, was developed in 2021, by Antohe *et al.* [74]. An unclad core of an optical fiber was successively coated with platinum and polyaniline, resulting in a surface plasmon resonance pH sensor with a sensitivity of 2.77 nm/pH from 1 to 7 and 3.18 nm/pH from 7 to 14.

Lastly, in 2019, Khanikar *et al* [75] developed a multimode fiber sensor, in which the cladding is replaced with a polyaniline-polyvinyl alcohol (PANI-PVA) composite layer coating, with the PANI synthesized as stable aqueous dispersion in the presence of PVA. The detection mechanism depends on the light absorption capability and RI of the PANI-PVA layer changes, leading to a sensitivity of −2.79 μW/pH in the pH range from 2 to 9 with fast response time in the pH extreme regions and no cross sensitivity towards temperature and ionic strength [75].

3. Manufacture and the functioning of pH sensors

In this chapter, a description of the methodology used to produce the pH sensors is presented as well as the equipment used, manufacturing process and reagents. Two types of geometry-modified sensors were explored: i) a tapered SMF with a FBG, and ii) a D-shaped POF. Regarding the latter, two different methods are used, one using a home-made polishing machine, and the other one reusing a former cortisol D-shaped POF sensor. To develop optical fibers sensitive to pH, a layer of polyaniline was produced on the fibers surface resorting to synthetic oxidative polymerization. A study was carried out for the polymeric coating regarding synthesis parameters, the properties, oxidation states and base forms of the polymer.

3.1. Fiber Bragg Grating inscribed in a taper

3.1.1. Taper

Tapering means applying a reduction in width or thickness in any object elongated towards both ends. This concept can be applied to optical fibers intended to be used as sensors, since changing the waist diameter, waist length, and overall shape, changes the way light propagates inside the fiber [26,56]. The most common way to obtain these tapered structures is to heat a short section of the optical fiber [76], while its ends are simultaneously pulled in opposite directions using a constant tension, ensuring that the fiber is fully stretched [46]. Nevertheless, other methods can also be applied, such as high-power laser radiation [77] and arc discharges [78]. A tapered optical fiber consists of three sections: the waist, the reduced section of the fiber that was reduced with an uniform diameter; the transition section, which by conical sections connects the tapered region to the last section; the fiber without changes in its geometry and properties [26,56,69,79,80].

In general, the slope and sharpness of the taper angle at the transition region determines its features and which taper it is [81]. If the taper angle is small and has very small local changes in the transition region, it has a more gradual geometry, and it is classified as adiabatic. In this case, most of the light remains in the fundamental mode and does not couple to higher modes. Alternatively, if the taper has more of an abrupt geometry, its transition region has a steep slope, and the taper angle is sharp and large enough so that the local taper length-scale is much smaller than the coupling length. This leads to the coupling of the fundamental core mode in the non-tapered fiber and the higher modes in the tapered region, HE_{11} and HE_{12} [70,80,82].

In order to enhance the intensity and the penetration depth of the EW, it is reported that tapers with smaller waist result in sensors with higher EW and, consequently, higher sensitivity because, as the diameter of the core decreases, the fundamental mode becomes less confined in the core and couples with the higher order cladding modes. This makes tapers more sensitive than other evanescent wave-based sensors where the core dimensions remain unchanged, such as thinned cladding fibers or other sensors with the cladding removed by any method, if the core is exposed to the surrounding medium [26,69,70].

The properties mentioned above make tapered optical fibers flexible sensors, since with appropriate coatings and/or functionalization it is possible to sense all kinds of analytes, such as ammonia, acetone, uric acid, creatinine, alanine, *p*-Cresol and many more [26,56,83,84].

As mentioned above, the most common method to produce tapered optical fibers is to heat a short section of the optical fiber while its ends are simultaneously pulled in opposite

directions, using constant tension, to ensure that the fiber is fully stretched [76]. The technique applied to produce tapered optical fibers in this study is similar, but instead of using, for example, an oxygen flame, it uses a plasma technique employed in a combiner manufacturing system (CMS, model 3SAE Technologies Inc., Japan) [54,56,82,85,86]. CMS is a semi-automated fiber processing station, which can operate in both two and three-electrode mode and provide a far greater degree of positional adjustment than conventional splicers, which are based on a plasma field that surrounds the fiber for even heat distribution during the tapering process. So, in order to produce the tapered optical fiber, a pre-treatment of the fiber is necessary, alongside the preparation of the CMS machine and the setting of the duration of the tapering process [54].

For the treatment of the optical fiber, around 3 cm of the plastic coating surrounding the middle of the fiber were removed, ensuring that there was enough length for the tapering process, and, with the cladding exposed, the fiber is lightly cleaned with ethanol and placed on two fiber clamps on the CMS platform, as schematized in Figure 3.1. As for the CMS, it is operated in the three-electrode mode, since it offers a more evenly heated environment for the fiber during the discharge, and it is more efficient than the two-electrode mode. Furthermore, there are needed accurate adjustments of the stretching platform, setting the appropriate parameters for the tapered optical fiber in the computer program (transition region and waist profile, tensioning, start speed and arc balance of the electrodes) and a vacuum level of 2.5 *psia*. In theory, the lower the vacuum, the lower the necessary temperature to heat the fiber, which provides better taper shapes, however, it is more important to maintain a stable vacuum during the entire tapering process. As for the parameters set by the program, it is important to note that there needs to be a balance between the tension and speed imposed, so that the heating produces uniform diameter variations of the fiber during the heating process [54]. The fiber is affixed to a platform while its ends are stretched, and the glass is heated to the point of reducing its viscosity. Consequently, by relaxing the perpendicular tensions and increasing the tensions in the direction of the fiber axis, the fiber will stretch, increasing its length and decreasing its diameter. This whole process lasts a total of 39 seconds [46,54].

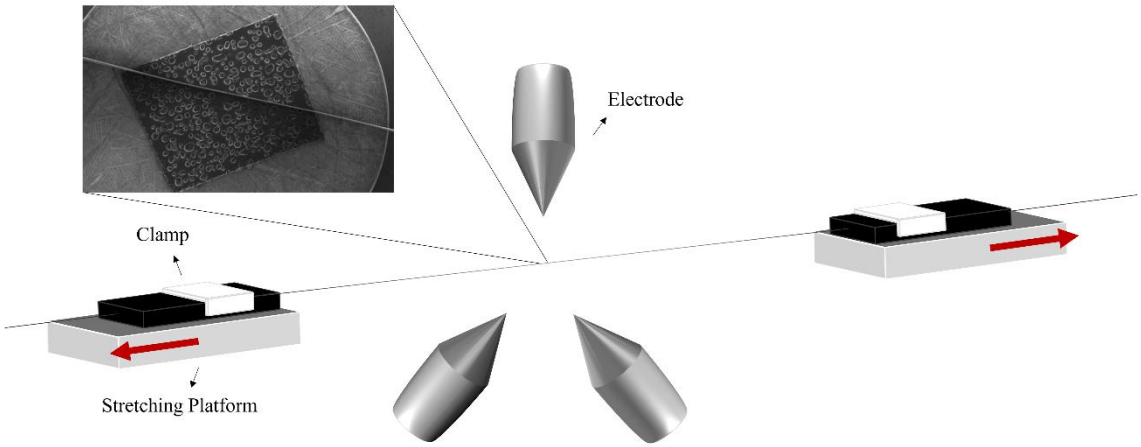

Figure 3.1 – Schematic representation of the CMS equipment during the tapering process of a SMF. Inset: Microscopy photo of a tapered fiber.

The produced tapers have a waist diameter of 40 µm, with its core at 2.624 µm, a waist-length of 4 mm and a transition length of 5 mm. The use of the CMS allows a better control of the taper profile, regarding its dimensions, low surface roughness, quick fabrication, economic viability and better reproducibility than other tapering methods [54,56,82,85–87]. All the tapers used in this work were provided by Liaocheng University, China.

3.1.2. Fiber Bragg Grating

As mentioned in the previous section, a FBG is only inherently sensitive to temperature and strain, thus, to make the FBG sensitive to other parameters of the surrounding medium it is necessary to open access to the evanescent wave, and that can be accomplished by either polishing, etching, or, by the process mentioned in the previous section, tapering [40,46,77,88].

The equation that describes the λ_{Bragg} in a taper is written in the same way when compared to traditional FBGs inscribed in a SMF, depending on the same variables, n_{eff} and Λ. The difference is visualized in the n_{eff} dependence with new variables associated with the taper manufacturing process and the evanescent field created, which makes the FBG inscribed in a taper sensitive to external media, in contrast to traditional FBGs which are only sensitive to strain and temperature, as equation (11) [89]:

$$\lambda_{FBG} = 2n_{eff}(r_{taper}, n_f, n_{ext}, \varepsilon, T)\Lambda(\varepsilon, T) \tag{11}$$

For a FBG inscription, UV laser systems are the most used ones, which follow one of these three methods: phase mask, interferometry or point-to-point [90]. Out of these three methods, the most common one, which was utilized in this work, since it is the easiest, simplest, and most practical method, is the phase mask method. A phase mask consists of a diffraction grating with small periodic grooves produced on the face of a silica plate, with a high degree of purity and transparent to UV radiation. The principle of operation is based on a diffraction grating. After the incidence of a monochromatic UV laser beam on the phase mask, there is the transmission of several beams of different diffraction orders and the multiple interferences between two of these orders form a periodic modulation of UV radiation. This way, it will change the RI of the fiber periodically and the grating is inscribed in the optical fiber core. When the incidence is normal, the efficiency for the orders m = + 1 and m = −1 are maximized and the FBG is inscribed, as schematized in Figure 3.2 [42].

As the FBGs were inscribed in the tapered region, this required additional care. The most traditional way of inscribing FBGs is to dope an SMF with boron or germanium, making them more photosensitive. Thus, its exposure to UV radiation will produce an FBG with high reflectivity [91]. Although the supplied tapers do not have such doping, many of the commercial fibers available usually have a high germanium doping that guarantees some photosensitivity in their cross section [70,92]. However, when trying to inscribe an FBG in one of the tapers, the peak of the FBG produced did not have a satisfactory reflectivity. Thus, to increase their photosensitivity and produce FBGs with greater reflectivity, the tapers were hydrogenated at room temperature, at a pressure of 120 bar, for approximately 7 days [93]. Additionally, since it is intended that the grating is centered as much as possible in the waist region, and due to the fragility of the taper, associated with its reduced diameter, the SMF needs to be placed in the inscription platform very carefully. Furthermore, the pump energy and the time of exposure to the laser cannot be too high, because, otherwise, there is a risk that the laser pierces through the taper.

The laser used to manufacture the FBGs is a Q-switched Nd:YAG pulsed UV laser (model LS-21137U, from LOTIS TII) that emits at a wavelength of 266 nm, using a pumping energy of 25.4 J. The time of exposure of the fiber to the laser was approximately 2 minutes. The phase masks used (from IBSEN) are specific for UV radiation at 266 nm and have typical pitches around 1064±14 nm, producing FBGs with a Bragg wavelength centered at approximately 1520-1560 nm. To monitor the produced FBGs, the fiber was connected to an optical interrogator (Micron Optics, model SM125-500, with a resolution of 1 pm, acquisition frequency of 1 Hz and spectral range of 1520-1570 nm).

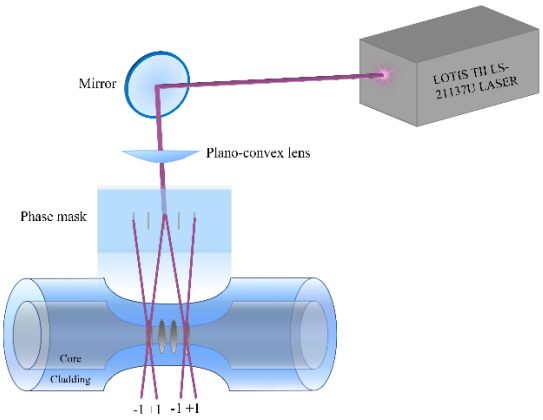

Figure 3.2 – Schematic representation of the platform used to inscribe FBGs.

The setup where the pH characterization takes place uses the same interrogator as mentioned above, and the tapered FBG was carefully handled and set in an oval container using cellophane tape, as shown in Figure 3.3. Since the FBG produced has low reflectivity, its visibility in the interrogator can be highly influenced by back-reflections if the end of the fiber is not perpendicularly cut. Thus, to mitigate this problem, an index-matching gel was used at the end of the fiber.

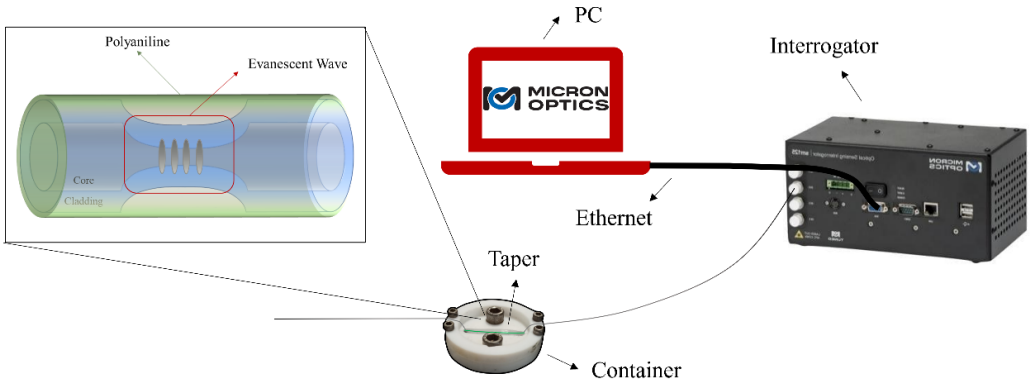

Figure 3.3 – Schematic of the experimental setup used for pH characterization of the tapered optical fibers with a FBG inscribed coated with polyaniline. Inset: Schematic of the sensor's full structure.

3.2. D-shape in POF

As mentioned above, changes in the fiber's geometry can lead to light leaking into the surrounding medium as an evanescent wave, which is useful for sensors, just as seen in tapered optical fibers. The next proposed solution for sensors consists in utilizing fibers with other geometry changes, D-shapes. These structures are achieved by removing part of the cladding in one side of the fiber, therefore exposing the core [63,65,94,95]. One benefit of implementing the D-shape geometry is its versatility, since depending on the parameter of interest, the sensing material can be easily applied on the region that the cladding was removed [65,96].

The most conventional method to produce D-shape fibers is through polishing techniques, usually by setting the fiber in a V-groove while its cladding is polished away by interacting with a rolling disk covered with an abrasive sheet [63,65,94,95,97,98]. Alternatively, methods using lasers are also employed, namely CO_2 and femtosecond lasers [99]. Lastly, there are also chemical etching processes [100]. Each one of these methods has their limitations depending on: a) the chosen fiber, either SMF or POF, and b) the reproducibility obtained. The laser methods are characterized by their higher precision, with CO_2 being useful to remove the plastic cladding,

whereas for silica fiber a femtosecond laser is usually used. However, the issue with these lasers is the machining complexity and costs associated with it [99,101,102]. As for chemical etching, these methods make use of strong acids, and a rigorous and very precise control of the area exposed to the acid medium and the exposure time is necessary to produce multiple sensors with the same properties [100]. Therefore, the most popular way to produce D-shapes is through polishing techniques. Reports show that to ease the polishing process, fibers are permanently glued in a cut-carved V-groove block, which can be either quartz, fused silica or resin. This procedure can limit the advantages of optical fibers, such as low size, portability and difficulty to access the sensitive area [94,95,98]. Additionally, there are a lot of precautions and measures to take if the fibers intended to be polished are made of silica, in order to assure that they neither break nor crack, which makes it hard to produce [95].

For these reasons, and since the proposed taper solution will be made in a silica SMF in the C-band (1550 nm), to offer a different alternative, the D-shapes will be made in MMF POF using the visible and near-infrared band (400-900 nm).

To produce the POF D-shapes, two different methods were employed. The first one consists of a low-cost and home-made method using a polishing machine, and the other one involved reutilizing a POF D-shape which previously functioned as a cortisol sensor.

3.2.1. Home-made

Starting with the home-made method, a segment of a POF was cut with a length of approximately 30 cm and was fixed on two clamps, each one on opposite sides of the fiber, so it stayed stretched and steady throughout the whole polishing process. Part of the black plastic jacket that covers the PMMA was removed near the center of the fiber with the assistance of a plier and a blade, and this section was placed on the V-Groove where the polishing will take place. It is important to note that this removed section of plastic needs to have a length higher than the polishing blade, which has a length of 1 cm, so usually 5 cm of plastic are taken off. The last step before starting the polishing was to connect the POF to a light source in one of the ends, and a powermeter in the other end, to monitor the power loss throughout the whole polishing process. The V-Groove in which the POF was placed is a custom one, which has a depth of approximately 700 µm, leaving approximately 300 µm of the PMMA uncovered, which was removed by the polishing machine.

The polishing machine is held by a claw, which is attached to a 3D platform, the V-Groove, where the POF is placed and attached to a 3D platform, as Figure 3.4 shows. The 3D movement for both the claw and the V-Groove is important to ensure that the polishing machine is as parallel as possible to the fiber, to guarantee that the D-shape is as centered as it can be, and the sides of the fiber are not polished. Once it is parallel, only the bolts related to the z-axis movement are needed.

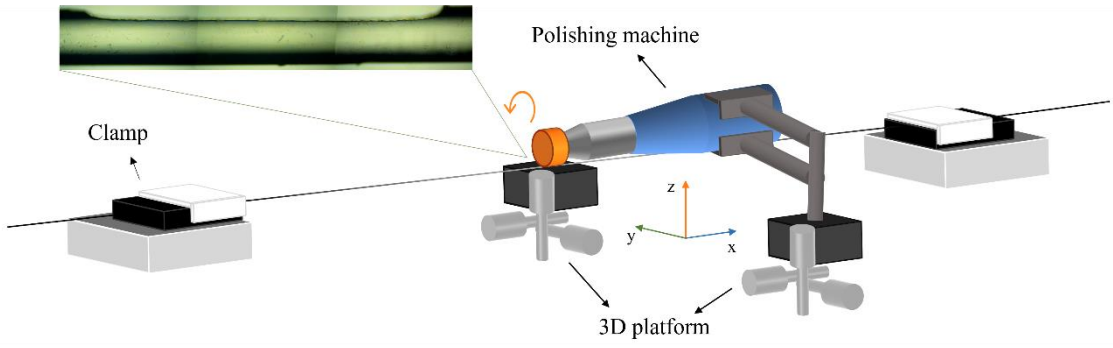

Figure 3.4 – Schematic of the custom setup used to manufacture POF D-shape using a polishing machine. Inset: Microscope photo of a manufactured POF D-shape home-made.

After the polishing starts, the time it takes can vary due to the speed of the polishing machine and the degree of movement done on the z-axis bolts. Thus, to ensure reproducibility between the D-shapes, the power loss during the process is measured, and as soon as a 3 dB loss was registered, the polishing stops [94]. Lastly, sandpaper was used to correct a few irregularities and scratches that happened during the polishing, guaranteeing a smooth and homogeneous D-shape surface, since there is excessive loss in the scratches, due to light scattering [98].

3.2.2. Reused

The other option involves the regeneration of a D-shaped POF that through surface plasmon resonance phenomena were used as immunosensors for cortisol detection by other laboratory colleagues [103]. These D-shapes consist of a POF completely stripped of the black plastic jacket glued and set on a resin block, which was done aiming to ease the polishing process. This procedure was done by using polishing papers until the cladding and half of the core was removed. After that, through spin coating, a photoresist buffer was deposited on the surface with a thickness of about 1.5 µm and on top of that, through sputtering, the fiber was coated with a gold film with a thickness of 60 nm [96,104–106]. This Au coated D-shaped POF was functionalized and exploited as cortisol sensor. Therefore, to be used in this work, the bioorganic layer as well as the gold coating was chemically removed, yielding a reused bare D-shaped POF. For that, it was used aqua regia, a strong acid that consists in a mixture of hydrochloric acid and nitric acid (3 HCl: 1 HNO_3 v/v). The most common use of this acid is to remove noble metals, such as gold, platinum, and palladium, from substrates. Due to its highly corrosive and highly oxidizing nature, it needs to be handled with extreme caution, therefore the need of using gloves during the whole process and the process was done inside a fume hood since, by corroding metals, brown fumes of NO_2 are released, which are toxic [107,108]. The POF is set in a watch glass and a few drops of aqua regia are released on the Au-coated D-shape section, as depicted in Figure 3.5 [107,108]. After 1 or 2 minutes of exposure, most of the gold contained on the resin block, and therefore on the D-shape section, was removed, and then the fiber was exhaustively rinsed with water before it was placed on the customized container, on which the polyaniline reaction will take place.

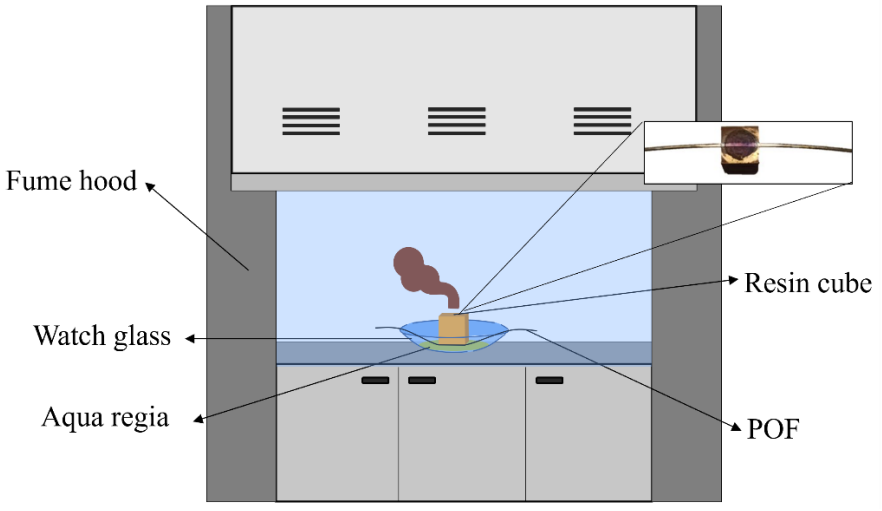

Figure 3.5 – Schematic of the reaction occurring inside the fume hood when the resin cube containing the POF D-shape is exposed to aqua regia. Inset: Photo of the POF D-shape attached to the resin cube.

For all the tests using POFs, the light source used was a 7 W tungsten lamp (model LS-W7, brand Sarspec) with an emission range between 380 nm to 2500 nm, and a spectrometer (model FLAME-T-UV-vis manufactured by Ocean Optics, USA), with a detection range of 180 nm to 890 nm, and the transmission spectra were acquired using the Ocean View software as shown in Figure 3.6.

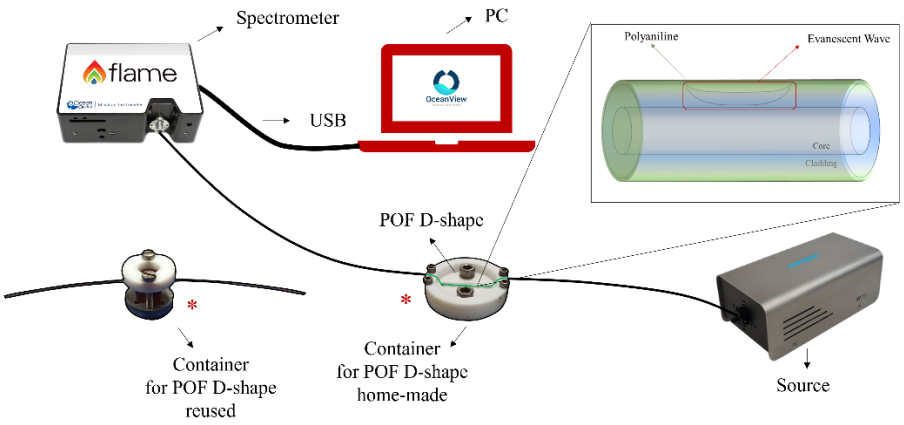

Figure 3.6 – Schematic of the experimental setup used for pH characterization of the home-made POF D-shape coated with polyaniline. Inset: Schematic of the sensor's full structure.

3.3. Synthesis of polyaniline

Up until the latter half of the 20th century, a lot of the organic materials, including polymers, were thought to be insulators. However, reports of low resistance observed in polypyrrole [109], and electrochemical chains that resulted in high conductivities observed in polyaniline [110], culminated in the synthesis of the highly conductive polyacetylene done by Alan J. Heeger, Alan MacDiarmid and Hideki Shirakawa [111,112], which were later awarded, in 2000, with the Nobel Prize in Chemistry for the discovery and development of a new generation of polymers, conducting polymers [111,113]. Since these materials present good electric and optical properties, associated with conductors or semiconductors, and the good mechanical and processing properties, characteristics of polymers, these makes them promising materials to use in a wide variety of technological application.

The research conducted by Alan J. Heeger and his colleagues that lead to the Nobel Prize was done around polyacetylene. However, since it was unstable when exposed to air and difficult to process, this hindered its possibility of being used in applications. Therefore, the conductive polymers that stand out are polyaniline (PANI), polythiophene (PTH) and polypyrrole (PPY). The difference between these three polymers resides in the atoms present in the main chain. Both PPY and PANI contain nitrogen, nevertheless the difference between the two is associated with its presence in the aromatic ring: in PPY it is inside the aromatic ring and in PANI it is on the outside of the aromatic ring. Finally, PTH contains sulfur in the aromatic ring [114].

Of the three conducting polymers mentioned above, the one which will be used in this work is PANI. This polymer possesses easy synthesis, low cost, excellent stability, anticorrosive and biochemical compatibility [73,115,116]. These properties make this material interesting to use in a variety of applications, such as gas detection [117], photovoltaic cells [118], electromagnetic shielding [119] and as modified coatings applied in optical fibers [73,75,120,121], just like how it will be used in this work, for pH sensing. As for its disadvantages, it has low processing capability, lacking flexibility, absence of biodegradability and poor solubility. These disadvantages inhibit the use of PANI in biological applications, which is not the case of this work. However, there are techniques that can overcome these problems by chemically modifying, by doping or by derivatives in the PANI structure [122].

PANI can be observed in three oxidation states and all these structures can exist in the base forms (deprotonated), or in their salt form (protonated), which is achieved by exposing the base form to an acid, as seen in Figure 3.7 [73,116,123].

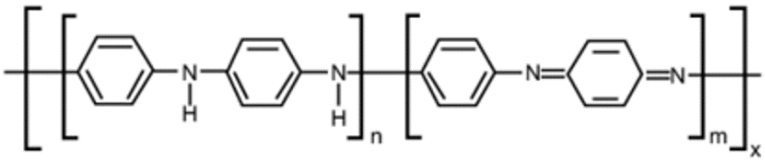

Figure 3.7 – Basic structure of polyaniline, where n + m = 1 and x is the degree of polymerization – number of monomeric units in a polymer (adapted from [124]*).*

As just mentioned, PANI can be easily protonated and deprotonated being a polymer sensitive to pH changes. Furthermore, the different forms of PANI present different colors depending not only on the oxidation state but also on the degree of protonation, as depicted in Figure 3.8. For instance, the completely reduced state, leucoemeraldine (n = 1 and m = 0), contains only benzenoid rings, and has a clear/white color. Emeraldine presents a partially oxidated state, (n = 0.5 and m = 0.5), and finally, the fully oxidated state is pernigraniline (n = 0 and m = 1), that contains benzenoid and quinonoid rings and presents a purple color [116,124,125]. The most stable and common form is the emeraldine base. However, by doping it with acid, emeraldine salt is achieved, which reveals a green color, and has higher conductivity when compared to all other possible configurations [73,126].

In order to synthetize polyaniline, there are a variety of techniques, including chemical, electrochemical and even physical methods. Nevertheless, the most common techniques are the chemical ones, with the one utilized in this work being the synthetic oxidative polymerization of aniline [127].

As soon as the polymerization starts, an initial polymer product is formed, the fully oxidized pernigraniline base, due to the high oxidizing power of ammonium persulfate. When the oxidant is fully consumed, the left-over aniline will reduce the pernigraniline to the emeraldine salt. As mentioned above, the PANI emeraldine structure has poor solubility, which is due to its rigid structure associated with the hydrogen bonds between adjacent chains and the strong π electron structures, precipitating in a dark green powder [116].

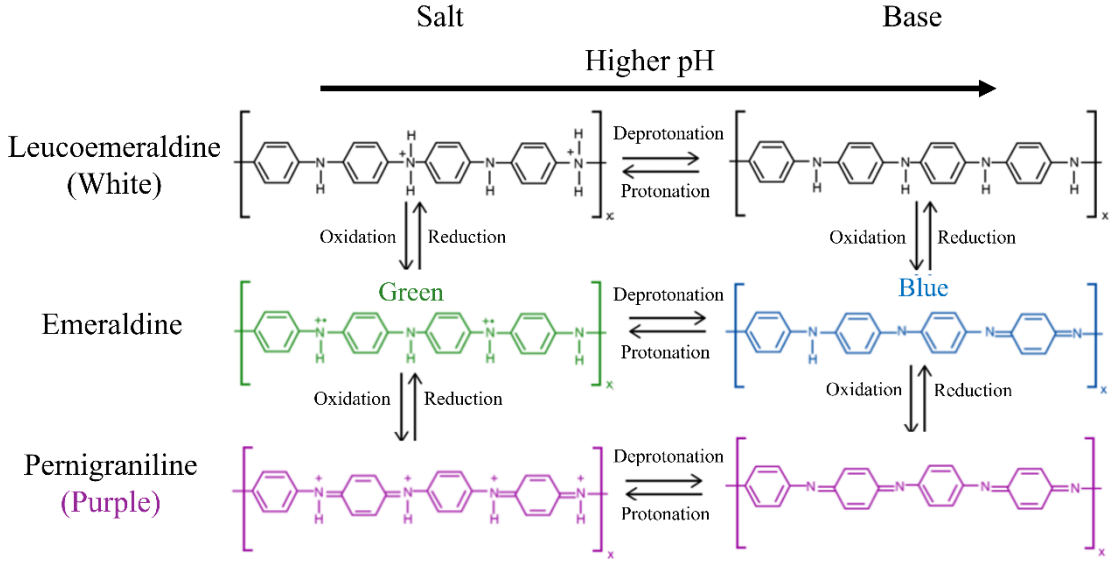

Figure 3.8 – All base and salt forms of polyaniline and its respective protonation/deprotonation and redox reactions (adapted from [125]*).*

As regards the experimental procedure followed in this work to coat the fiber with PANI, the oxidative polymerization of aniline was carried out onto the fiber surface. To do so, the fiber was fixed in a Teflon container and, after cleaning the fiber surface, it was immersed in 300 µL of an

aniline solution (0.133 M) prepared in 1.0 M of HCl and then 100 μL of 0.4 M of ammonium persulfate dissolved in HCl (1.0 M) was added to start the polymerization reaction. After the desired reaction time, the coated fiber was washed abundantly with deionized water to ensure the complete removal of the precursors and detached PANI. During the washing step, as the water has neutral pH, the deprotonation of emeraldine is observed, going from the green color to blue.

Note that, during the inscription of the FBG, it was necessary to apply some minor adjustments to one of the mirrors to align the laser with the core of the taper. Ideally, it is necessary to minimize these adjustments as much as possible, however, since the core of the taper is reduced, this alignment is very sensitive to the slightest movements, which affects the period of the FBG, and consequently the interference fringes. This leads to the interference of higher modes ± 2, instead of only the intended ± 1, which affects the cladding modes, causing the appearance of lateral lobes with low reflectivity in the FBG spectrum, alongside the first order mode of the FBG. As the cladding is so thin, by adding the polyaniline coating, it blocks the propagation of these cladding modes, consequently disappearing from the spectrum, which leaves only the first order Bragg mode, since this is the only one inscribed in the core, and not in the cladding. The first order Bragg mode only suffers a slight decrease in transmission, i.e., its reflectivity. A similar phenomenon also happens during the coating process in the POF D-shape, observing a slight decrease in transmission of the main peak of the spectrum.

3.4. pH measurements

For the characterization of the sensors, eight solutions with different pH were prepared using 0.01 M of the mixture of sodium phosphate dibasic heptahydrate ($Na_2HPO_4 \cdot 7H_2O$, *Sigma-Aldrich*) and sodium phosphate monobasic monohydrate ($NaH_2PO_4 \cdot H_2O$, *Sigma-Aldrich*) dissolved in physiologic solution (0.137 M NaCl and 0.027 M KCl). The ratio between phosphate ions is what determines the pH of the solution, and it works as a buffer in the pH range from 5.8 and 8. Eight different solutions were prepared, with intended pH values approximately of: 2, 4, 5.4, 6.2, 6.6, 7.4, 8 and 10. For the solution at pH of 7.4, commercial tablets purchased from Fisher Bioreagents were used. HCl and NaOH were used to adjust the pH of the solutions when it was necessary. The pH of each solution was confirmed and measured using a pH electrode (*Hannah Instruments*). During this work, there was the need to prepare different sets of these solutions.

The fiber was placed in the teflon container, and, at the beginning of every characterization test, the sensors were immersed in HCl (0.1 M) for at least 10 minutes, which served as the reference value. Then, the HCl was removed and replaced with the solution with a pH of 2 during a few minutes and the spectrum was recorded. Afterwards, it was replaced with the solution with the next pH and the procedure was repeated for all the solutions in an increasing pH order. At the end, the same steps were followed for the solutions in a decreasing order of pH. It is important to note that, since it was unknown how the sensor would react and how long it would take to stabilize, the sensor was initially exposed to the solutions more time than necessary, usually between seven and ten minutes, but since the characterization is done by gradually incrementing the pH step, and then decreasing it, three minutes per step is long enough for the spectrum to stabilize. During the characterization of the sensors, three different batches of tapers were supplied. The first batch was used to determine the synthesis time and, subsequently, the other batches were used mainly for the reproducibility and repeatability tests.

For the ionic strength characterization of the sensors, six solutions were prepared. All the solutions contain 10 mM of phosphate ions, using the same reagents as when the different pH solutions were made to keep the pH at 7.4 (7.5 mM $Na_2HPO_4 \cdot 7H_2O$ and 2.5 mM $NaH_2PO_4 \cdot H_2O$). A stock solution of 50 mL containing a total salt concentration of 0.5 M is

prepared using sodium chloride and potassium chloride (0.42 M NaCl and 0.08 M KCl). With the appropriate mixture between this stock solution and deionized water, six different solutions with the intended ionic strength concentrations were prepared: 0, 0.0001, 0.001, 0.01, 0.1 and 0.5 M.

3.5. Other characterization techniques

To determine additional characteristics of the polyaniline, regarding its molecular structure, as well as its topography and morphology when coated in the fibers, Fourier transform infrared (FTIR) and scanning electron microscopy (SEM) were used, respectively.

FTIR spectroscopy is a vibrational technique that through the interaction of an infrared beam focused on an interferometer and the sample of interest, an IR spectrum of the sample will be retrieved where certain wavelengths will be absorbed depending on the molecular structure and chemical composition of the sample [128].

The equipment used was an ATR-FTIR (Attenuated Total Reflection Fourier Transform Infrared) and at the tip of the equipment there is a crystal, which in this case is diamond, that has a high refractive index and transparent to IR. As light passes through the crystal, there is total internal reflection happening in the interface between the crystal and the sample. Thus, there is EW leaking to the sample which will be absorbed, and the reflected light beams have lower intensity leading to the ATR phenomena [128]. The spectra acquisition was performed in an infrared spectrometer (Bruker Alpha Platinum, Germany) equipped with the ATR crystal with a resolution of 4 cm^{-1} and 32 scans, in the mid-infrared region (4000-500 cm^{-1}). The tests were performed in a room with a controlled temperature of 25 ºC and humidity of 35 %.

SEM is a technique that uses an electron beam to scan the surface of a given sample, and the interaction between these two elements will cause the emission of secondary electrons, which its detection will produce a highly magnified image of the sample [129].

The images were retrieved using the SEM (Vega 3 SBH, TESCAN) at a high voltage of 30 kV with a secondary electron detector. The tapered optical fiber, non-coated and coated with polyaniline, were set on an aluminum sample holder, and were attached using double sided carbon tape. The sample holder is placed in a vacuumed chamber where the images will be taken and the carbon tape is a conductive surface to minimize charge effect build-up in the sample, induced by the electron beam, with this to ensure as much image quality as possible.

4. Results and analysis

In this chapter, an extensive characterization of all the sensors produced will be done, including the optimal synthesis time regarding the polyaniline coating, the sensors' components and the reason the sensors behave the way they do when exposed to pH variations, reproducibility and repeatability tests, the stabilization time, and the effect of different temperature and ionic strength values on the sensors. Moreover, for the POF D-shape sensor, the employment of a cost-effective method making use of a powermeter is proposed. All these tests were performed with the goal to deploy these sensors in aquaculture and subsequently integrate them in the hybrid platform with the electrochemical nitrites' sensor.

4.1. PANI synthesis time

After manufacturing the fibers with the geometry changes mentioned in sections 3.1 and 3.2, in the form of tapered SMF and POF D-shape, respectively, the fibers were coated with polyaniline as the pH sensitive layer. The literature shows that different synthesis times, and consequently PANI thickness, affect the behavior of the sensor regarding different parameters, such as sensitivity and hysteresis [73]. Therefore, three different synthesis times were tested: 10 (Figure 4.1), 20 (Figure 4.2) and 30 minutes (Figure 4.3), with the intent of finding the best experimental conditions to produce the pH sensor. It should be noted that for both the wavelength and power characterization, a reference spectrum, using HCl, was subtracted from the spectra.

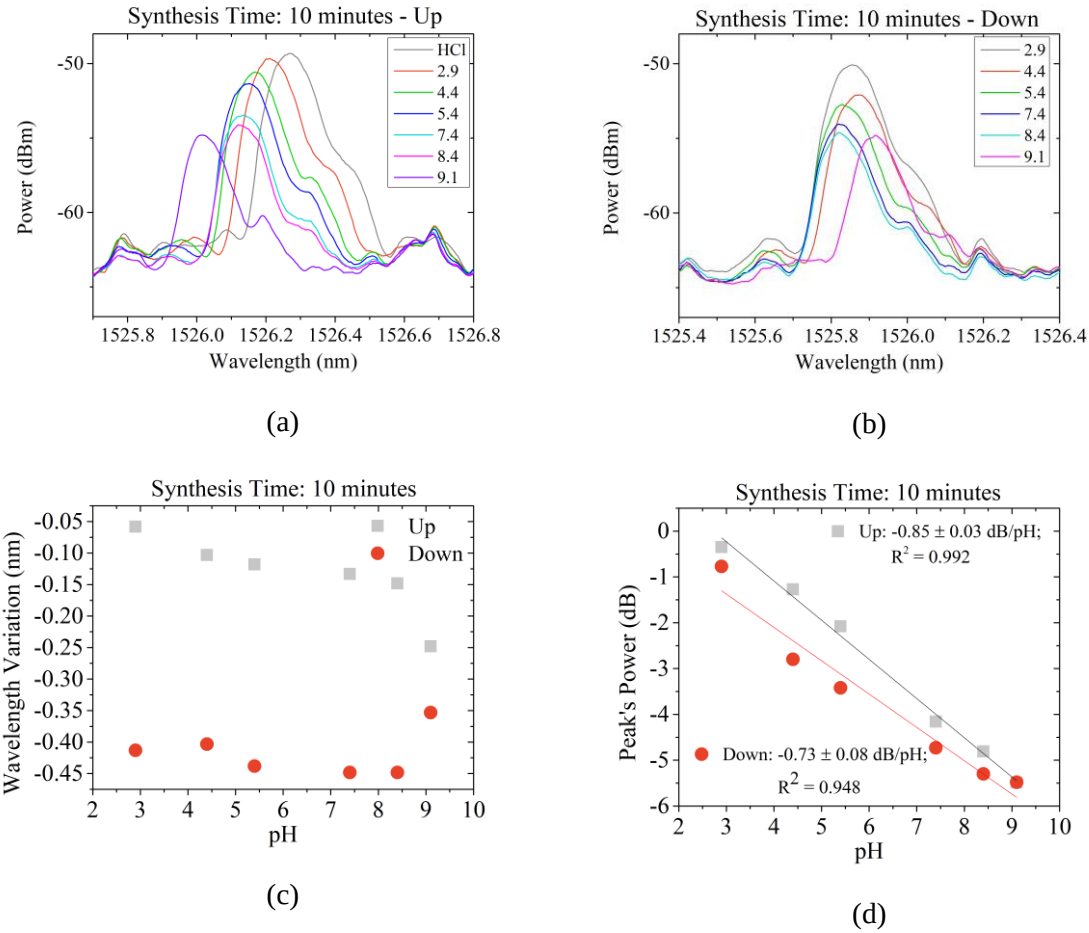

Figure 4.1 – Example of spectral evolution of a tapered fiber coated with PANI synthesized during 10 minutes, for (a) increasing pH order – Up and (b) decreasing pH order – Down; (c) Wavelength and (d) Power variations as a function of pH.

Both wavelength and power variations associated with the Bragg's peak were monitored during this initial phase of the pH characterization tests. In Figure 4.1(c) is observed that while increasing and decreasing the pH, slight decreases in the wavelength variations are observed, but in neither case it is possible to define a tendency. Regarding power variations (Figure 4.1(d)), by increasing the pH a decrease in power is observed, whereas when decreasing the pH an increase in power occurs. In this parameter, a linear tendency can be defined for both increasing and decreasing orders, however a slight hysteresis is noticeable.

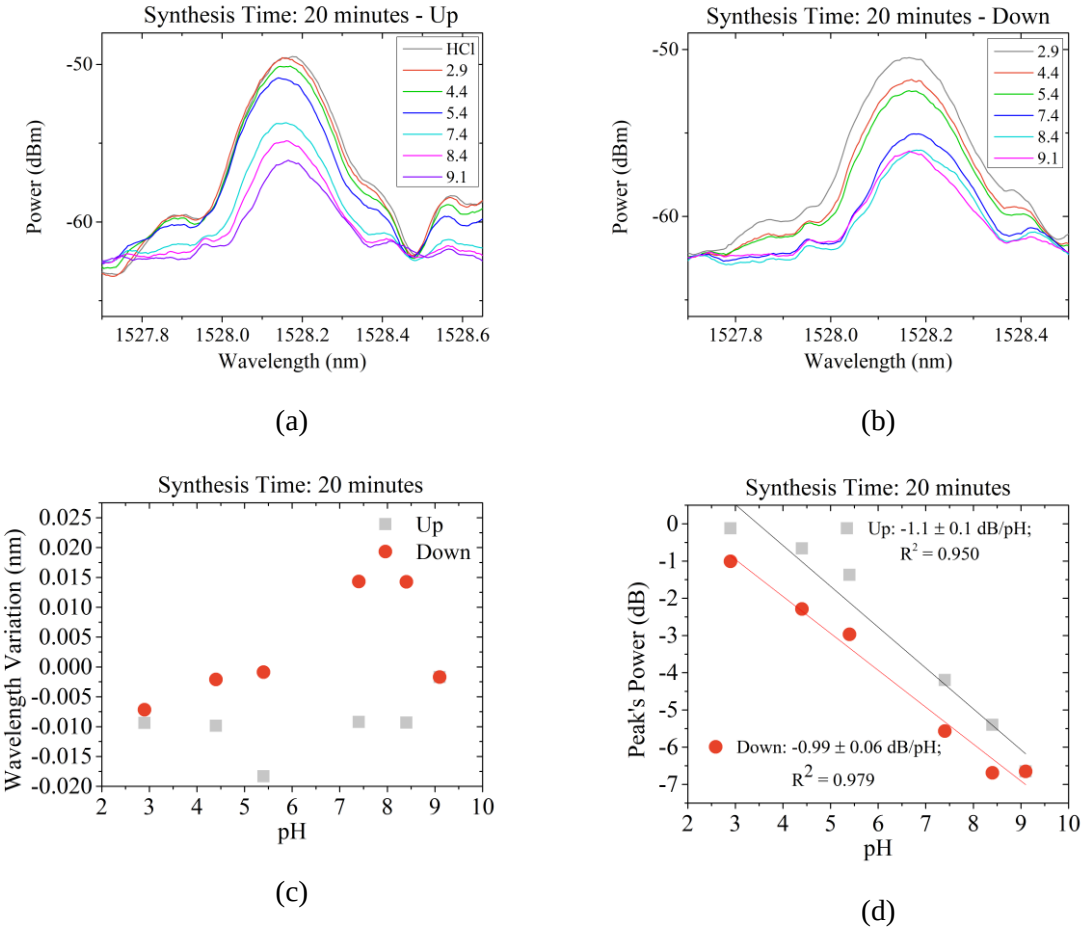

Figure 4.2 – Example of spectral evolution of a tapered fiber coated with PANI synthesized during 20 minutes, for (a) increasing pH order – Up and (b) decreasing pH order – Down; (c) Wavelength and (d) Power variations as a function of pH.

As for the synthesis of 20 and 30 minutes, similar results were achieved, with the wavelength (Figure 4.2(c) and Figure 4.3(c)) showing smaller total variations when compared to a synthesis of 10 minutes, and, once again, an erratic behavior incapable of defining a tendency was observed. As for the power variations, see Figure 4.2(d) and Figure 4.3(d), linear tendencies were once again applied and, in the case of 20 minutes, higher sensitivities were achieved, in contrast to the 10 minutes followed by the 30 minutes. Also, a slight hysteresis with a similar shape was observed for the three different synthesis times of PANI.

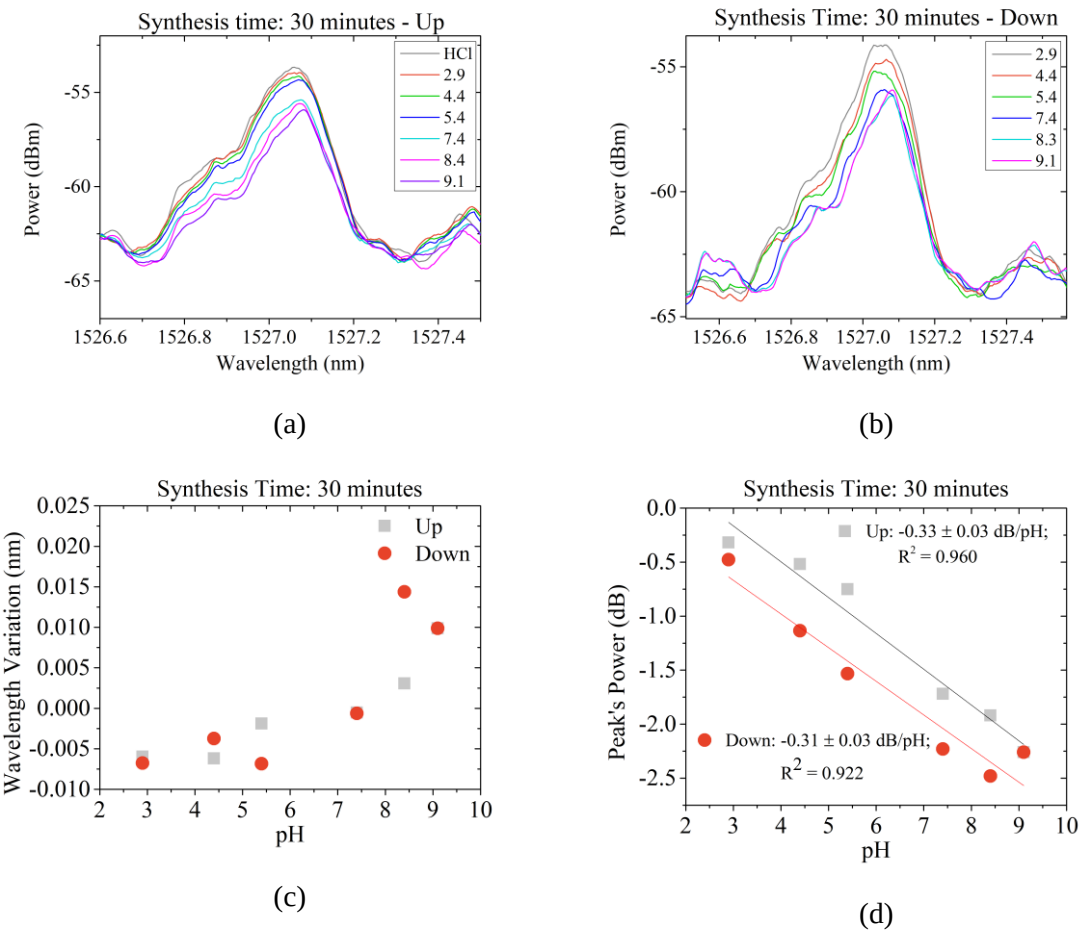

Figure 4.3 – Example of spectral evolution of a tapered fiber coated with PANI synthesized during 30 minutes, for (a) increasing pH order – Up and (b) decreasing pH order – Down; (c) Wavelength and (d) Power variations as a function of pH.

The optical characterization for the three different PANI synthesis times showed that the wavelength variation is either null or extremely inconsistent. On the other hand, the power variation shows some tendency, hence, to simplify the analysis, a linear fit was applied to this parameter for an easier comparison. The power variations are observed based on a relationship between the evanescent wave produced by the tapers and its interactions with the polyaniline coating after exposure to the different pH solutions. As already mentioned, polyaniline is a pH sensitive polymer that is swollen when it is protonated and shrinks gradually when increasing to higher pH. As a result, this leads to an increase of the RI of the layer as the pH increases, thus, the peak power of the FBG decreases, i.e., a decrease in transmission.

The synthesis time of PANI influences the thickness of the polymer and consequently could affect the pH sensitivity. Therefore, all the tapers were characterized by Scanning Electron Microscopy (SEM), as seen in Figure 4.4, determining the thicknesses of the polyaniline for the different synthesis times, 10, 20 and 30 minutes.

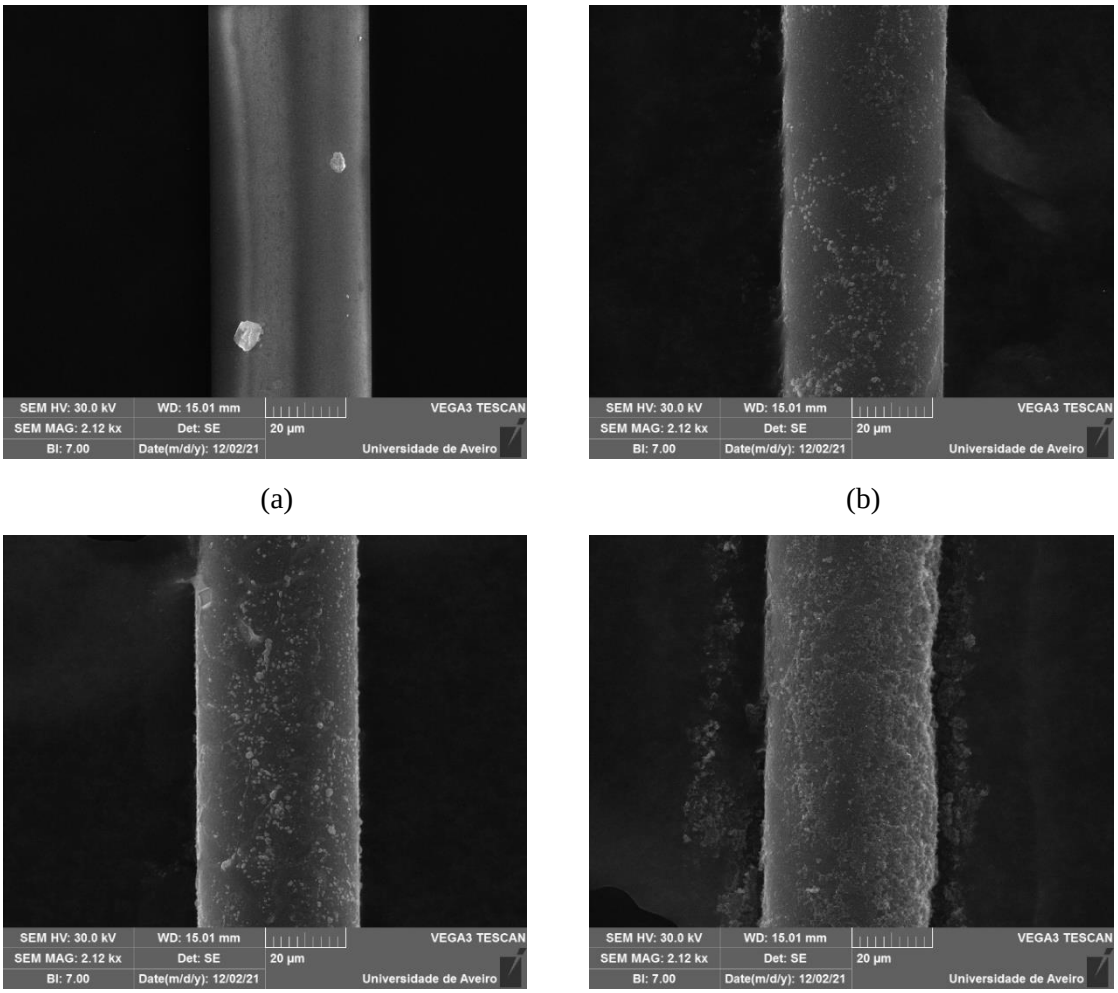

Figure 4.4 – SEM images of the (a) bare tapered fiber, and the fiber with PANI synthesized during (b) 10, (c) 20 and (d) 30 minutes.

The bare tapered fiber, which has a diameter of 40 µm and a smooth surface, as observed in Figure 4.4(a), was used as a reference to determine the thickness of the polyaniline for the three different synthesis times. In Figure 4.4(b), for a synthesis time of 10 minutes, the coating has a thickness of 0.4 ± 0.1 µm and it has a few indentations, which makes it not completely uniform. Whereas in Figure 4.4(d), 30 minutes, the coating has a few clusters of polyaniline on the right side, making it the least uniform amongst the three synthesis times tested, with a coating of 3.2 ± 0.2 µm. For the 20 minutes of synthesis, Figure 4.4(c), is the most uniform of the three and has a thickness of 0.7 ± 0.1 µm.

Table 1 summarizes the pH sensitivity (S_{pH}) determined by the optical characterization, as well as the thickness of the PANI layer, followed by a discussion of these results.

Table 1 – pH sensitivity of the three sensors for three different synthesis times and the respective polyaniline thickness.

Synthesis Time		Sensitivity (dB/pH)	R^2	Thickness (μm)
10 min.	Up	-0.85 ± 0.03	0.992	0.4 ± 0.1
	Down	-0.73 ± 0.08	0.948	
20 min.	Up	-1.1 ± 0.1	0.950	0.7 ± 0.1
	Down	-0.99 ± 0.06	0.979	
30 min.	Up	-0.33 ± 0.03	0.960	3.2 ± 0.2
	Down	-0.31 ± 0.03	0.922	

The power variations, as already mentioned, are due to the relationship between the evanescent wave produced by the tapers and its interactions with the polyaniline coating. The sensitivity results, summarized in Table 1, allow to observe that $S_{pH,\ 30min} < S_{pH,\ 10min} < S_{pH,\ 20min}$. These results, given the determined thicknesses, allow to infer that for 10 minutes (0.4 μm), the layer of polyaniline is sufficient to observe a decrease in power, but by increasing the deposition time to 20 minutes and, consequently, the thickness (0.7 μm), greater sensitivities can be achieved. However, for a time of 30 minutes, the value of sensitivity reached is much lower compared to 10 and 20 minutes, accompanied by a considerable increase in thickness (3.2 μm) and a less uniform coating. It is possible to consider that there is a correlation between this increase of thickness and the decrease in sensitivity, since having a much thicker layer makes it difficult for the evanescent field to interact with the exterior, thus resulting in a decrease in the value of sensitivity.

It is important to have in mind that any type of changes in the waist diameter of a taper and the coating's surrounding layers can have a major impact on the sensitivity of the sensor. For example, before pH tests, the non-coated FBG tapers, with a diameter of 40 μm, were submitted to RI tests using glucose solutions with well-known RI, where a sensitivity value of 0.617 nm/RI was achieved. However, in the literature, it is possible to find tapers with a waist diameter of 10 μm, which can reach sensitivities of 100 nm/RI or even more [26,79], but also, tapers with such small waists can be extremely problematic to handle. That is, decreasing the taper diameter 4 times can translate into an increase in sensitivity by more than 100 times at the RI level. This is because the lower the diameter of the taper, the greater the evanescent field, which increases sensitivity. Also, between 10, 20 and 30 minutes, there is an increase followed by a decrease in sensitivity. Due to this, there is an ideal time of synthesis, and consequently, an optimal thickness for this pH sensor, and this value might be near 20 minutes, with a thickness of around 0.7 μm. Therefore, for further testing, for both the POF D-shapes and the tapers, the synthesis time was 20 minutes.

Additionally, FTIR spectroscopy was performed on a fiber after the synthesis of polyaniline was completed to confirm the chemical nature of the coating produced, as well as for a bare silica fiber for comparison and better identification of the vibrational modes, as Figure 4.5 presents.

The silica spectrum has two characteristic peaks at 800 cm^{-1} and 1097 cm^{-1}, which are associated with the Si−O stretching and Si−O−Si asymmetric stretching vibrations, respectively [130]. As for the PANI coated fiber, the FTIR spectrum presents the characteristic vibrational modes of PANI. The peaks observed at 569, 610 and 648 cm^{-1} are associated with the aliphatic C−H stretching and aromatics C−Cl out of plane bend modes. The large band peak between 900 and 1250 cm^{-1} is assigned to the vibrations of the $-NH^{+}=$ structure and the plane bending of C−H

quinoid and benzenoid rings, which overlap with the vibrational mode from the silica fiber. Lastly, the three peaks situated at 1298, 1484 and 1572 cm^{-1} are stretching modes, related to the C−N benzenoid ring, C=C benzenoid ring and C=N quinoid ring [131,132]. Therefore, FTIR spectroscopy corroborates that the oxidative polymerization of aniline occurred and PANI is coating the optical fiber.

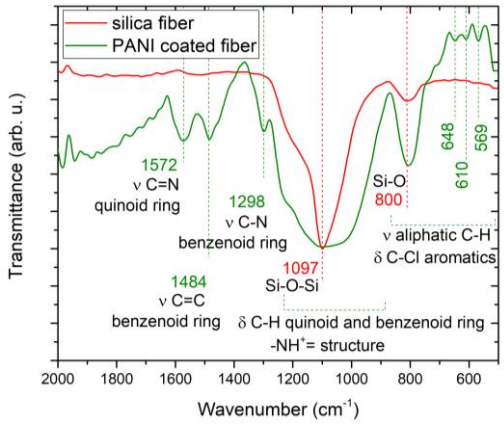

Figure 4.5 – FTIR spectra of silica fiber coated with polyaniline and bare silica fiber.

4.2. Influence of sensors' components

In the literature, several optical fiber sensors based on polyaniline for pH or other chemical compounds are documented that, like the work carried out here, their sensitivity is determined by quantifying a change in light transmission [75,120,133–135]. Thus, the reflectivity variations observed at the FBG peak may be associated with this occurrence. In this work, a tapered fiber with an inscribed Bragg grating and a coating of polyaniline is being explored, thus, to understand the influence of these elements that comprise the sensor and the respective spectral behavior observed, tests were carried out for two other configurations: FBG SMF (non-tapered) coated with polyaniline and tapered FBG without the PANI coating.

For the non-tapered FBG coated with polyaniline, the spectral evolution and characterization, in both wavelength and power variation, are displayed in Figure 4.6. In this case, although the fiber is coated with polyaniline, the variations recorded were practically null, in both wavelength and power, for the different pH measured. The polymer went through the protonation-deprotonation cycle during the pH variations, but since there is no taper structure, there is no evanescent wave, therefore the light trapped inside the core cannot interact with the surrounding medium, so, as expected, no variations in the spectra were observed.

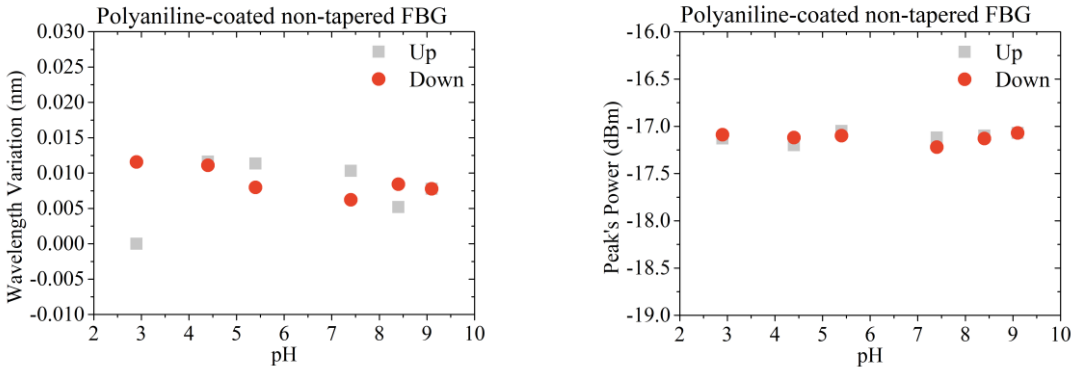

Figure 4.6 – Characterization of the response of a polyaniline-coated non-tapered FBG for different pH, performed for a polyaniline synthesized during 30 minutes for one trial: (a) wavelength and (b) power variation as function of pH.

For the second case, the non-coated tapered FBG, see Figure 4.7, the opposite occurs. Despite the existence of the evanescent wave, which enables the sensor to have a way to interact with the exterior, as there is no polyaniline, there is no component to sense the variations in the pH, which leads to no variation in the spectra, namely the power variation (Figure 4.7(b)). Note that this tapered structure depends only on the variables indicated in the equation (11), where none of them relates to pH.

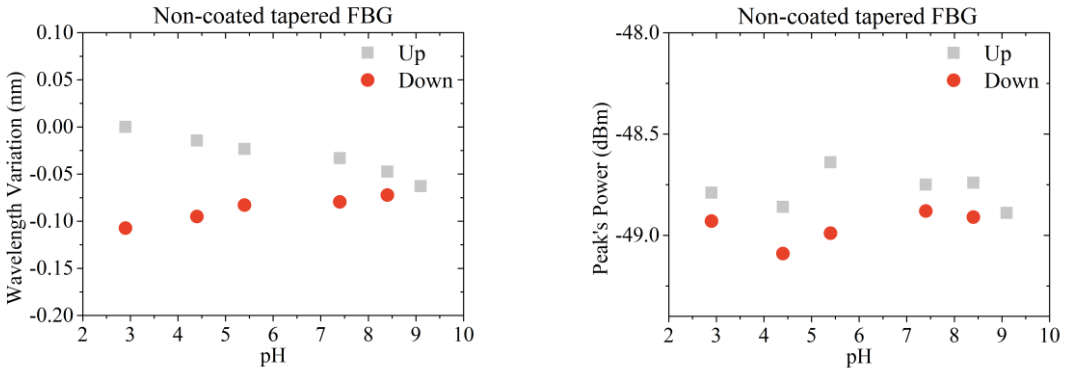

(a) (b)

Figure 4.7 – Characterization of the response of non-coated tapered FBG for different pH for one trial: (a) wavelength and (b) power variation as function of pH.

As for the wavelength variation, and this applies to all the fibers previously mentioned, as it can be seen in equation (11), there should be only observed wavelength variations when at least one of temperature, strain or RI of the surrounding medium suffers any variation. The characterization tests were conducted in a room with air conditioning at 20 °C, and all the solutions used have the same RI, so changes in the wavelength are not expectable. However, there were observed some variation in the λ_{Bragg}, especially in the tapered structures. Although wavelength variations do not necessarily affect the measurements, since they are based on power variations, it is better to minimize them as much as possible to avoid further confusion. When withdrawing the solutions from the container with a syringe, to change the pH solution, the slightest touch could induce permanent deformations in the fiber, which would be manifested through a variation in the λ_{Bragg} immediately verified in the interrogator. Moreover, just touching and applying pressure in the bottom of container with the tip of the syringe is enough to observe such variation, and as soon as the pressure stops, the spectra seem to center again on the previous λ_{Bragg}, but no spectra were recorded to confirm this hypothesis. These variations are more apparent in tapered FBGs, since they show more sensitivity to strain than normal non-tapered SMF inscribed FBGs. This was only a problem in the early stage of this work when these tests were conducted. Since then, new containers were home-made, being more robust with a deeper well, allowing a greater volume, and having deeper grooves for placing the fibers, so that they can stay fixed more easily, as Figure 4.8 presents.

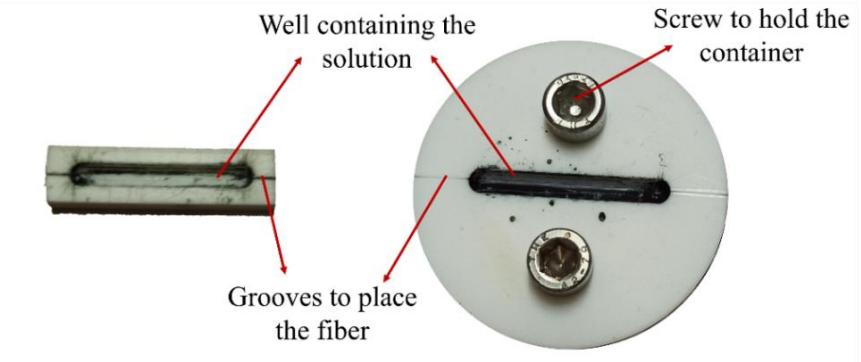

Figure 4.8 – Teflon containers used in experimental trials with the one on the left being the first version, and the one on the right the latest version. Note: the dark colour results from the PANI polymerization.

In conclusion, for the pH sensor to work, it must be a FBG inscribed in a tapered SMF coated with polyaniline. This is because the geometrically modified FBG, as a taper, promotes the interaction with the surrounding medium through the produced evanescent wave, and together with the polyaniline layer, which is pH responsive, allows the development of an optical fiber-based pH sensor.

4.3. Reproducibility

In this section, the results of the reproducibilit1y tests will be shown, aiming to understand if it is possible to produce different sensors with the same sensitivities for all three proposed configurations: a) tapers, b) POF D-shapes home-made and c) POF D-shapes reused. It shall be noted that the polyaniline synthesis time, from now on, was always 20 minutes.

For the tapers, there were available two additional batches to do these reproducibility tests, as seen in Figure 4.9, where the bar indicates the sensitivity value and the error bar the associated fitting error.

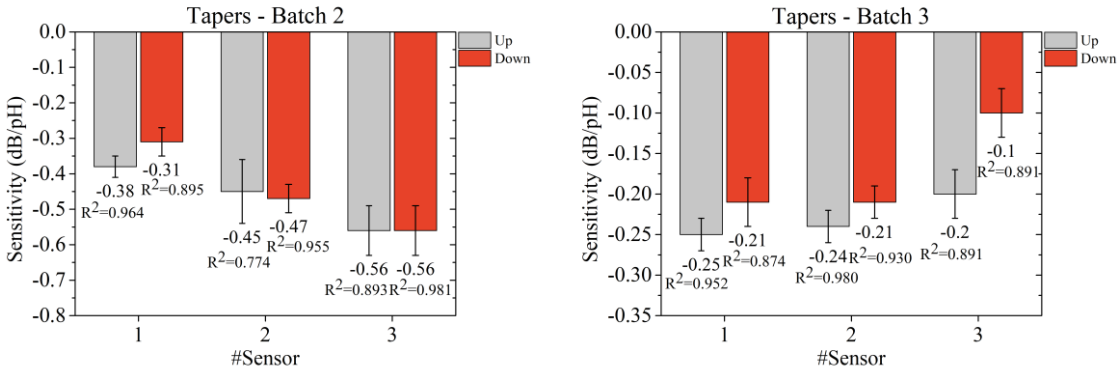

(a) (b)

Figure 4.9 – Reproducibility tests for three different sensors for (a) the second batch and (b) the third batch of a polyaniline coated tapered FBG.

Figure 4.9(a) shows that, in the second batch of fibers, for the increasing order of pH, the values of sensitivity were contained between −0.38 dB/pH and −0.56 dB/pH and for the decreasing order of pH, they were between −0.31 dB/pH and −0.56 dB/pH. For both increasing and decreasing orders, the values were both contained in short intervals and the error associated with the fitting overlaps. The main issue is the considerably lower sensitivity when comparing to the value obtained for the 20 minutes polyaniline synthesis in the first batch (Figure 4.2), which was −1.1 dB/pH.

Since the procedure regarding the FBG inscription and synthesis was the same, the university that supplied the tapers was inquired to understand the reasoning behind these differences. The main issue addressed was electrode aging due to overuse of electrodes, since there was an eight-month difference between the first batch and the second batch. Additionally, the proper maintenance on the water tank of the CMS machine may have some effect on the heat dissipation system and the high number of repetitions in a short period of time decreased the efficiency of the electrodes heating power. All of this can contribute to irregularities in the waist diameter of the taper, which were proved by a side camera being part of the CMS, that through an imaging module traced the whole surface side of the optical fiber, and determined the diameter of the tapers throughout the waist region for 5 different fibers of one of the supplied batches, as is presented in Table 2:

Table 2 –Waist diameter of five different tapers regarding the interval, average and median of its value.

Waist diameter of taper (μm)	1	2	3	4	5
Interval	[40,41]	[43.1,44.1]	[37.5,41.3]	[40.4,41.1]	[39.9,41.1]
Average	40.6 ± 0.6	43.6 ± 0.5	40.9 ± 3.4	40.7 ± 0.4	40.6 ± 0.7
Median	40.7	43.6	41	40.7	40.6

From the data retrieved by the side camera, it is possible to see slight deviations from the expected 40 μm diameter and, as mentioned above, these changes can have an impact on the evanescent wave, and consequently, on the sensitivity of the sensor.

For the third batch (Figure 4.9(b)), the sensitivities were even lower than on the second batch, however, especially in the increasing order, the sensitivities of the three sensors, between −0.20 dB/pH and −0.25 dB/pH, are in a narrower interval and contained within the fitting error. Therefore, for tapers from the same batch, there is some sort of reproducibility for the same synthesis time, unfortunately, when comparing fibers from different batches, which have different waist diameters, there is no way to obtain reproducibility.

All further tests, including repeatability (4.4), stabilization time (4.5), temperature (4.6) and ionic force (4.7) were done exclusively on fibers from the third batch.

The same process and analysis were applied for both POF D-shapes, for both the home-made method (Figure 4.10) and the reused method (Figure 4.11) by monitoring the peak centered at 650 nm. Once again, for the increasing order, the sensitivity values of the three sensors are contained in a tight interval and within the fitting error, between −471 Counts/pH and −563 Counts/pH, which shows some reproducibility, as shown in Figure 4.10(a). This is due to the fabrication process that is consistent, using the same grinder, the same V-groove and monitoring the power loss to around 3 dB, producing D-Shapes with the same dimensions, 1 cm long. Therefore, the interaction length between the evanescent wave produced and the polyaniline is kept constant and, consequently, reproducibility is obtained.

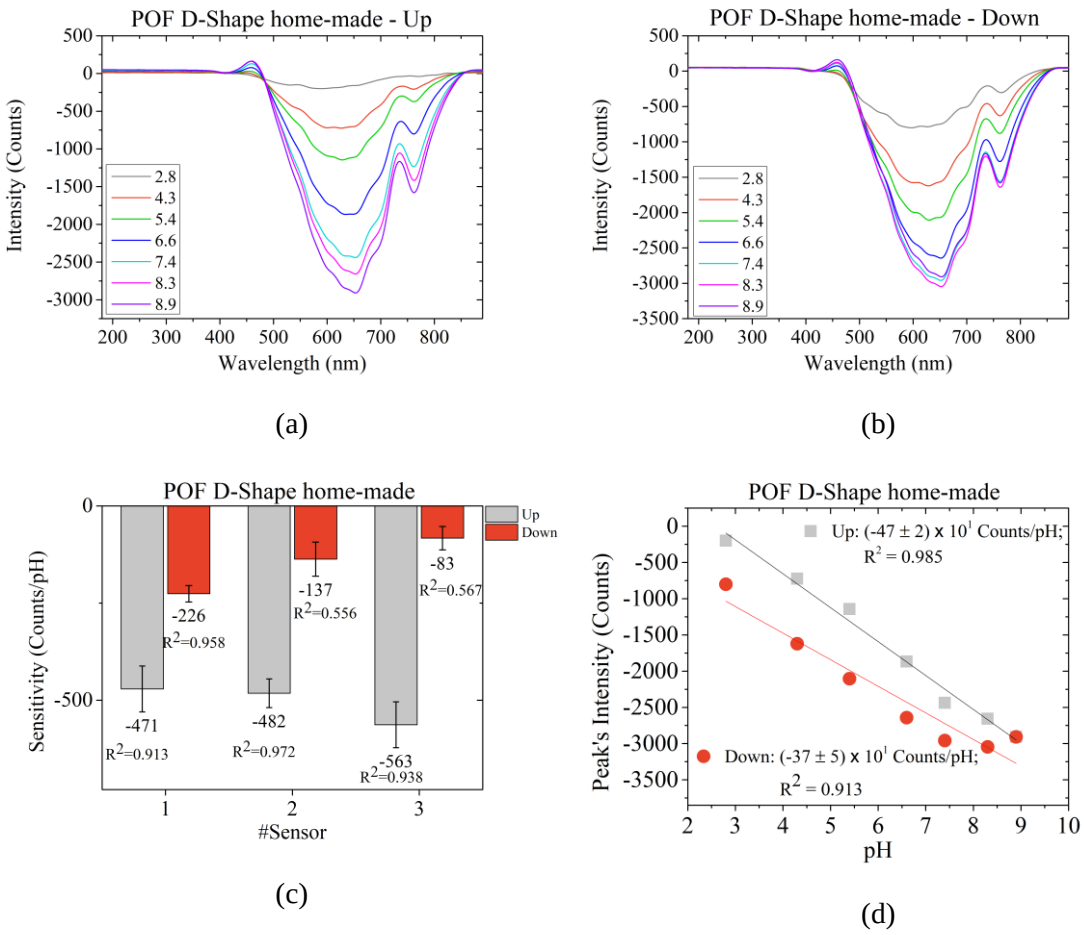

Figure 4.10 – Example of spectral evolution of a polyaniline coated POF D-shape home-made for (a) increasing pH order – Up and (b) decreasing pH order – Down; as well as (c) reproducibility tests for three different sensors and (d) an example of the power variation as a function of pH.

As for the reused D-shapes, as shown in Figure 4.11(a), the sensitivities registered for the pH increasing order were between −2248 counts/pH and −2499 counts/pH, respectively, and, once again, this short interval is overlapped within the error of each fitting. However, in the case of the reused D-shapes, they had different dimensions regarding the length, which are 1.2 cm, 2.2 cm and 2.3 cm for the first, second and third sensors, respectively. The amount of core exposed is the same for every D-shape, around 500 µm. However, despite the different lengths, due to the setup used for these D-shapes, the synthesis reaction was kept inside a small circle with a diameter of 0.8 cm. Therefore, the coating of the polyaniline, for every D-shape reused, only covered 0.8 cm of length, so, since the interaction length was kept consistent, the results obtained are similar between the three different sensors.

Thus, there is a degree of reproducibility between the sensors for both methodologies employed despite the way the coating is implemented being different. As for the home-made method, the coating covers the whole D-shape. So, if the interaction length was kept consistent, there is no trouble replicating different sensors with similar sensitivities.

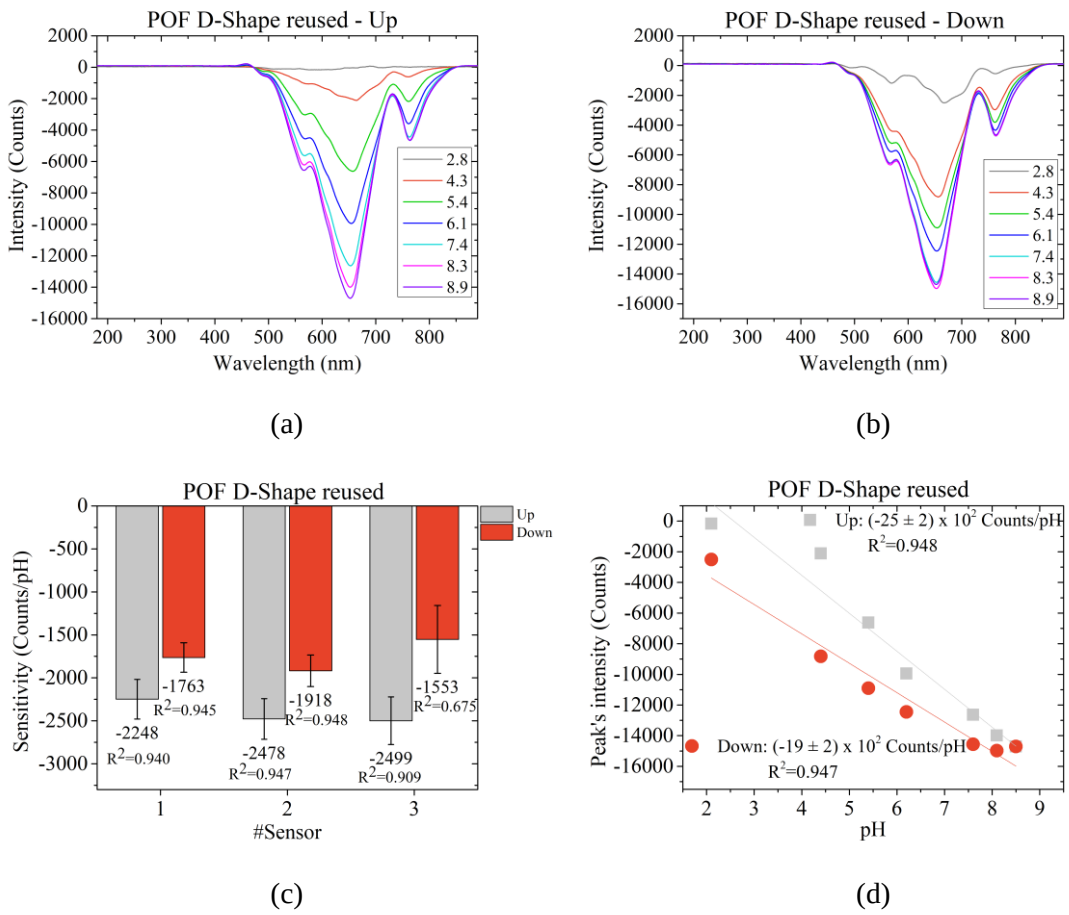

Figure 4.11 – Example of spectral evolution of a polyaniline coated POF D-shape reused for (a) increasing pH order – Up and (b) decreasing pH order – Down; as well as (c) reproducibility tests for three different sensors and (d) an example of the power variation as a function of pH.

It is important to note that the sensitivity achieved for the reused D-shapes is much higher than for the home-made method, around four to five times higher. This is due to the amount of core that is polished, leaving more core exposed in the reused D-shapes, 500 μm, when compared to the home-made method, around 300 μm, leading to a higher evanescent wave field, which enhances the sensitivity.

4.4. Repeatability

Repeatability tests were carried out to understand if each sensor can be applied for multiple usages in different days without loss of sensitivity. For that, after the first trial, the sensors were washed with deionized water and stabilized with 0.1 M of HCl before the next repetition. The results can be found for the three different sensors' configurations in study: tapers, POF D-shape home-made and POF D-shape reused (Figure 4.12).

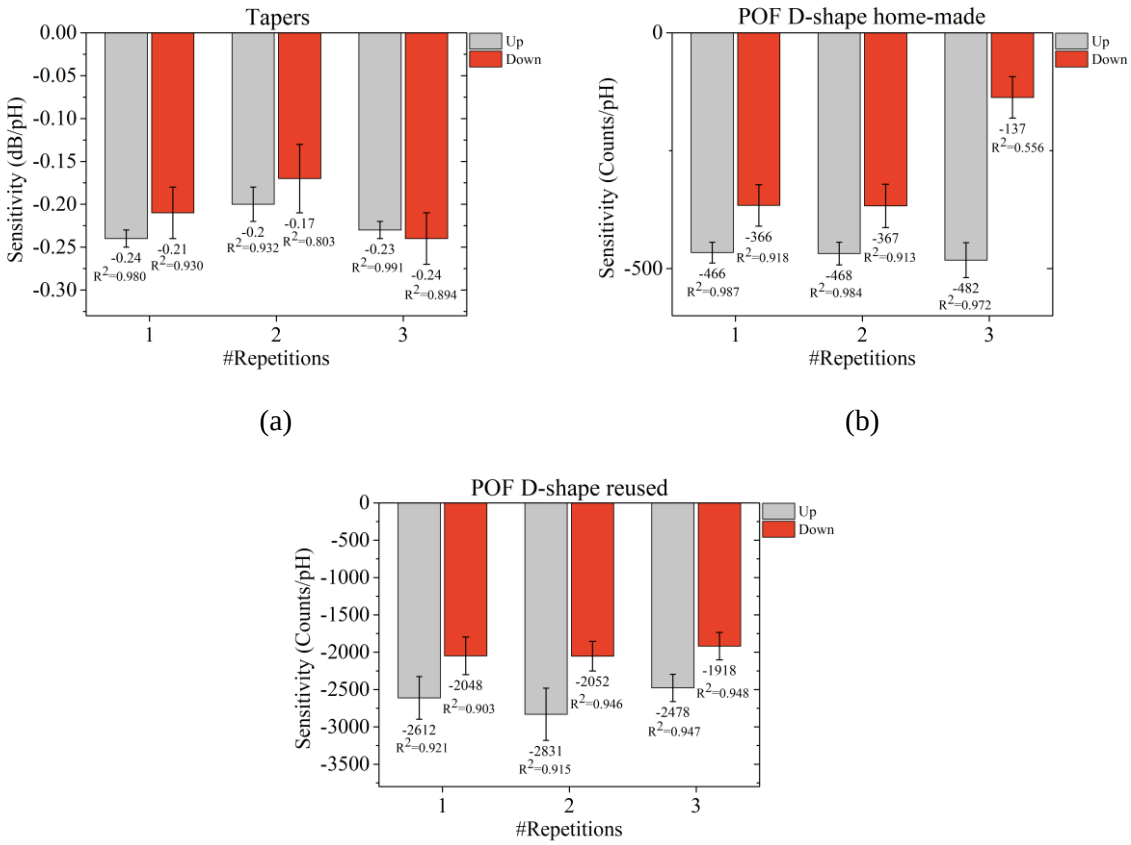

Figure 4.12 – Repeatability tests for three repetitions for one polyaniline coated (a) tapered FBG, (b) POF D-Shape home-made and (c) POF D-Shape reused.

All three of the proposed sensors show a degree of repeatability for the increasing order, with the tapers between -0.20 dB/pH and -0.24 dB/pH, the POF D-shape home-made between -466 Counts/pH and -482 Counts/pH and the POF D-shape reused between -2479 Counts/pH and -2831 Counts/pH, for the lower and upper values, respectively.

As seen so far, usually both reproducibility and repeatability are only achieved while increasing the pH, giving more consistent results regarding the sensitivity values and higher linearity, as opposed to the decreasing order, giving disparate results for the sensitivity and lower linearity. To add to this, counting not only the results showed in this document, but all the trials for all the sensors produced, 77% of the trials done showed more linearity while increasing the pH.

Literature reports that the hysteresis present in all characterizations and the lack of linearity, especially in the decreasing order, occur due to different reaction rates during the protonation and deprotonation process of the polyaniline and the higher the pH value, the higher the hysteresis observed [136]. When the polyaniline is protonated, it is in a swollen conformation, whereas when it is in its deprotonated form, it is in a shrank conformation. The swollen polyaniline coating is positively charged, increasing the pore size and consequently the permeability, and it has a faster ion diffusion, which results in a fast response time when slightly increasing the pH. But, as it starts to transition to the deprotonated form, the opposite happens: the pore size and, therefore, the permeability, decreases, leading to slower ion diffusions and slower response times [133,137].

However, at this stage of the work, 3 minutes per pH solution are given to the sensor, so its response fully stabilizes, but the hysteresis is still observed. This can be explained by the fact that while the decreasing pH order is taking place, and the polyaniline is in its deprotonated form, only fractions of the polyaniline are available and can interact with the pH solutions. Furthermore, the polyaniline only fully becomes accessible again after the coating is exposed to a pH value low enough, so that it can be fully swelled and protonated.

The above-mentioned reasons give the sensor a hysteresis that cannot be neglected, so it is not recommended to use this sensor while decreasing the pH. Ideally, there would always be a step of HCl calibration to obtain the most accurate measurements. Therefore, only the increasing order is necessary to evaluate the reproducibility and repeatability of the sensor.

4.5. Stabilization Time

Literature reports that when the polyaniline is protonated the ion diffusion is faster, resulting in a fast response for slight increases of pH and, while transitioning to the deprotonated form, the ion diffusion is slower [133,136,137]. To evaluate and validate the statements made in the previous sections that the 3 minutes were enough to stabilize the PANI in each pH solution, stabilization time tests were done, for all three different sensors: tapers, POF D-shape home-made and POF D-shape reused (Figure 4.13). To monitor these tests, for both the interrogator used in the tapers and the spectrometer used for the POF D-shapes, spectra were collected with 5 seconds intervals.

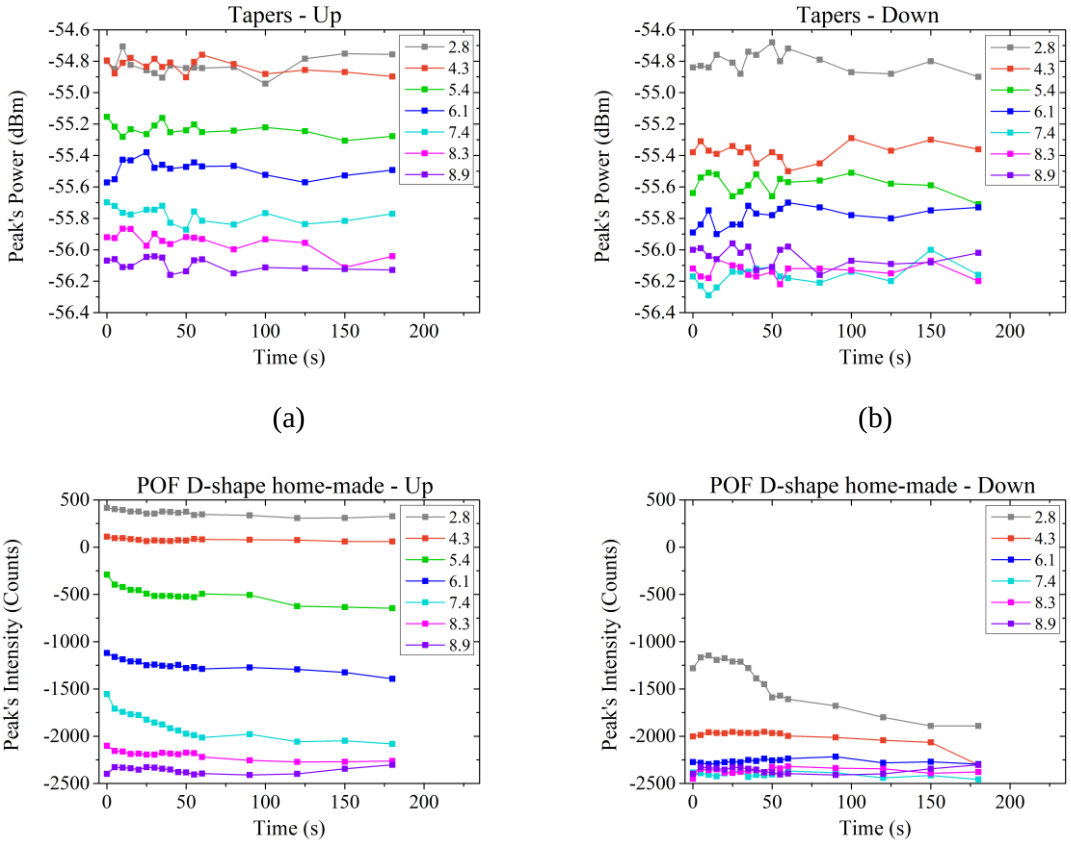

(a) (b)

(c) (d)

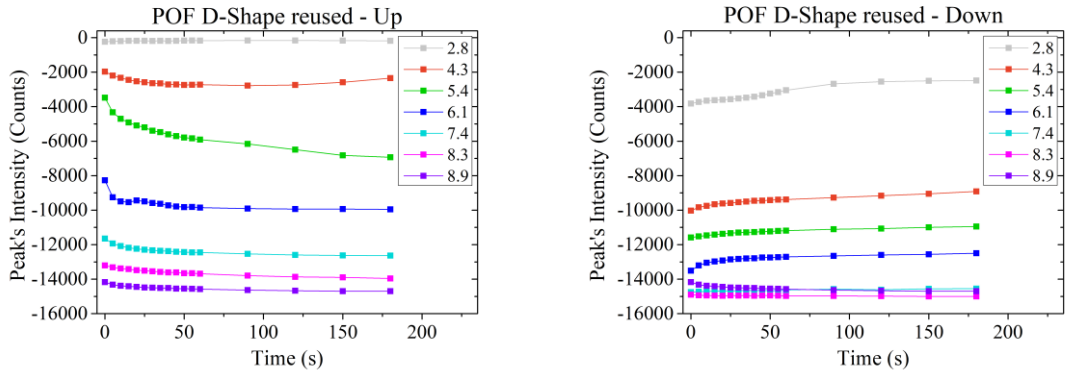

(e) (f)

Figure 4.13 – Stabilization time of the polyaniline coated (a), (b) tapered FBG, (c), (d) POF D-shape home-made and (e),(f) POF D-shape reused, for the pH increasing order (Up) and the pH decreasing order (Down), respectively.

An observation of the stabilization time plots for all three sensors show that it is easier to analyze and draw conclusions for the POF D-shapes, with the tapers showing more volatility and more instability, even after applying some smoothing signal processing. Overall, the stabilization time for the tapers is around 60 seconds, except in the increasing order nearing basic pH values, or, when decreasing it back to acid pH values, showing more instability in the regions where the polyaniline transitions between its protonated and unprotonated states, and vice-versa. This may be caused by the acquisition method of the equipment and the reflectivity of the FBGs. In the case of the interrogator, it has a 0.01 dB resolution and the total variations registered in the FBG when doing a full trial is around −1.6 dB, and since the latest batch of FBGs only had a reflectivity of 6 dB at its highest, when it is in acid medium, this results in a lower signal-to-noise ratio (SNR) and, thus, slight variations were more notorious in the case of the tapers. Whereas the spectrometer has a 0.01 count resolution and, when doing a full trial, the total variations registered in the POF D-shapes home-made and reused were 3000 and 16000 counts, respectively, and the transmission peak of the raw spectra is set to 60000 counts for both sensors, and although there are still variations, they are not notorious enough. Additionally, the interrogator has a frequency acquisition of 1 Hz, and consequently the spectrum is updated every second. When observing the spectrum in real time at the interrogator, it shows a lack of stability, which is more apparent since the SNR is smaller, while in the spectrometer the average time of every scan was set to around 5 seconds to reduce the noise observed.

The reasons mentioned above make the POF D-shapes, for both cases, easier to evaluate and to observe the changes polyaniline undergoes in a full increasing order and decreasing order of the pH cycle. In the beginning of the increasing order, in the first two steps, since the polyaniline is in its protonated form, the stabilization time is fast, taking around 25 seconds, or even less, to stabilize. But as the solutions take a pH of approximately between 5 and 7, the stabilization time increases roughly to 60 seconds, which means the polyaniline is transitioning from the protonated to the deprotonated form. After that, since the polyaniline is fully in its deprotonated form, the end of the increasing order and the beginning of the stabilization time is once again fast, taking about 30 seconds to stabilize. The stabilization time, once again, increases to 60 seconds, when the polyaniline starts to transition from the deprotonated to the protonated form for pH values between 5 and 7. Finally, at the end of the decreasing order, when the polymer is exposed to an acid medium, and it is turning back to its fully protonated form, the stabilization time is the highest, 150 seconds or even higher.

4.6. Ionic Strength

Since the exploited sensors have the purpose to be implemented in the aquaculture field, it is necessary to evaluate if they are susceptible to cross sensitivities regarding environmental changes that they may experience. A factor that may have an impact on cross-sensitivity measurements is the influence of the salinity/ionic strength. In aquaculture, the salinity observed is roughly 35 mg/L (0.0006 M). Therefore, aiming to observe the sensors behaviors, the ionic strength solutions prepared contain lower and higher concentrations: 0, 0.0001, 0.001, 0.01, 0.1 and 0.5 M. The solutions were prepared to keep the pH value as close to 7.4 as possible, nevertheless, the pH value of each solution was measured with the pH electrode, giving the results presented in Table 3.

Table 3 – pH values for the different ionic strength solutions considered.

Ionic Strength (M)	0	0.0001	0.001	0.01	0.1	0.5
pH	7.311	7.487	7.350	7.430	7.410	7.230

The measured pH values for the ionic strength solutions were between 7.4 ± 0.1, except for the higher ionic strength of 0.5 M, which was near 7.2. Because of these pH deviations, a slight variation in the intensity is expected. However, if these variations are according to the sensitivity of the sensor, conclusions regarding the increase of ionic strength can still be drawn. It is important to note that the spectrum immersed in 0 M solution was used as the reference spectrum.

As seen in Figure 4.14, the tendency is the same for all three sensors, showing little variations from 0.0001 to 0.1 M, that are according to the sensitivities of the sensors. This is specially seen when comparing the POF D-shape home-made with the reused method, with the latter showing four to five times the variations, just as observed when comparing the sensitivities. However, a bigger variation of the response was observed when increasing from 0.1 to 0.5 M for all three cases, since the ionic strength affects the level of protonation of the polyaniline due to the Donnan effect and the distribution of ions, changing the electronic structure of the polyaniline. Thus, ionic strengths higher than 0.5 M result in lower degrees of protonation for the polyaniline, which in turn change the sections of the polyaniline available, affecting the sensors response. However, since the aquaculture medium has ionic strengths of around 0.0006 M, the sensors are suitable for this field.

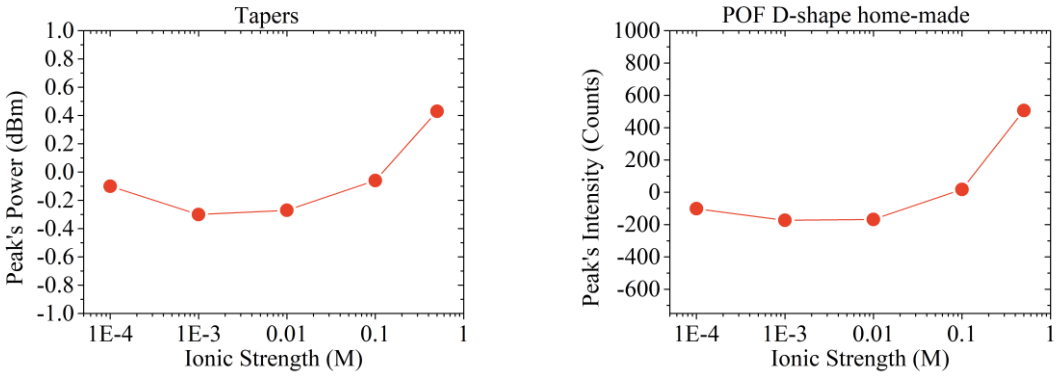

(a) (b)

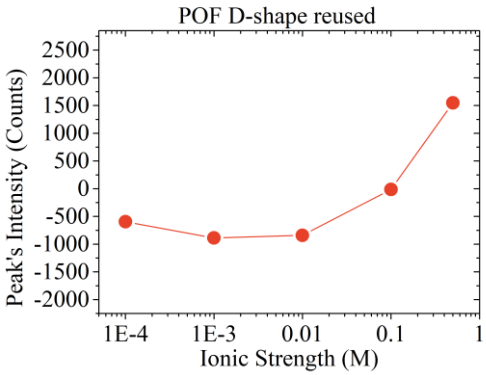

(c)

Figure 4.14 – Ionic strength characterization for polyaniline coated (a) tapers, (b) POF D-shape home-made and (c) POF D-shape reused.

4.7. Temperature

Up until this point, all the tests were done in a room with the air conditioner set to 20 ºC, the temperature that is usually measured at the fish tanks in aquaculture. Therefore, it is of interest to measure the temperature changes in the vicinity of this value, for 17, 20 and 23 ºC, for three different pH that are usually observed at aquaculture tanks, between 6.1 and 8.7.

The temperature tests were done in a thermal chamber with its relative humidity set to 0%. There were approximately 15 minutes for each temperature step, to ensure that not only was the temperature of the chamber stable, but also that the desired temperature for the solution was reached. This process was done for each of the three sensors, as seen in Figure 4.15, and the changes in the temperature have practically no effect on the sensor's behavior. The only subtle changes observed are mainly on the 6.1 pH value, which may be due to the thermal chamber being pre-set to 17 ºC, therefore the chamber stabilized quicker and the jump from HCl to 6.1 was big enough for the polyaniline to undergo transition from protonated to deprotonated, meaning that the pH variation had not fully stabilized yet. It is important to note that at this stage of the work, the interrogator stopped working and the taper's temperature characterization was done using an OSA. Additionally, there was the need to add connectors and fiber extensions to the D-shape home-made, since the temperature characterization was done on the thermal chamber, which may contribute to the lower counts observed in Figure 4.15(b).

For these temperature tests, all three of the sensors were set at a time inside a climatic chamber (Model L C/64/70/3, Weiss Technik). The temperature ranges from 17 to 23 ºC, with steps of 3 ºC and 10 minutes per step in order for the temperature of the chamber and solution to stabilize, and at a constant humidity of 0 %RH. Unfortunately, at this stage of the work the interrogator started malfunctioning making it impossible to use, so these temperature tests were carried on an optical spectrum analyzer (OSA), where the used light source (Amonics, model ALS-CL-17-B-FA), has a bandwidth of 80 nm, centered at 1570 nm, and the OSA (Anritsu, MS9740A), with a resolution of 0.05 nm, were utilized.

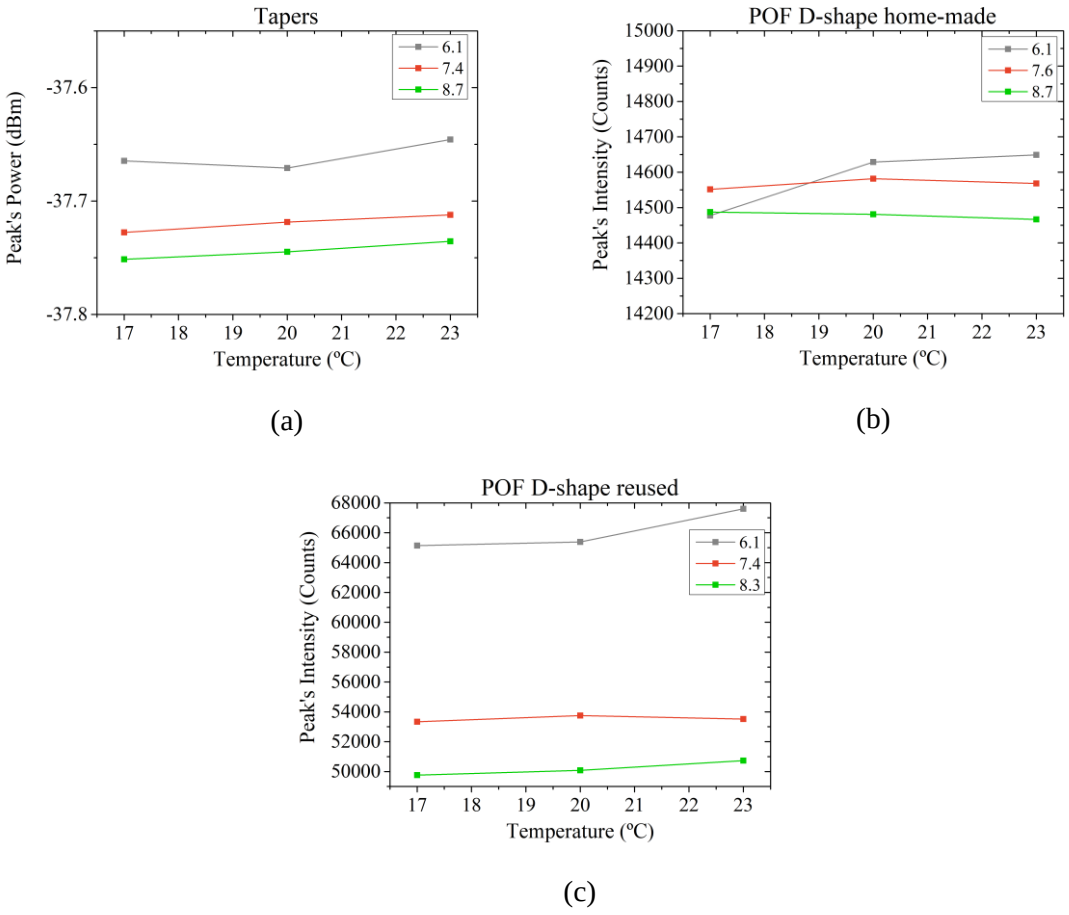

Figure 4.15 – Temperature characterization for a polyaniline coated (a) tapered FBG, (b) POF D-shape home-made and (c) POF D-shape reused.

4.8. Powermeter

Instead of utilizing the spectrometer, it is of interest to explore a low-cost alternative. Therefore, the use of a powermeter was implemented to measure the intensity losses, while the pH increases, in two of the three proposed sensors, the ones that use a POF, as this equipment is easy to implement in those fibers. The power characterization is shown as follows (Figure 4.16):

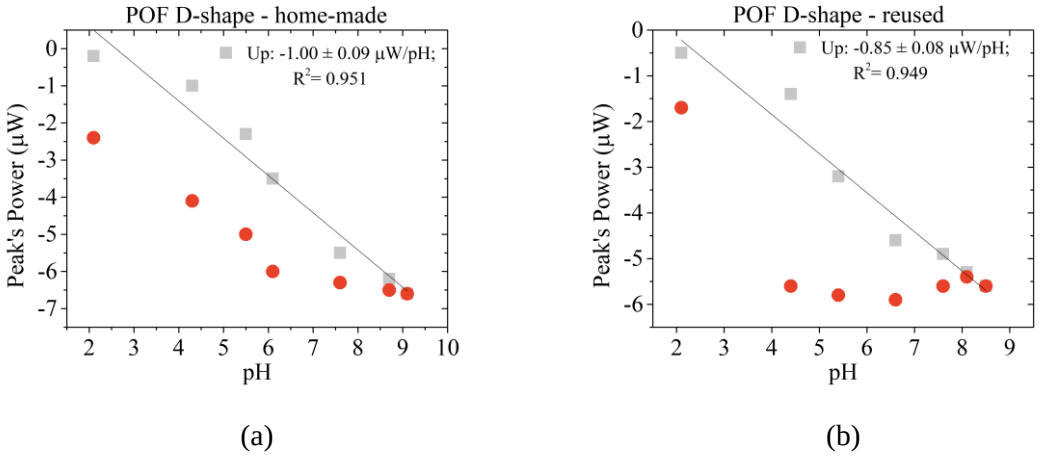

Figure 4.16 – Power variation for the polyaniline coated POF D-shape (a) home-made and (b) reused using a powermeter.

The characterization shows that a higher sensitivity was recorded for the home-made method (−1.00 ± 0.09 μW) when comparing to the reused method (−0.85 ± 0.09 μW), in contrast to what happens when using the spectrometer. One of the reasons may be the initial power value at which the POF are set. Due to the short fiber length associated with the reused method, there is the need to use two connectors and an additional POF length to connect the D-shape to the source and spectrometer or powermeter, resulting in an initial power of around 50 μW. For the home-made method, the fiber length is enough to connect the D-shape to the source and spectrometer or powermeter, without the use of connectors and extended fiber lengths, leading to lower losses and a recorded initial power of 200 μW. The additional losses, and the approximately four times lower initial power associated with the reused method, eventually led to a lower sensitivity when using the powermeter. The reason for not observing this when using the spectrometer is because before each test, for both the home-made and reused method, the intensity of the higher peak is set at around 60000 counts.

This characterization took place using a powermeter (Thorlabs, PM100D) capable of attaching different sensing heads, such as photodiode, thermal or pyroelectric sensors. The sensing head (ThorLabs, S121C) used was a silicon photodiode with a wavelength range of 400 to 1100 nm, and in this case, it was centered at 650 nm, power range of 500 nW to 500 mW with a resolution of 10 nW.

4.9. Integration in a hybrid platform

One of the main objectives of this work is, after producing an optical pH sensor, to integrate it in a hybrid sensing platform with an electrochemical sensor of nitrites. Since high levels of nitrites can be a major contributor to toxicity, leading possibly to the mortality of the fish, and literature reports that one major factor the nitrites toxicity is dependent on, is the pH of the water [10]. Thus, the importance of integrating both sensors in the same structure.

The other part of the hybrid system, developed by a laboratory colleague, consists of an optical fiber coated with laser induced graphene (LIG) functionalized with gold nanoparticles (Au NPs), which was exploited for nitrite detection by using differential pulse voltammetry (DPV) through a Versastat3 electrochemical station (Princeton Applied Research). The experimental setup consisted of an electrochemical cell, where a three-electrode setup is used in contact with phosphate buffered saline (PBS) solution as electrolyte. Here, the Au NPs-functionalized LIG is the working electrode (WE), which corresponds to the transduction element. By applying a range of potential values to the WE, electron transfer processes are promoted between the WE surface and the electrolyte, and current begins to flow. A saturated calomel reference electrode (RE) has a stable independent potential and provides a reference point against which the potential on the WE can be applied. A platinum counter electrode (CE) establishes a connection to the electrolyte, closing the electrical circuit. The resulting current has a peak value specific to the reduction/oxidation of nitrite dissolved in the electrolyte, and a linear relationship between this electrical signal and the concentration of nitrites can be attained, within a certain range. The calibration curve was determined by adding small volumes of nitrites containing solution to the electrolyte and the voltammogram was recorded.

Although the pH is a key parameter to determine the water's quality and for the well-being of the fish, it is also important as a parameter to calibrate other sensors accordingly, such as this nitrites sensor, in which the calibration curve depends on the pH of the electrolyte solution.

The WE and the tapered optical pH sensor were integrated in the same fiber, by splicing them together using a fusion machine (Fujikura, model FSM-40s), and then this fiber was inserted in a graduated cylinder. The pH sensor was located near the bottom of the graduated cylinder, allowing to ease the calibration step where the HCl is needed. The graduated cylinder is closed by a lid with three different holes, the main one, designated for the fiber with the pH sensor and

the WE, which will connect to the interrogator, and two additional holes, designated for the RE and CE, needed for the sensor of nitrites. Moreover, to make use of the work that was done on the POF D-shapes, two small holes, on opposite sides, were made at the bottom of the graduated cylinder, and after the D-shape goes through them, making it centered, glue is used at the holes, ensuring no liquid leakage. This offers the opportunity of having two different pH sensors in the same structure, which is beneficial to see if the pH values are in agreement, as Figure 4.17 presents. Unfortunately, the interrogator malfunctioning continued, and the tests proceeded with just the POF D-shape home-made. But since both showed similar behaviors throughout the whole work and share the same sensing principle, the spectral behavior while increasing the nitrites concentration in the POF D-shape should be similar to the one that would be observed in the tapers.

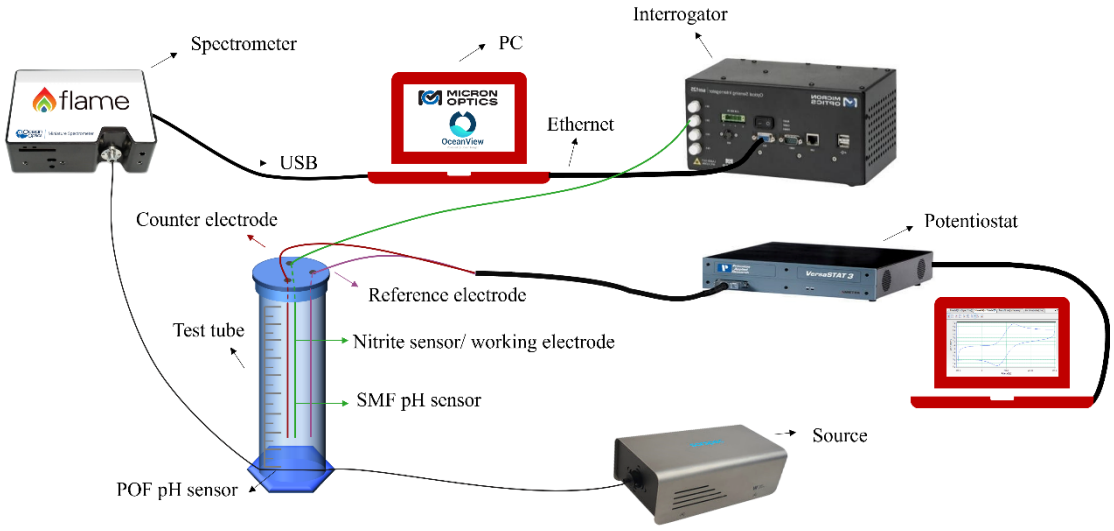

Figure 4.17 – Schematic of the hybrid platform used to test the pH sensors produced during this work, as well as the sensor of nitrites.

Afterwards, the calibration step using HCl (0.1 M) took place, then, after removing HCl, PBS was added. As the polyaniline is transitioning from a protonated to a deprotonated state, since PBS has a defined pH of 7.4, instead of a gradual increase, as was done during the characterization, and, to ensure the full stabilization, the sensor was immersed in PBS during 10 minutes. Subsequently, nitrites were added in steps of 50 µM up until 150 µM. For every single step the solutions were subject to a homogenization using a magnetic stirrer and, after the solution is properly homogenized, the stirring stops and DPV was run. During this time, the spectrometer is saving spectra with intervals of 30 seconds. A reference spectrum using HCl was subtracted from all the spectra, and the evolution throughout time is as Figure 4.18 follows.

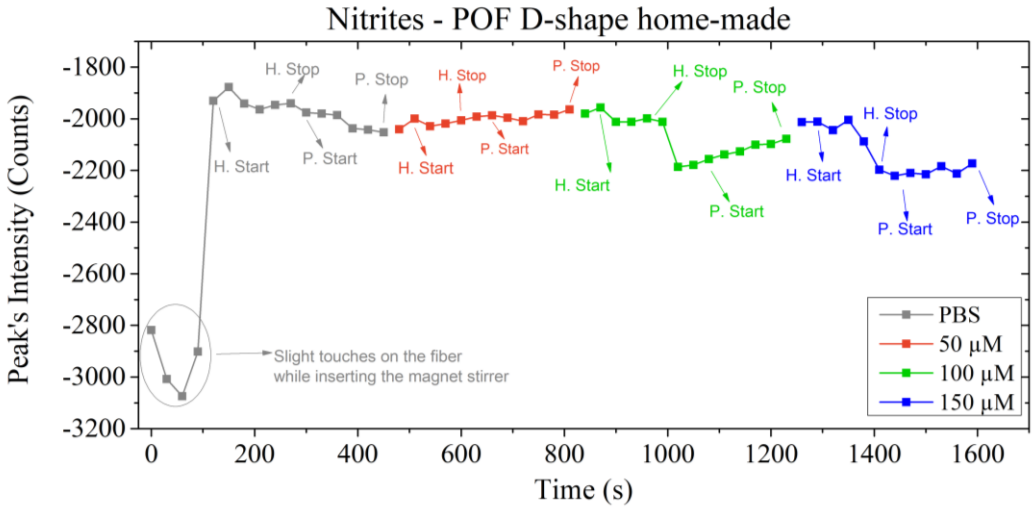

Figure 4.18 – Monitoring the peak's evolution throughout the process of adding nitrites in three different steps of 50 µM. Where "H. Start" and "H. Stop" stand for homogenize start and stop, respectively, and "P. Start" and "P. Stop" stand for potentiostat start and stop, respectively.

As Figure 4.18 shows, a slight decrease in transmission as nitrites are added is observed, totaling just about 250 counts when the 150 µM of nitrites are fully added. As a solution gets more basic, according to the sensor's behavior, this would translate to a decrease in transmission. Although nitrites are a weak base, any major changes were not expected, since PBS is a buffer solution. Additionally, the tested nitrites' concentrations greatly outspan the possible concentrations observed in aquaculture, which are usually between 20 and 40 µM, thus the changes observed were not significant. However, it is important to note that aquaculture water is not a buffer solution, consequently, bigger changes are to be expected in this case.

4.10. Advantages and disadvantages of the proposed sensors

Given the produced sensors, both in the SMF Taper and the POF D-shape, it is of interest to do a comparison and evaluate the performance of the sensors in four different levels: very good, good, modest, and challenging or unknown, for a diversity of different parameters, as seen in Figure 4.19.

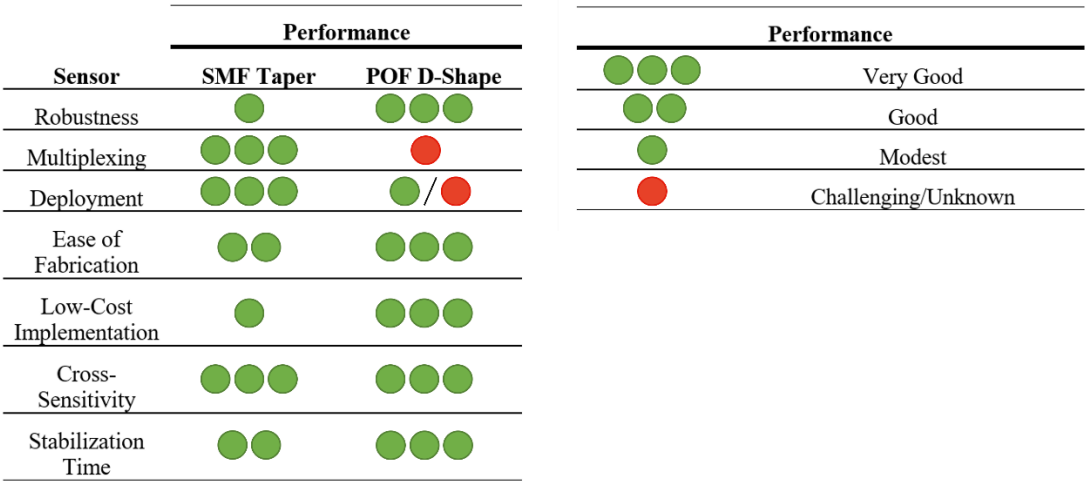

Figure 4.19 – Comparing of the relative performance for a variety of different parameters for the manufactured sensors, SMF Taper and the POF D-shape (Left); symbols code (Right).

For most of the parameters mentioned above (see Figure 4.19), the POF D-shape has an equal or better performance than the SMF taper. For the temperature and ionic strength, both sensors showed practically no cross-sensitivity for both these two parameters, having similar behaviors.

As for the stabilization time, although it is around 60 seconds for both sensors, it can be even lower, in the case of the extreme regions in the protonated or unprotonated form of the polyaniline. However, when recording the spectra, the tapers show more volatility and more instability, due to a lower SNR and the acquisition method, when comparing it to the POF D-shapes.

Additionally, although if handled with care it does not break that easily, the robustness of a tapered fiber is not comparable to that of a POF. Concerning the fabrication method, the geometry-modifying processes are simple for both fibers. For the POF D-shapes only a defined volume of PMMA is polished and, as for a taper, if the CMS parameters regarding the tension and speed are set accordingly, the heating process leaves the waist diameter uniform. However, in the taper, there is the need to inscribe the FBG, which due to the reduced core diameter and the handling of the taper, is a slightly difficult process.

Moreover, the overall cost and implementation is a lot cheaper in the case of the POF when compared to the tapers, not only regarding the manufacturing, but also the sensing equipment, with the interrogation system for the tapers being a lot more expensive than the low-cost solution, using a powermeter.

However, these advantages that the POF has come at the cost of two key parameters, if the sensors are to be deployed in a practical application, such as aquaculture. One of the main advantages of a SMF is its ability to multiplex different sensors in the same fiber, as was seen in the previous section when the pH sensor produced was spliced to a nitrite's sensor. However, the nitrites' sensor uses polyimide transformed as LIG, and currently there are no reports of applying LIG on PMMA. The other key parameter is its deployment in aquaculture tanks, which is a lot easier in the case of a SMF. An SMF has lower attenuations, which allows remote sensing for great distances. This can be a minor issue for the POF, as they have higher losses when compared to the latter. However, in aquaculture it is not extremely problematic, since all the tanks are contained within a tight space, thus, the fiber length would be only a few meters long. The main problem, which was seen when integrating the sensor on the hybrid platform, is that the POF needs to be as stable as possible, otherwise any touches on it can cause major changes in the spectrum, which makes it difficult to interpret the results. Additionally, their large size hinders their miniaturization potential, especially the reused POF, that has a resin cube attached to the fiber, making this sensor unfeasible to apply in aquaculture.

5. Conclusions and future work

The continuous increment of the world population, combined with the overexploitation of the fish species present in the oceans and seas, demands for an alternative to provide the high-quality protein needed for humans, with aquaculture being the industry at the fore front of this change. However, as aquaculture grows more intensely, new technology needs to be developed to ensure the fish well-being, and quality of the food for human consumption. Optical fiber sensors can fill this void on the market, as they offer valuable advantages, such as immunity to electromagnetic interference and miniaturization, as well as the possibility of *in situ* and real time measurements of the properties of the tanks, with pH being one of the key parameters that determines the fish's health.

For that reason, two different types of geometry-modified optical fiber sensors were produced: single mode tapered fibers and D-shaped plastic optical fibers. The tapers, provided by Liaocheng University, were produced using a combiner manufacturing system that uses a plasma field for even heat distribution to produce tapered optical fibers with a waist diameter of 40 µm, with its core at 2.624 µm, a waist-length of 4 mm and a transition length of 5 mm. Subsequently, the tapers had a fiber Bragg grating inscribed in them using a UV laser with the phase mask method. Regarding the D-shaped POF, two different methods were used. One uses a home-made polishing machine, producing D-shapes with approximately 300 µm of core exposed. The other reuses a former cortisol D-shape sensor, that is attached to a resin block with 500 µm, i.e., half the core was exposed through a polishing process as well. This cortisol sensor had a gold coating, which was removed resorting to aqua regia, a strong acid that dissolves noble metals, leading to the bare POF D-Shape ready to be used. All three of the modified sensors have an evanescent wave output surrounding the fiber, but there is still the need to coat the fibers surface with a pH sensitive material. The material of choice was polyaniline, produced using synthetic oxidative polymerization. The most common form of polyaniline is its partially oxidated state, emeraldine, and the polymer changes between protonated and deprotonated depending on the pH. At acidic values, the polyaniline is protonated and swollen (emeraldine salt), revealing a green color, whereas at basic values, the polyaniline is deprotonated and deswollen (emeraldine base form), which has a blue color.

When characterizing these sensors, it is possible to see a tendency regarding power variations, this is due to the transition between protonated and deprotonated polyaniline as pH increases, which leads to an increase of the refractive index of the layer and, thus, a decrease in transmission is observed. Furthermore, there is the need to evaluate which synthesis time is more appropriate to use for further testing. The tapered fibers were coated with polyaniline for three different times: 10, 20 and 30 minutes. The best sensitivity was achieved for 20 minutes and, by using Scanning Electron Microscopy, it was possible to observe coating and the thickness associated with this time is the most uniform, while also being thick enough to promote interactions between the evanescent wave and the polyaniline. This fiber achieved better sensitivities than the one with a synthesis time of 10 minutes, whilst not being so thick that it starts trapping the evanescent wave, which reduces its sensitivity, as it is observed for 30 minutes.

The tapers and the homemade and reused D-shapes all exhibit some degree of reproducibility and repeatability, with their sensitivities being about −0.25 dB/pH, −500 counts/pH, and −2500 counts/pH, respectively. Although there is a certain level of uncertainty regarding the reproducibility of the tapers themselves when comparing the sensitivity achieved for the three different batches at disposal, since the profile of a few tapers showed slight variations along the waist diameter, resulting in variations of the evanescent wave and, consequently, the sensitivity. The results for the D-shapes are also in agreement, since there is more core exposed in the reused method when compared to the home-made one, thus, there is more evanescent wave,

and consequently the sensitivity obtained is higher. However, these considerations regarding the sensitivity values are only valid for the increasing order of pH, since for the decreasing order, a lower linearity was observed.

As for the stabilization time, the D-shaped POF can exhibit a stabilization period of around 25 seconds, or less, when the polymer is either totally protonated or deprotonated, which happens in acidic and basic mediums, respectively. It can rise to 60 seconds for the transitioning pH values, or even more, especially in the decreasing order. Regarding the tapers, the stabilization period can take around 60 seconds, and even more in the transition regions, although it is quite difficult to analyze these situations for the tapers, due to a lower signal-to-noise ratio associated with the fiber Bragg grating peak and a lower power resolution of the equipment. Concerning possible environmental cross-sensitivities, the parameters tested were temperature and ionic strength, between 17 and 23 ºC, and from 0 to 0.5 M, respectively, and practically no spectral response was observed for both cases.

Afterwards, and since the interrogator used to monitor the tapered fibers was malfunctioning, the POF D-shape home-made sensor was integrated in the same structure as the electrochemical nitrites' sensor. By adding the nitrites, up to 150 μM which is a weak base, to the PBS, a buffer solution that acts as an electrolyte, only a very minimal decrease in transmission is observed.

When comparing the advantages and disadvantages of the proposed sensors: D-shaped plastic optical fibers and tapered silica fibers, are somewhat complementary. Whereas the ones that use plastic optical fiber are characterized by their mechanical robustness, ease of fabrication and implementation cost, they lack multiplexing and remote sensing capabilities, while in the tapers it is the exact opposite, it is easy to multiplex various sensors in the same fiber and to implement remote sensing, but they are troublesome regarding their robustness and fabrication.

The possibilities of future work involving the pH sensors produced are mainly concerning their direct application in aquaculture tanks and further work on the hybrid sensing platforms.

For the application in aquaculture, the first step would be acquiring various samples of water, before and after passing through the recirculating systems, and determine the pH to see if they are according to the expected values. Afterwards, the implementation and real time monitoring of the pH directly in the aquaculture tanks would come. Additionally, there is also improvements to be done in the hybrid platform and the structure surrounding it, so the tests for both nitrites and pH measurement to be carried out more accurately and less disturbances. For example, adding extra space to fit in a glass electrode to compare the spectral evolution while adding nitrites to the values measure in the glass electrode.

About the improvements and further work on the implementation of the hybrid platform, it would be best to try to find alternative sensors for tapers, since they are hard to handle and splicing the tapered fiber to the fiber containing the sensor of nitrite was a difficult process. So, to avoid this splicing process, an alternative would be to inscribe some grating structure directly on the fiber with polyimide, such as tilted fiber Bragg gratings. As already mentioned, there are currently no reports of applying laser induced graphene on PMMA, which is the material of the core of the plastic optical fiber. Hence, an idea to avoid this problem would be to find a way to place and connect the polyimide sheets to the PMMA, and afterwards proceed with the laser induced graphene. A possibility would be to place liquid polyimide, however, the problem in this case is the difficulty to control its thickness and homogeneity.

Additionally, it would also be interesting to introduce novel parameters, besides nitrites and pH, in the hybrid platform, that may be of interest to aquaculture, such as monitoring bacteria, micro-plastics, bromine and turbidity present in the water.

6. References

[1] Population, United Nations. (2019). https://www.un.org/en/global-issues/population (accessed September 26, 2022).

[2] FAO, The State of World Fisheries and Aquaculture: Towards Blue Transformation, Rome, 2022. https://www.fao.org/3/ca9229en/online/ca9229en.html#chapter-1_1.

[3] A. Ahmad, S. Rozaimah, S. Abdullah, H. Abu, A. Razi, N. Izzati, Aquaculture industry : Supply and demand , best practices , effluent and its current issues and treatment technology, J. Environ. Manage. 287 (2021) 112271. https://doi.org/10.1016/j.jenvman.2021.112271.

[4] The Sustainable Development Goals Report, United Nations. (2022). https://unstats.un.org/sdgs/report/2022/.

[5] N. Afspan, Aquaculture for Food Security, Poverty Alleviation and Nutrition (AFSPAN) Final Technical Report 2014, (2014).

[6] DNV, DNV Marine Aquaculture Forecast: Oceans' future for 2050, (2021).

[7] M. Badiola, O.C. Basurko, R. Piedrahita, P. Hundley, D. Mendiola, Aquacultural Engineering Energy use in Recirculating Aquaculture Systems (RAS): A review, Aquac. Eng. 81 (2018) 57–70. https://doi.org/10.1016/j.aquaeng.2018.03.003.

[8] E. Proksch, pH in nature, humans and skin, J. Dermatol. 45 (2018) 1044–1052. https://doi.org/10.1111/1346-8138.14489.

[9] Y. Tang, L. Zhong, W. Wang, Y. He, T. Han, L. Xu, X. Mo, Z. Liu, Y. Ma, Y. Bao, S. Gan, L. Niu, Recent Advances in Wearable Potentiometric pH Sensors, Membranes (Basel). 12 (2022) 1–20. https://doi.org/10.3390/membranes12050504.

[10] L.C.B. Silva, B. Lopes, M.J. Pontes, I. Blanquet, M.E.V. Segatto, C. Marques, Fast decision-making tool for monitoring recirculation aquaculture systems based on a multivariate statistical analysis, Aquaculture. 530 (2021) 735931. https://doi.org/10.1016/j.aquaculture.2020.735931.

[11] M.I. Khan, K. Mukherjee, R. Shoukat, H. Dong, A review on pH sensitive materials for sensors and detection methods, Microsyst. Technol. 23 (2017) 4391–4404. https://doi.org/10.1007/s00542-017-3495-5.

[12] G.L. Allan, G.B. Maguire, Effects of pH and salinity on survival, growth and osmoregulation in Penaeus monodon Fabricius, Aquaculture. 107 (1992) 33–47. https://doi.org/10.1016/0044-8486(92)90048-P.

[13] L. Jiao, N. Zhong, X. Zhao, S. Ma, X. Fu, D. Dong, Recent advances in fiber-optic evanescent wave sensors for monitoring organic and inorganic pollutants in water, TrAC - Trends Anal. Chem. 127 (2020) 115892. https://doi.org/10.1016/j.trac.2020.115892.

[14] M.F. Camões, A Century of pH Measurements, Chem. Int. (2010) 3–7.

[15] P. Muller, Glossary of terms used in physical organic chemistry (IUPAC Recommendations 1994), Pure Appl. Chem. 66 (1994) 1077–1184. https://doi.org/doi:10.1351/pac199466051077.

[16] A.K. Covington, R.G. Bates, R.A. Durst, Definition of pH scales, standard reference values, measurement of pH and related terminology (Recommendations 1984), Pure Appl. Chem. 57 (1985) 531–542. https://doi.org/doi:10.1351/pac198557030531.

[17] R. Myers, The Basics of Chemistry, Greenwood Press, 2003. https://books.google.pt/books?id=oS50J3-IfZsC.

[18] R.J. Myers, One-hundred years of pH, J. Chem. Educ. 87 (2010) 30–32. https://doi.org/10.1021/ed800002c.

[19] W.B. Jensen, The Symbol for pH, J. Chem. Educ. 81 (2004) 21–22.

[20] P. Spitzer, K.W. Pratt, The history and development of a rigorous metrological basis for pH measurements, J. Solid State Electrochem. 15 (2011) 69–76. https://doi.org/10.1007/s10008-010-1106-9.

[21] J.G. Nørby, The origin and the meaning of the little p in pH, Trends Biochem. Sci. 25 (2000) 36–37. https://doi.org/10.1016/S0968-0004(99)01517-0.

[22] S. Karastogianni, S. Girousi, S. Sotiropoulos, pH: Principles and Measurement, Encycl. Food Heal. (2015) 333–338. https://doi.org/10.1016/B978-0-12-384947-2.00538-9.

[23] H.N. Po, N.M. Senozan, The Henderson – Hasselbalch Equation : Its History and Limitations, 78 (2001).

[24] M. Toledo, A Guide To pH, 2011.

[25] K.F. Lim, Negative pH does exist, J. Chem. Educ. 83 (2006) 1465. https://doi.org/10.1021/ed083p1465.

[26] S. Korposh, S.W. James, S.W. Lee, R.P. Tatam, Tapered Optical Fibre Sensors: Current Trends and Future Perspectives, Sensors (Basel). 19 (2019). https://doi.org/10.3390/s19102294.

[27] O. Korostynska, K. Arshak, E. Gill, A. Arshak, Review on state-of-the-art in polymer based pH sensors, Sensors. 7 (2007) 3027–3042. https://doi.org/10.3390/s7123027.

[28] L. Manjakkal, D. Szwagierczak, R. Dahiya, Metal oxides based electrochemical pH sensors: Current progress and future perspectives, Prog. Mater. Sci. 109 (2020) 100635. https://doi.org/10.1016/j.pmatsci.2019.100635.

[29] M. Khalil, N. Liu, R.L. Lee, Super-Nernstian potentiometric pH sensor based on the electrodeposition of iridium oxide nanoparticles, Int. J. Technol. 9 (2018) 446–454. https://doi.org/10.14716/ijtech.v9i3.1263.

[30] R. Mohammad-Rezaei, S. Soroodian, G. Esmaeili, Manganese oxide nanoparticles electrodeposited on graphenized pencil lead electrode as a sensitive miniaturized pH sensor, J. Mater. Sci. Mater. Electron. 30 (2019) 1998–2005. https://doi.org/10.1007/s10854-018-0471-5.

[31] T.D. Singewald, I. Traxler, G. Schimo-Aichhorn, S. Hild, M. Valtiner, Versatile, low-cost, non-toxic potentiometric pH-sensors based on niobium, Sens. Bio-Sensing Res. 35 (2022) 100478. https://doi.org/10.1016/j.sbsr.2022.100478.

[32] H.J. Park, J.H. Yoon, K.G. Lee, B.G. Choi, Potentiometric performance of flexible pH sensor based on polyaniline nanofiber arrays, Nano Converg. 6 (2019) 9. https://doi.org/10.1186/s40580-019-0179-0.

[33] F. Mazzara, B. Patella, C. D'agostino, M.G. Bruno, S. Carbone, F. Lopresti, G. Aiello, C. Torino, A. Vilasi,

A. O'riordan, R. Inguanta, Pani-based wearable electrochemical sensor for ph sweat monitoring, Chemosensors. 9 (2021) 1–14. https://doi.org/10.3390/chemosensors9070169.
[34] F. Vivaldi, D. Santalucia, N. Poma, A. Bonini, P. Salvo, L. Del Noce, B. Melai, A. Kirchhain, V. Kolivoška, R. Sokolová, M. Hromadová, F. Di Francesco, A voltammetric pH sensor for food and biological matrices, Sensors Actuators, B Chem. 322 (2020). https://doi.org/10.1016/j.snb.2020.128650.
[35] W.J. Cho, C.M. Lim, Sensing properties of separative paper-based extended-gate ion-sensitive field-effect transistor for cost effective pH sensor applications, Solid. State. Electron. 140 (2018) 96–99. https://doi.org/10.1016/j.sse.2017.10.025.
[36] S. Sinha, R. Mukhiya, R. Sharma, P.K. Khanna, V.K. Khanna, Fabrication, characterization and electrochemical simulation of AlN-gate ISFET pH sensor, J. Mater. Sci. Mater. Electron. 30 (2019) 7163–7174. https://doi.org/10.1007/s10854-019-01033-5.
[37] H. Kadhum Hisham, Optical Fiber Sensing Technology: Basics, Classifications and Applications, Am. J. Remote Sens. 6 (2018) 1. https://doi.org/10.11648/j.ajrs.20180601.11.
[38] E. Frankforter, Fiber Optic Guided Wave Sensors For Structural Health Monitoring, (2017).
[39] S.J. M, Optical Fiber Communications: Principles and Practice, Pearson Education, 2009. https://books.google.pt/books?id=ok0XX-3MgMoC.
[40] K.M. Chung, Z. Liu, C. Lu, H.Y. Tam, Single reflective mode fiber bragg grating in multimode microfiber, IEEE Photonics J. 4 (2012) 437–442. https://doi.org/10.1109/JPHOT.2012.2188098.
[41] X. Cao, M. Zopf, F. Ding, Telecom wavelength single photon sources, J. Semicond. 40 (2019). https://doi.org/10.1088/1674-4926/40/7/071901.
[42] R. Kashyap, Fiber Bragg Gratings (Second Edition), Academic Press, Boston, 2010.
[43] B. Culshaw, A. Kersey, Fiber-Optic Sensing : A Historical Perspective, 26 (2008) 1064–1078.
[44] S. Yin, P.B. Ruffin, F.T.S. Yu, Fiber Optic Sensors, CRC Press, 2017. https://books.google.pt/books?id=5KdCOguH9CsC.
[45] W. Zhang, W. Zhuang, M. Dong, L. Zhu, F. Meng, Dual-Parameter Optical Fiber Sensor for Temperature and Pressure Discrimination Featuring Cascaded Tapered-FBG and Ball-EFPI, IEEE Sens. J. 19 (2019) 5645–5652. https://doi.org/10.1109/JSEN.2019.2905635.
[46] C.C. Moura, V. Oliveira, C.R. Biazoli, C.M.B. Cordeiro, H.J. Kalinowski, Manufacture of tapered fibers and FBG writing, J. Microwaves, Optoelectron. Electromagn. Appl. 17 (2018) 638–645. https://doi.org/10.1590/2179-10742018v17i41549.
[47] D. Lo Presti, C. Massaroni, C.S. Jorge Leitao, M. De Fatima Domingues, M. Sypabekova, D. Barrera, I. Floris, L. Massari, C.M. Oddo, S. Sales, I.I. Iordachita, D. Tosi, E. Schena, Fiber bragg gratings for medical applications and future challenges: A review, IEEE Access. 8 (2020) 156863–156888. https://doi.org/10.1109/ACCESS.2020.3019138.
[48] T. Guo, Á. González-Vila, M. Loyez, C. Caucheteur, Plasmonic optical fiber-grating Immunosensing: A review, Sensors (Switzerland). 17 (2017) 1–20. https://doi.org/10.3390/s17122732.
[49] M.S. Soares, M. Vidal, N.F. Santos, F.M. Costa, C. Marques, S.O. Pereira, C. Leitão, Immunosensing based on optical fiber technology: Recent advances, Biosensors. 11 (2021). https://doi.org/10.3390/bios11090305.
[50] S.W. James, R.P. Tatam, Optical fibre long-period grating sensors: Characteristics and application, Meas. Sci. Technol. 14 (2003). https://doi.org/10.1088/0957-0233/14/5/201.
[51] F. Chiavaioli, F. Baldini, S. Tombelli, C. Trono, A. Giannetti, Biosensing with optical fiber gratings, Nanophotonics. 6 (2017) 663–679. https://doi.org/10.1515/nanoph-2016-0178.
[52] T. Guo, F. Liu, B.O. Guan, J. Albert, Tilted fiber grating mechanical and biochemical sensors, Opt. Laser Technol. 78 (2016) 19–33. https://doi.org/10.1016/j.optlastec.2015.10.007.
[53] X. Dong, H. Zhang, B. Liu, Y. Miao, Tilted fiber bragg gratings: Principle and sensing applications, Photonic Sensors. 1 (2011) 6–30. https://doi.org/10.1007/s13320-010-0016-x.
[54] Z. Wang, G. Zhu, Y. Wang, M. Li, R. Singh, B. Zhang, S. Kumar, Fabrication techniques and stability analysis of SMF-/MMF-based differently tapered optical fiber structures, Appl. Opt. 60 (2021) 2077. https://doi.org/10.1364/ao.418875.
[55] Y. Bai, Y. Miao, H. Zhang, J. Yao, Simultaneous Measurement of Temperature and Relative Humidity Based on a Microfiber Sagnac Loop and MoS2, J. Light. Technol. 38 (2020) 840–845. https://doi.org/10.1109/JLT.2019.2947644.
[56] Y. Wang, G. Zhu, M. Li, R. Singh, C. Marques, R. Min, B.K. Kaushik, B. Zhang, R. Jha, S. Kumar, Water Pollutants p-Cresol Detection Based on Au-ZnO Nanoparticles Modified Tapered Optical Fiber, IEEE Trans. Nanobioscience. 20 (2021) 377–384. https://doi.org/10.1109/TNB.2021.3082856.
[57] A. Leung, P.M. Shankar, R. Mutharasan, A review of fiber-optic biosensors, Sensors Actuators, B Chem. 125 (2007) 688–703. https://doi.org/10.1016/j.snb.2007.03.010.
[58] J. Liu, Y. Xing, X. Zhou, G.Y. Chen, H. Shi, Light-sheet skew rays enhanced U-shaped fiber-optic fluorescent immunosensor for Microcystin-LR, Biosens. Bioelectron. 176 (2021) 112902. https://doi.org/10.1016/j.bios.2020.112902.
[59] Y.E. Monfared, Overview of recent advances in the design of plasmonic fiber-optic biosensors, Biosensors. 10 (2020). https://doi.org/10.3390/BIOS10070077.
[60] V. Semwal, B.D. Gupta, Highly selective SPR based fiber optic sensor for the detection of hydrogen peroxide, Sensors Actuators, B Chem. 329 (2021) 129062. https://doi.org/10.1016/j.snb.2020.129062.
[61] A.L. Khalaf, P.T. Arasu, H.N. Lim, S. Paiman, N.A. Yusof, M.A. Mahdi, M.H. Yaacob, Modified plastic optical fiber with CNT and graphene oxide nanostructured coatings for ethanol liquid sensing, Opt. Express. 25 (2017) 5509. https://doi.org/10.1364/oe.25.005509.

[62] X. Cheng, J. Bonefacino, B.O. Guan, H.Y. Tam, All-polymer fiber-optic pH sensor, Opt. Express. 26 (2018) 14610. https://doi.org/10.1364/oe.26.014610.
[63] Y. Han, Z. Chen, D. Cao, J. Yu, H. Li, X. He, J. Zhang, Y. Luo, H. Lu, J. Tang, H. Huang, Side-polished fiber as a sensor for the determination of nematic liquid crystal orientation, Sensors Actuators, B Chem. 196 (2014) 663–669. https://doi.org/10.1016/j.snb.2014.02.076.
[64] K. Gasior, T. Martynkien, G. Wojcik, P. Mergo, W. Urbanczyk, D-shape polymer optical fibres for surface plasmon resonance sensing, Opto-Electronics Rev. 25 (2017) 1–5. https://doi.org/10.1016/j.opelre.2017.01.003.
[65] C.L. Tien, H.Y. Lin, S.H. Su, High Sensitivity Refractive Index Sensor by D-Shaped Fibers and Titanium Dioxide Nanofilm, Adv. Condens. Matter Phys. 2018 (2018). https://doi.org/10.1155/2018/2303740.
[66] S. Chandra, S. Mukherji, Polyaniline modified u-bent fiber optic pH sensor for physiological use, 2018 3rd Int. Conf. Microw. Photonics, ICMAP 2018. 2018-Janua (2018) 1–2. https://doi.org/10.1109/ICMAP.2018.8354478.
[67] C. Zhang, Z. Li, S.Z. Jiang, C.H. Li, S.C. Xu, J. Yu, Z. Li, M.H. Wang, A.H. Liu, B.Y. Man, U-bent fiber optic SPR sensor based on graphene/AgNPs, Sensors Actuators, B Chem. 251 (2017) 127–133. https://doi.org/10.1016/j.snb.2017.05.045.
[68] S.K. Khijwania, B.D. Gupta, Maximum achievable sensitivity of the fiber optic evanescent field absorption sensor based on the U-shaped probe, Opt. Commun. 175 (2000) 135–137. https://doi.org/10.1016/S0030-4018(00)00465-X.
[69] Y. Xu, P. Lu, L. Chen, X. Bao, Recent developments in micro-structured fiber optic sensors, Fibers. 5 (2017). https://doi.org/10.3390/fib5010003.
[70] Y. Zhang, B. Lin, S.C. Tjin, H. Zhang, G. Wang, P. Shum, X. Zhang, Refractive index sensing based on higher-order mode reflection of a microfiber Bragg grating, Opt. Express. 18 (2010) 26345. https://doi.org/10.1364/oe.18.026345.
[71] A. Iadicicco, S. Campopiano, A. Cutolo, M. Giordano, A. Cusano, Thinned fiber Bragg gratings for sensing applications, Proc. WFOPC2005 - 4th IEEE/LEOS Work. Fibres Opt. Passiv. Components. 2005 (2005) 216–221. https://doi.org/10.1109/WFOPC.2005.1462129.
[72] H. Wen, J. Weng, C. Chiang, pH Sensor Through a Self-Assembled Multifunctional Layer With Clitoria Ternatea Based on Long-Period Fiber Gratings, 21 (2021) 12137–12145.
[73] A. Lopez Aldaba, González-Vila, M. Debliquy, M. Lopez-Amo, C. Caucheteur, D. Lahem, Polyaniline-coated tilted fiber Bragg gratings for pH sensing, Sensors Actuators, B Chem. 254 (2018) 1087–1093. https://doi.org/10.1016/j.snb.2017.07.167.
[74] I. Antohe, L. Jinga, V. Antohe, Sensitive pH Monitoring Using a Polyaniline-Functionalized Fiber Optic — Surface Plasmon Resonance Detector, Sensors. 21 (2021) 1–11.
[75] T. Khanikar, V.K. Singh, PANI-PVA composite film coated optical fiber probe as a stable and highly sensitive pH sensor, Opt. Mater. (Amst). 88 (2019) 244–251. https://doi.org/10.1016/j.optmat.2018.11.044.
[76] R. Jarzebinska, C.S. Cheung, S.W. James, R.P. Tatam, Response of the transmission spectrum of tapered optical fibres to the deposition of a nanostructured coating, Meas. Sci. Technol. 20 (2009) 34001. https://doi.org/10.1088/0957-0233/20/3/034001.
[77] K. Mullaney, R. Correia, S.E. Staines, S.W. James, R.P. Tatam, Monitoring techniques for the manufacture of tapered optical fibers, Appl. Opt. 54 (2015) 8531–8536. https://doi.org/10.1364/AO.54.008531.
[78] G. Rego, Fibre optic devices produced by arc discharges, J. Opt. 12 (2010) 113002. https://doi.org/10.1088/2040-8978/12/11/113002.
[79] J. Lu, Z. Chen, F. Pang, T. Wang, Theoretical analysis of fiber-optic evanescent wave sensors, Proc. 2008 China-Japan Jt. Microw. Conf. CJMW 2008. (2008) 583–587. https://doi.org/10.1109/CJMW.2008.4772500.
[80] A.J. Fielding, K. Edinger, C.C. Davis, Experimental observation of mode evolution in single-mode tapered optical fibers, J. Light. Technol. 17 (1999) 1649–1656. https://doi.org/10.1109/50.788571.
[81] M.I. Zibaii, H. Latifi, M. Karami, M. Gholami, S.M. Hosseini, M.H. Ghezelayagh, Non-adiabatic tapered optical fiber sensor for measuring the interaction between alpha-amino acids in aqueous carbohydrate solution, Meas. Sci. Technol. 21 (2010) 105801. https://doi.org/10.1088/0957-0233/21/10/105801.
[82] N. Agrawal, B. Zhang, C. Saha, C. Kumar, B.K. Kaushik, S. Kumar, Development of dopamine sensor using silver nanoparticles and peg-functionalized tapered optical fiber structure, IEEE Trans. Biomed. Eng. 67 (2020) 1542–1547. https://doi.org/10.1109/TBME.2019.2939560.
[83] M. Li, R. Singh, M.S. Soares, C. Marques, B. Zhang, S. Kumar, Convex fiber-tapered seven core fiber-convex fiber (CTC) structure-based biosensor for creatinine detection in aquaculture, Opt. Express. 30 (2022) 13898. https://doi.org/10.1364/oe.457958.
[84] Z. Wang, R. Singh, C. Marques, R. Jha, B. Zhang, S. Kumar, Taper-in-taper fiber structure-based LSPR sensor for alanine aminotransferase detection, Opt. Express. 29 (2021) 43793. https://doi.org/10.1364/oe.447202.
[85] L. Singh, R. Singh, B. Zhang, S. Cheng, B. Kumar Kaushik, S. Kumar, LSPR based uric acid sensor using graphene oxide and gold nanoparticles functionalized tapered fiber, Opt. Fiber Technol. 53 (2019) 102043. https://doi.org/10.1016/j.yofte.2019.102043.
[86] Q. Yang, X. Zhang, S. Kumar, R. Singh, B. Zhang, C. Bai, X. Pu, Development of Glucose Sensor Using Gold Nanoparticles and Glucose-Oxidase Functionalized Tapered Fiber Structure, Plasmonics. 15 (2020) 841–848. https://doi.org/10.1007/s11468-019-01104-7.
[87] S. Kumar, R. Singh, B.K. Kaushik, N.K. Chen, Q.S. Yang, X. Zhang, Lspr-based cholesterol biosensor using hollow core fiber structure, IEEE Sens. J. 19 (2019) 7399–7406. https://doi.org/10.1109/JSEN.2019.2916818.
[88] H.A. Mohammed, M.H. Yaacob, A novel modified fiber Bragg grating (FBG) based ammonia sensor coated

with polyaniline/graphite nanofibers nanocomposites, Opt. Fiber Technol. 58 (2020) 102282. https://doi.org/10.1016/j.yofte.2020.102282.
[89] J.L. Kou, M. Ding, J. Feng, Y.Q. Lu, F. Xu, G. Brambilla, Microfiber-based bragg gratings for sensing applications: A review, Sensors (Switzerland). 12 (2012) 8861–8876. https://doi.org/10.3390/s120708861.
[90] C.A.F. Marques, R. Min, A.L. Junior, P. Antunes, A. Fasano, G. Woyessa, K. Nielsen, H.K. Rasmussen, B. Ortega, O. Bang, Fast and stable gratings inscription in POFs made of different materials with pulsed 248 nm KrF laser, Opt. Express. 26 (2018) 2013. https://doi.org/10.1364/oe.26.002013.
[91] A. Othonos, K. Kalli, G.E. Kohnke, Fiber Bragg Gratings: Fundamentals and Applications in Telecommunications and Sensing, Phys. Today. 53 (2000) 61. https://doi.org/10.1063/1.883086.
[92] F. Bilodeau, Y. Hibino, M. Abe, B. Malo, J. Albert, M. Kawachi, D.C. Johnson, K.O. Hill, Photosensitization of optical fiber and silica-on-silicon/silica waveguides, Opt. Lett. 18 (1993) 953. https://doi.org/10.1364/ol.18.000953.
[93] C.L. Liou, L.A. Wang, M.C. Shih, Characteristics of hydrogenated fiber Bragg gratings, Appl. Phys. A. 64 (1997) 191–197. https://doi.org/10.1007/s003390050463.
[94] H.H. Qazi, A.B. Mohammad, H. Ahmad, M.Z. Zulkifli, D-shaped polarization maintaining fiber sensor for strain and temperature monitoring, Sensors (Switzerland). 16 (2016). https://doi.org/10.3390/s16091505.
[95] J. Zhao, G. Yin, C. Liao, S. Liu, J. He, B. Sun, G. Wang, X. Xu, Y. Wang, Rough side-polished fiber with surface scratches for sensing applications, IEEE Photonics J. 7 (2015) 1–8. https://doi.org/10.1109/JPHOT.2015.2423288.
[96] N. Cennamo, L. Zeni, P. Tortora, M.E. Regonesi, A. Giusti, M. Staiano, S. D'Auria, A. Varriale, A High Sensitivity Biosensor to detect the presence of perfluorinated compounds in environment, Talanta. 178 (2018) 955–961. https://doi.org/10.1016/j.talanta.2017.10.034.
[97] L. Bilro, N.J. Alberto, L.M. Sá, J. De Lemos Pinto, R. Nogueira, Analytical analysis of side-polished plastic optical fiber as curvature and refractive index sensor, J. Light. Technol. 29 (2011) 864–870. https://doi.org/10.1109/JLT.2011.2105462.
[98] S. Tseng, C. Chen, Side-polished fibers, Appl. Opt. 31 (1992).
[99] L. Jiang, L. Zhao, S. Wang, J. Yang, H. Xiao, Femtosecond laser fabricated all-optical fiber sensors with ultrahigh refractive index sensitivity: modeling and experiment, Opt. Express. 19 (2011) 17591. https://doi.org/10.1364/oe.19.017591.
[100] C. Zhong, C. Shen, Y. You, J. Chu, X. Zou, X. Dong, Y. Jin, J. Wang, A polarization-maintaining fiber loop mirror based sensor for liquid refractive index absolute measurement, Sensors Actuators, B Chem. 168 (2012) 360–364. https://doi.org/10.1016/j.snb.2012.04.035.
[101] C.H. Chen, T.C. Tsao, J.L. Tang, W. Te Wu, A multi-D-shaped optical fiber for refractive index sensing, Sensors. 10 (2010) 4794–4804. https://doi.org/10.3390/s100504794.
[102] C.H. Chen, T.C. Chao, W.Y. Li, W.C. Shen, C.W. Cheng, J.L. Tang, L.K. Chau, W. Te Wu, Novel D-type fiber optic localized plasmon resonance sensor realized by femtosecond laser engraving, J. Laser Micro Nanoeng. 5 (2010) 1–5. https://doi.org/10.2961/jlmn.2010.01.0001.
[103] M.S. Soares, D. Rodrigues, M. Vidal, M. Facão, N. Cennamo, L. Zeni, C. Caucheteur, F.M. Costa, C. Leitão, S.O. Pereira, N. Santos, C.F. Marques, D-shape optical fiber immunosensors based on SPR for cortisol detection: simulation and experimental procedure, (2022) 15. https://doi.org/10.1117/12.2620806.
[104] N. Cennamo, G. Alberti, M. Pesavento, G. D'Agostino, F. Quattrini, R. Biesuz, L. Zeni, A simple small size and low cost sensor based on Surface Plasmon Resonance for selective detection of Fe(III), Sensors (Switzerland). 14 (2014) 4657–4671. https://doi.org/10.3390/s140304657.
[105] N. Cennamo, D. Massarotti, L. Conte, L. Zeni, Low cost sensors based on SPR in a plastic optical fiber forbiosensor implementation, Sensors. 11 (2011) 11752–11760. https://doi.org/10.3390/s111211752.
[106] M. Pesavento, N. Cennamo, L. Zeni, L. De Maria, A molecularly imprinted polymer based spr sensor for 2-furaldehyde determination in oil matrices, Appl. Sci. 11 (2021). https://doi.org/10.3390/app112110390.
[107] Agua Regia, Princet. Univ. - Off. Enviaronmental Heal. Saf. - Chem. Saf. (2022). https://ehs.princeton.edu/laboratory-research/chemical-safety/chemical-specific-protocols/aqua-regia (accessed July 25, 2022).
[108] Aqua Regia Laboratory Safety Guideline, Harvard Environ. Heal. Saf. (2019) 1–2. https://www.ehs.harvard.edu/sites/default/files/lab_safety_guideline_aqua_regia.pdf (accessed July 25, 2022).
[109] B.A. Bolto, R. McNeill, D.E. Weiss, Electronic conduction in polymers. Iii. Electronic properties of polypyrrole, Aust. J. Chem. 16 (1963) 1090–1103. https://doi.org/10.1071/CH9631090.
[110] R. De Surville, M. Jozefowicz, L.T. Yu, J. Pepichon, R. Buvet, Electrochemical chains using protolytic organic semiconductors, Electrochim. Acta. 13 (1968) 1451–1458. https://doi.org/10.1016/0013-4686(68)80071-4.
[111] A.J. Heeger, Semiconducting and Metallic Polymers: The Fourth Generation of Polymeric Materials (Nobel Lecture) Copyright(c) The Nobel Foundation 2001., Rev. Mod. Phys. 73 (2001) 681.
[112] H. Shirakawa, E.J. Louis, A.G. MacDiarmid, C.K. Chiang, A.J. Heeger, Synthesis of electrically conducting organic polymers: Halogen derivatives of polyacetylene, (CH)x, J. Chem. Soc. Chem. Commun. (1977) 578–580. https://doi.org/10.1039/C39770000578.
[113] H. Heeger, Alan J. ; MacDiarmid, Alan G. ; Shirakawa, Advanced Information - The Nobel Prize in Chemistry 2000, Nobel Media AB 2019. (1974) 1–16. https://doi.org/10.1007/978-1-84996-290-2.
[114] H. Naarmann, Polymers, Electrically Conducting, in: Ullmann's Encycl. Ind. Chem., John Wiley & Sons, Ltd, 2000. https://doi.org/https://doi.org/10.1002/14356007.a21_429.
[115] G. Liao, Q. Li, Z. Xu, The chemical modification of polyaniline with enhanced properties: A review, Prog.

Org. Coatings. 126 (2019) 35–43. https://doi.org/10.1016/j.porgcoat.2018.10.018.
[116] M. Beygisangchin, S.A. Rashid, S. Shafie, A.R. Sadrolhosseini, Polyaniline Thin Films — A Review, Polymers (Basel). 13 (2021) 1–46.
[117] D. Thomas, A. Thomas, A.E. Tom, K.K. Sadasivuni, D. Ponnamma, S. Goutham, J.J. Cabibihan, K. Venkateswara Rao, Highly selective gas sensors from photo-activated ZnO/PANI thin films synthesized by mSILAR, Synth. Met. 232 (2017) 123–130. https://doi.org/10.1016/j.synthmet.2017.08.006.
[118] E.A. Gizzie, J. Scott Niezgoda, M.T. Robinson, A.G. Harris, G. Kane Jennings, S.J. Rosenthal, D.E. Cliffel, Photosystem I-polyaniline/TiO2 solid-state solar cells: Simple devices for biohybrid solar energy conversion, Energy Environ. Sci. 8 (2015) 3572–3576. https://doi.org/10.1039/c5ee03008k.
[119] J.A. Marins, B.G. Soares, M. Fraga, D. Müller, G.M.O. Barra, Self-supported bacterial cellulose polyaniline conducting membrane as electromagnetic interference shielding material: effect of the oxidizing agent, Cellulose. 21 (2014) 1409–1418. https://doi.org/10.1007/s10570-014-0191-9.
[120] Z. Ge, C.W. Brown, L. Sun, S.C. Yang, Fiber-Optic pH Sensor Based on Evanescent Wave Absorption Spectroscopy, Anal. Chem. 65 (1993) 2335–2338. https://doi.org/10.1021/ac00065a028.
[121] S.A. Ibrahim, N.A. Rahman, M.H. Abu Bakar, S.H. Girei, M.H. Yaacob, H. Ahmad, M.A. Mahdi, Room temperature ammonia sensing using tapered multimode fiber coated with polyaniline nanofibers, Opt. Express. 23 (2015) 2837. https://doi.org/10.1364/oe.23.002837.
[122] K. Kenry, B. Liu, Recent Advances in Biodegradable Conducting Polymers and Their Biomedical Applications, Biomacromolecules. 19 (2018) 1783–1803. https://doi.org/10.1021/acs.biomac.8b00275.
[123] Y. Chen, A review of polyaniline based materials as anodes for lithiumion batteries, IOP Conf. Ser. Mater. Sci. Eng. 677 (2019) 1–7. https://doi.org/10.1088/1757-899X/677/2/022115.
[124] E.T. Kang, Z.F. Li, K.G. Neoh, Y.Q. Dong, K.L. Tan, Protonation and deprotonation of polyaniline films and powders: Effects of acid and base concentrations on the surface intrinsic oxidation states, Synth. Met. 92 (1998) 167–171. https://doi.org/10.1016/S0379-6779(98)80107-0.
[125] H. Behniafar, K. Malekshahinezhad, A. Alinia-pouri, One-pot methods for preparing polyaniline/Ag nanocomposites via oxidative polymerization of aniline, J. Mater. Sci. Mater. Electron. 27 (2016) 1070–1076. https://doi.org/10.1007/s10854-015-3853-y.
[126] A.G. MacDiarmid, A.J. Epstein, "Synthetic metals": A novel role for organic polymers, Makromol. Chemie. Macromol. Symp. 51 (1991) 11–28. https://doi.org/10.1002/masy.19910510104.
[127] C.K. Arakawa, C.A. DeForest, Chapter 19 - Polymer Design and Development, in: A. Vishwakarma, J.M. Karp (Eds.), Biol. Eng. Stem Cell Niches, Academic Press, Boston, 2017: pp. 295–314. https://doi.org/https://doi.org/10.1016/B978-0-12-802734-9.00019-6.
[128] M.A. Mohamed, J. Jaafar, A.F. Ismail, M.H.D. Othman, M.A. Rahman, Chapter 1 - Fourier Transform Infrared (FTIR) Spectroscopy, in: N. Hilal, A.F. Ismail, T. Matsuura, D. Oatley-Radcliffe (Eds.), Membr. Charact., Elsevier, 2017: pp. 3–29. https://doi.org/https://doi.org/10.1016/B978-0-444-63776-5.00001-2.
[129] J.I. Goldstein, D.E. Newbury, P. Echlin, D.C. Joy, C.E. Lyman, E. Lifshin, L. Sawyer, J.R. Michael, Electron Beam--Specimen Interactions, in: Scanning Electron Microsc. X-Ray Microanal. Third Ed., Springer US, Boston, MA, 2003: pp. 61–98. https://doi.org/10.1007/978-1-4615-0215-9_3.
[130] K. Panwar, M. Jassal, A.K. Agrawal, In situ synthesis of Ag-SiO2Janus particles with epoxy functionality for textile applications, Particuology. 19 (2015) 107–112. https://doi.org/10.1016/j.partic.2014.06.007.
[131] V.S. Jamadade, D.S. Dhawale, C.D. Lokhande, Studies on electrosynthesized leucoemeraldine, emeraldine and pernigraniline forms of polyaniline films and their supercapacitive behavior, Synth. Met. 160 (2010) 955–960. https://doi.org/10.1016/j.synthmet.2010.02.007.
[132] D. Geethalakshmi, N. Muthukumarasamy, R. Balasundaraprabhu, Effect of dopant concentration on the properties of HCl-doped PANI thin films prepared at different temperatures, Optik (Stuttg). 125 (2014) 1307–1310. https://doi.org/10.1016/j.ijleo.2013.08.014.
[133] I. Mihai, F. Addiego, D. Ruch, V. Ball, Composite and free standing PANI-PVA membranes as flexible and stable optical pH sensors, Sensors Actuators, B Chem. 192 (2014) 769–775. https://doi.org/10.1016/j.snb.2013.11.042.
[134] N. Abu-Thabit, Y. Umar, E. Ratemi, A. Ahmad, F.A. Abuilaiwi, A flexible optical pH sensor based on polysulfone membranes coated with pH-responsive polyaniline nanofibers, Sensors (Switzerland). 16 (2016). https://doi.org/10.3390/s16070986.
[135] T. Lindfors, L. Harju, A. Ivaska, Optical pH measurements with water dispersion of polyaniline nanoparticles and their redox sensitivity, Anal. Chem. 78 (2006) 3019–3026. https://doi.org/10.1021/ac052252u.
[136] T. Khanikar, V.K. Singh, PANI-PVA composite film coated optical fiber probe as a stable and highly sensitive pH sensor, Opt. Mater. (Amst). 88 (2019) 244–251. https://doi.org/10.1016/j.optmat.2018.11.044.
[137] Z. Jin, Y. Su, Y. Duan, Improved optical pH sensor based on polyaniline, Sensors Actuators, B Chem. 71 (2000) 118–122. https://doi.org/10.1016/S0925-4005(00)00597-9.